Szkoła Główna Gospodarstwa Wiejskiego
w Warszawie
Instytut Inżynierii Mechanicznej

mgr inż. Michał Piątek
Numer albumu 2543

Modelowanie kinetyki procesu wytwarzania biogazu z materiałów lignocelulozowych

Modeling the kinetics of the biogas production process from lignocellulosic materials

Praca doktorska
Doctoral thesis

Praca wykonana pod kierunkiem:

Promotora: prof. dr. hab. inż. Aleksandra Lisowskiego
Promotora pomocniczego: dr inż. Magdaleny Dąbrowskiej

Warszawa, 2021

Streszczenie:

W niniejszej pracy zaprezentowano matematyczny opis procesu fermentacji anaerobowej biomasy lignocelulozowej w kontekście wstępnej obróbki mechanicznej. Na podstawie szerokiego przeglądu literatury wykazano luki w wiedzy obejmujące brak wiarygodnych modeli matematycznych uwzględniających dostępną powierzchnię materiału dla fazy hydrolizy oraz brak wiedzy dotyczącej wpływu lignin w formie stałej na fazę produkcji metanu w procesie fermentacji anaerobowej. W toku realizacji pracy zaprojektowano oraz wykonano stanowisko badawcze do prowadzenia procesu fermentacji anaerobowej. Do badań wykorzystano substraty modelowe: celulozę mikrokrystaliczną oraz ligniny kraft. Opracowano nowe modele matematyczne uwzględniające ubytek dostępnej powierzchni hydrolizowanego materiału oraz wykazano ich adekwatność na podstawie porównania z modelem kinetyki rzędu I. Wykazano również, że w określonych warunkach ligniny w formie stałej mogą mieć negatywny wpływ na proces metanogenezy.

Słowa kluczowe: modelowanie, geometria cząstki, kinetyka procesu degradacji powierzchni, inhibicja, fermentacja anaerobowa

Summary:

A mathematical description of the anaerobic fermentation process of lignocellulosic biomass in the context of mechanical pre-treatment was presented in this thesis. Based on an extensive literature review, knowledge gaps were identified, including the lack of reliable mathematical models taking into account the available surface area of the material for the hydrolysis phase, and the lack of knowledge on the effect of solid lignins on the methane production phase in the anaerobic fermentation process. During work a research stand for the anaerobic fermentation process was designed and constructed. Model substrates: microcrystalline cellulose and kraft lignin were used for the research. New mathematical models were developed, taking into account the loss of the available surface of the hydrolysed material, and their adequacy was demonstrated on the basis of a comparison with the 1st order kinetic model. It was also shown that under certain conditions, solid lignin may have a negative impact on the methanogenesis process.

Keywords: modeling, particle geometry, surface-related kinetics, inhibition, anaerobic digestion

Wykaz publikacji stanowiących pracę doktorską:

Publikacja nr 1:

Piątek M., Lisowski A., Dąbrowska M., 2021. Surface-Related Kinetic Models for Anaerobic Digestion of Microcrystalline Cellulose: The Role of Particle Size. Materials 14, 487. **(140 pkt., IF = 3.057)**
Udział w publikacji: 90%

Publikacja nr 2:

Piątek M., Lisowski A., Dąbrowska M., 2021. The effects of solid lignin on the anaerobic digestion of microcrystalline cellulose and application of smoothing splines for extended data analysis of its inhibitory effects. Bioresource Technology 320, 124262. **(140 pkt. IF= 7.539)**
Udział w publikacji: 90%

Spis treści

1. Wprowadzenie

Biomasa lignocelulozowa stanowi ogromne źródło substratu do produkcji biogazu w procesie fermentacji anaerobowej (Mustafa et al., 2016). Lignoceluloza charakteryzuje się unikalną, strukturą, która utrudnia jej efektywne wykorzystanie w procesie fermentacji anaerobowej (Solé-Bundó et al., 2017). Fakt ten powoduje, że w celu jej efektywnego wykorzystania, lignoceluloza powinna być poddana odpowiedniej obróbce wstępnej, pozwalającej na zwiększenie kinetyki produkcji oraz uzysku biogazu z jednostki substratu (Li et al., 2019). Wadą wielu metod obróbki wstępnej jest wytwarzanie inhibitorów procesu fermentacji takich jak hydroksymetylofurfural i furfural z celulozy i hemicelulozy (Atelge et al., 2020). Często stosowaną obróbką wstępną jest oddziaływanie na materiał substancjami o wysokim pH, takimi jak wodorotlenek sodu (Sołowski et al., 2020). W efekcie powstają fenole oraz rozpuszczalne w wodzie ligniny (Lorenci Woiciechowski et al., 2020; Venturin et al., 2018), które są inhibitorami nie tylko hydrolizy, ale również kwasogenezy i metanogenezy (Koyama et al., 2017). Należy jednak zaznaczyć, że całość lignin nie zostaje rozpuszczona, a w materiale pozostaje część lignin w formie nierozpuszczonej, stałej. Możliwy, negatywny wpływ lignin w formie stałej nie został dobrze zbadany. W szczególności wpływ lignin w formie stałej na fazę metanogenezy pozostaje luką w wiedzy. Co istotne, inhibicja tej fazy może doprowadzić do niebezpiecznych zaburzeń procesu takich jak nadmierna akumulacja lotnych kwasów tłuszczowych (LKT), prowadząca do zatrzymania procesu (Ma et al., 2013; Nguyen et al., 2019; Zhang et al., 2015). Zagadnienie to nabiera szczególnej wagi w kontekście obróbki mechanicznej materiału, podczas której nie dochodzi do rozkładu lignin, a jedynie do zmiany fizycznych właściwości materiału, zatem całość lignin pozostaje w formie stałej. Należy również zaznaczyć, że w wyniku obróbki mechanicznej nie powstaje szkodliwy hydroksymetylofurfural i furfural, a zatem ligniny w formie stałej pozostają jedynym potencjalnym źródłem inhibicji fazy metanogenezy. Jednocześnie istnieje konieczność redukcji wymiaru cząstek lignocelulozy, do wartości 1-2 mm celem uniknięcia zaburzeń transportu masy w trakcie procesu (Bochmann and Montgomery, 2013; Kratky and Jirout, 2011). Kluczowymi parametrami są wymiar i geometria cząstek, które zmieniają się w wyniku różnych obróbek wstępnych materiału lignocelulozowego niezbędnych do przeprowadzenia efektywnego procesu fermentacji anaerobowej. Parametry te mają wpływ przede wszystkim na dostępność wyspecjalizowanych mikroorganizmów do powierzchni celulozy i wynikający z tego zwiększony uzysk gazu oraz zwiększoną kinetykę tego procesu. W przypadku fermentacji anaerobowej lignocelulozy hydroliza jest etapem decydującym o wydajności

całego procesu, a obróbka wstępna ma na celu skrócenie czasu trwania tego etapu (De Sanctis et al., 2019; Karimi and Taherzadeh, 2016). Problematyczna, niska kinetyka hydrolizy celulozy jest związana z reakcjami enzymatycznymi, takimi jak warunki reakcji, aktywność celulazy, blokowanie się enzymów (ang. enzyme jamming), inhibicja kompetycyjna i niekompetycyjna oraz właściwościami materiału takimi jak stopień krystaliczności, stopień polimeryzacji, dostępność i struktura powierzchni czy wymiar cząstek (Kumar and Wyman, 2009; Monschein et al., 2013). Istnieje więc potrzeba rozwijania wiedzy naukowej dotyczącej związku właściwości celulozy z kinetyką jej hydrolizy (Koyama et al., 2017; Li et al., 2016), w szczególności z dostępnością powierzchni dla enzymów hydrolitycznych (Fierobe et al., 2002). Bardzo istotną właściwością celulozy, mającą wpływ na przebieg procesu fermentacji, jest jej stopień krystaliczności (Li et al., 2019; Yu et al., 2012). Na podstawie wyników badań stwierdzono, że spadek krystaliczności celulozy, będący efektem obróbki mechanicznej, jest nieodłącznie związany ze zmianą innych właściwości takich jak powierzchnia właściwa i wymiar cząstek (Yu et al., 2012; Yuan et al., 2014). Brak jest natomiast wiedzy dotyczącej wpływu wymiaru cząstek na kinetykę procesu, w sytuacji gdy stopień polimeryzacji i krystaliczności celulozy jest taki sam między porównywanymi próbkami celulozy różniącymi się wymiarami cząstek oraz powiązaną z tym powierzchnią właściwą materiału. Co więcej, w procesie fermentacji anaerobowej celuloza jest hydrolizowana przez cellulosomy, które są wieloenzymatycznymi kompleksami pośredniczącymi w procesie hydrolizy między cząstkami celulozy a mikroorganizmami (Adams et al., 2010; Bayer and Lamed, 1986). Po przyłączeniu do cząstki celulozy, cellulosomy utrzymują kontakt między bakterią a cząstką celulozy oraz szybko rosną (Bayer and Lamed, 1986). Uwzględnienie zmian powierzchni w modelu opisującym proces ma zatem istotne znaczenie. Kinetyka reakcji enzymatycznych kontroluje proces, w sytuacji gdy ilość enzymów przekracza ilość dostępnych miejsc adsorpcji. W tym przypadku reakcja hydrolizy celulozy może być dobrze opisana z wykorzystaniem równania kinetyki pierwszego rzędu (Batstone et al., 2002; García-Gen et al., 2015; South et al., 1995; Vavilin et al., 2008). Model ten nie uwzględnia jednak ubytku dostępnych miejsc adsorpcji enzymów w czasie, powiązanego z wymiarem i kształtem cząstek, co stanowi kolejną lukę w wiedzy. Dotychczas zaproponowano kilka modeli biorących pod uwagę zjawisko ubytku dostępnej powierzchni w procesie hydrolizy cząstek stałych, niemniej zagadnienie to wymaga dalszego rozwoju (da Rocha et al., 2013; Sakimoto et al., 2017; Vavilin et al., 1996). W niniejszej pracy podjęto próbę uzupełnienia zidentyfikowanych luk w wiedzy. Sformułowano hipotezy i cele badawcze. Przedstawiono dyskusje wyników oraz najważniejsze

wnioski. Wszystkie zagadnienia prezentowane w niniejszej pracy zostały w szczegółach rozwinięte i opisane w publikacjach naukowych stanowiących jej załączniki.

2. Problem i hipotezy badawcze

Na podstawie obszernego przeglądu literatury stwierdzono następujące luki w wiedzy:

1) Model kinetyki pierwszego rzędu nie wystarcza do prawidłowego opisu hydrolizy lignocelulozy w procesie fermentacji anaerobowej;
2) Brak informacji dotyczących wpływu lignin w formie stałej na fazę metanogenezy.

Sformułowano następujące hipotezy badawcze:

1) Modele uwzględniające ubytek dostępnej powierzchni celulozy lepiej opisują proces jej hydrolizy w procesie fermentacji anaerobowej;
2) Nierozpuszczone ligniny są inhibitorem zarówno hydrolizy, jak i metanogenezy.

3. Cel badań

Cele naukowe:

1) Opracowanie nowego modelu uwzgledniającego ubytek dostępnej powierzchni podczas hydrolizy celulozy w procesie fermentacji anaerobowej.
2) Zbadanie potencjalnego wpływu nierozpuszczalnych lignin na hydrolizę i metanogenezę procesu fermentacji.

Cel utylitarny:

Opracowanie wytycznych dotyczących projektowania reaktorów fermentacji anaerobowej materiałów lignocelulozowych.

4. Metodyka badań

4.1 Przygotowanie próbek – separacja sitowa

Celulozę mikrokrystaliczną (ang. microcrystalline cellulose, MCC) Flocel 102 zakupiono na lokalnym rynku i rozdzielono przy użyciu wibracyjnego separatora sitowego LAB-11-200/UP. Zestaw miał wymiary sit otwierających w kolejności od dołu do góry przy: 20, 32, 45, 56, 100, 150, 212 i 300 μm. Zestaw spoczywał na dnie bez otworów. Zestaw sit dobrano na podstawie wstępnego testu tak, aby około połowa próbki materiału przeszła przez oczka o średnim rozmiarze. Masa pojedynczej próbki celulozy poddanej separacji wynosiła 50 g. Czas przesiewania wynosił 300 s i był kontrolowany za pomocą stopera. Czas przesiewania określono na podstawie wstępnych eksperymentów. Otrzymano siedem próbek frakcji cząstek o wymiarach od 20 μm do 300 μm.

4.2 Oznaczenie wilgotności materiału

Wilgotność materiału zbadano z wykorzystaniem suszarki laboratoryjnej SLW 115. Materiał suszono w 105°C przez 24 h.

4.3 Mikroskopia elektronowa

Obrazy losowo wybranych próbek uzyskano metodą skaningowej mikroskopii elektronowej (ang. scanning electron microscopy, SEM, FEI Quanta 200 z modelem mikroanalizatora EDS i cyfrowym zapisem obrazu) w Centrum Analitycznym SGGW. Aby uzyskać obrazy SEM, pobrano kilka cząstek z każdej frakcji i umieszczono w komorze próżniowej.

4.4 Oznaczenie gęstości właściwej

Gęstość cząstek mierzono za pomocą stereopiknometrii helowej (piknometr Quantachrome Instruments). Próbkę MCC umieszczono w celi pomiarowej o pojemności V_C = 100 cm^3. Dla tego stanu rejestrowano ciśnienie p_1 helu w celi pomiarowej. Następnie otwierano zawór, przez który gaz kierowany był do celi referencyjnej o objętości V_A i mierzono jego ciśnienie p_2 (Gilvari et al., 2019). Rzeczywistą gęstość MCC określono jako:

$$\rho = \frac{m}{V_C - V_A/(\frac{p_1}{p_2} - 1)}, \quad (1)$$

gdzie ρ to rzeczywista gęstość ($g \cdot cm^{-3}$), m to masa próbki MCC (g), V_C to objętość celi pomiarowej (cm^3), V_A to referencyjna objętość celi (cm^3), p_1 to ciśnienie w celi pomiarowej (MPa), a p_2 to ciśnienie w celi odniesienia (MPa).

4.5 Oznaczenie stopnia polimeryzacji

Stopień polimeryzacji zmierzono metodą wiskozymetryczną. Lepkość roztworu zmierzono za pomocą wiskozymetru Ubbelohdego o średnicy kapilary 0,84 mm (Schott Instruments). Rejestrowano czas wypływu roztworu celulozy co 10 min przez 2 h dla każdej próbki ważącej około 0,4 g. Temperatura kapilary wynosiła 25 ± 0,1°C. Stopień polimeryzacji obliczono za pomocą równania Immerguta:

$$DP^{\alpha} = K \cdot [\eta], \tag{2}$$

gdzie *DP* to średni stopień polimeryzacji (-), $[\eta]$ to średnia (wagowo) lepkość istotna (-), a K i α to stałe równe odpowiednio 1,65 $g \cdot cm^{-3}$ i 0,9 (Evans and Wallis, 1989). Aby zminimalizować szkodliwy wpływ roztworu miedzi (II)-etylenodiaminy (CUEN), przez ekstrapolację obliczono stopień polimeryzacji dla zerowego czasu retencji.

4.6 Oznaczenie stopnia krystalizacji

Krystaliczność próbek MCC (około 0,5 g) oceniano metodą dyfraktometrii rentgenowskiej (ang. x-Ray diffraction, XRD) ze źródłem promieniowania Cu Kα (długość fali λ = 1,5418 Å) przy napięciu 30 kV i prądzie 25 mA. Zakres skanowania wynosił 2θ = 5–30° z krokiem 0,04°, a czas zliczania impulsów 3 s. Krystaliczność celulozy obliczono metodą dekonwolucji XRD (Hindeleh and Johnson, 1971; Park et al., 2010).

4.7 Oznaczenie powierzchni właściwej

Powierzchnię właściwą (ang. specific surface area, SSA) wyznaczono metodą Brunauer'a- Emmett'a-Teller'a (BET). Przed pomiarem próbki odgazowano w próżni przez 24 godziny w 105°C w celu usunięcia wody i innych zanieczyszczeń. Pomiary przeprowadzono

za pomocą analizatora pola powierzchni QUADRASORB SI. Wszystkie niezbędne obliczenia wykonano za pomocą oprogramowania analizatora.

4.8 Wyznaczenie wskaźnika retencji wody

Wyznaczenie wskaźnika retencji wody (ang, water retention value, *WRV*) wykonano zgodnie z opublikowanym protokołem (Gao et al., 2017; Lu et al., 2019). Próbkę 1 g MCC odważoną z dokładnością do 0,1 mg umieszczono w probówce wirówkowej zawierającej wodę dejonizowaną (10 ml), wymieszano i pozostawiono na 24 godziny. Następnie próbki odwirowano (3000 g przez 20 min), a supernatant zdekantowano. Pozostałe mokre próbki MCC zważono i suszono w piecu przez 10 godzin w 105 °C. Następnie obliczono wskaźnik retencji wody (*WRV*) jako:

$$WRV = \frac{W_{wet} - W_{dried}}{W_{dried}}, \quad (3)$$

gdzie *WRV* to wskaźnik retencji wody (g $H_2O \cdot g^{-1}$), W_{wet} to masa mokrej próbki po odwirowaniu (g), a W_{dried} to masa próbki po wysuszeniu (g).

4.9 Fermentacja anaerobowa

Badania fermentacji anaerobowej wykonano na specjalnie do tego celu zaprojektowanym stanowisku badawczym (rys. 1) zgodnym z normą VDI 4630 (Verein Deutscher Ingenieure, 2014). Pomiar ilości wyprodukowanego gazu opierał się na metodzie wypartej solanki (ang. brine displacement method) (Ran et al., 2018; Xin et al., 2018). Reaktory, do których uprzednio wprowadzono inokulum oraz badany substrat umieszczono w łaźni wodnej w temperaturze 37°C. Wyprodukowany gaz wypierał nasycony roztwór chlorku sodu z butelek umieszczonych poza łaźnią, do których gaz doprowadzono niebieskim (rys. 1) przewodem polietylenowym. Wyparta ciecz była następnie ważona na wadze elektronicznej z dokładnością +/- 0,1g, a następnie przeliczana na objętość suchego gazu.

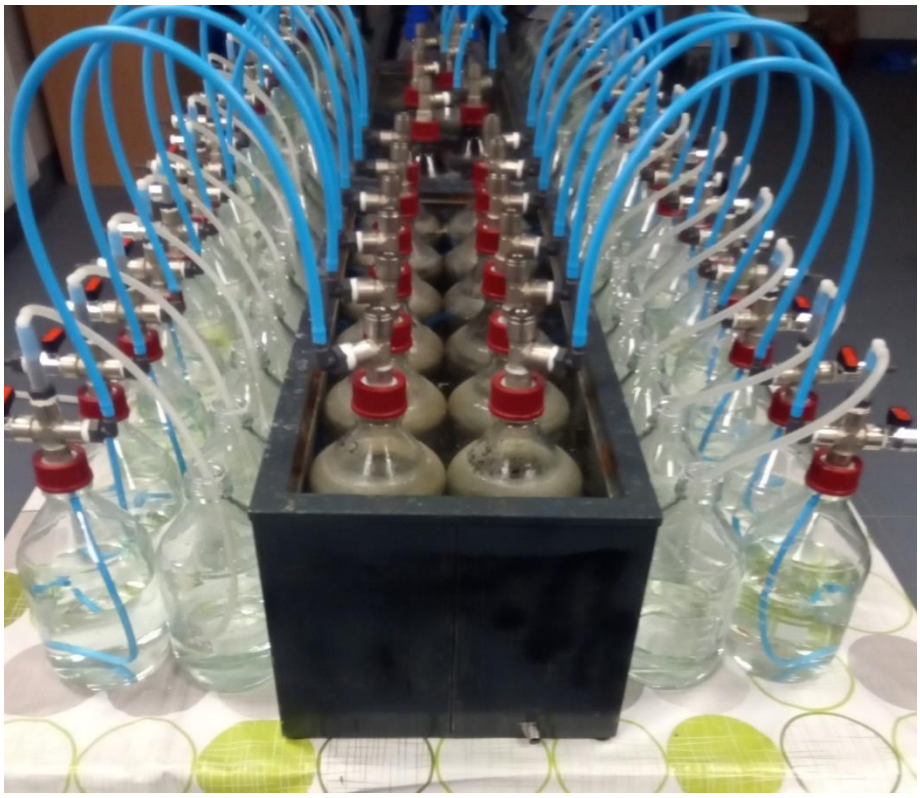

Rys. 1. Stanowisko do badań procesu fermentacji zgodne z VDI 4630

Pomiar składu gazu wykonywano za pomocą urządzenia GasData GFM 406 (rys. 2). Mierzono zawartość dwutlenku węgla oraz metanu w zakresie 0-100% z dokładnością do 1%.

Rys. 2. Analizator gazu GasData GFM 406

Eksperymenty wykonywano z wykorzystaniem inokulum pochodzącego z biogazowni rolniczej zlokalizowanej na terenie województwa mazowieckiego. Wykonano dwa podstawowe eksperymenty.

W pierwszym eksperymencie fermentacji poddano próbki MCC o różnych wymiarach cząstek. Do reaktorów wprowadzono 1800 ml inokulum oraz 10 g MCC. Badania wykonano trzykrotnie dla każdej z próbek. Inokulum zawierało 3,1% ±0,05% suchej substancji oraz 63,2% ± 0,05% suchej substancji organicznej. Stosunek inokulum do substratu w przeliczeniu na suchą substancję organiczną wynosił 3,5:1 Eksperyment prowadzono przez 25 dni zgodnie z zaleceniami normy VDI 4630.

W drugim eksperymencie, który miał na celu zbadanie wpływu lignin w formie stałej na fazę metanogenezy wykorzystano inokulum niezbalansowane. Był to materiał z celowo osłabioną kulturą organizmów prowadzących fazę metanogenezy, tak aby ta faza procesu stała się fazą limitującą proces, zamiast fazy hydrolizy. Do tego celu wykorzystano inokulum pochodzące z poprzedniego eksperymentu, które następnie było przechowywane w temperaturze 20°C przez około 3 miesiące, celem głodzenia i osłabienia organizmów fazy metanogenezy, które są najbardziej wrażliwe na niekorzystne zmiany środowiskowe (Wintsche et al., 2018). Czas wzrostu metanogenów jest dłuższy niż bakterii biorących udział w pozostałych etapach fermentacji anaerobowej (Manyi-Loh et al., 2013), co powoduje, że zaburzona równowaga między populacjami mikroorganizmów prowadzących poszczególne fazy procesu mogła utrzymywać się przez cały okres badania. W tym eksperymencie stosunek inokulum do substratu wynosił 3:1. Do reaktorów dodano 10 g MCC oraz ligniny kraft (370959, Sigma-Aldrich, USA) w dawkach 3, 7, 10, 13, 17 oraz 20 g. Przygotowano również próby z samą MCC (10 g) oraz ligninami (20 g). Odczyn pH inokulum wynosił 8.01 ±0.01 (phmetr WTW ProfLine pH 3110 z elektrodą SenTix® 41). Eksperyment trwał 70 dni.

4.10 Modelowanie

Efektem obróbki mechanicznej lignocelulozy jest zwiększenie uzysku biogazu oraz zwiększenie kinetyki produkcji. W przeciwieństwie do wielu innych metod dzieje się to poprzez mechaniczne struktury materiału, a nie przez modyfikację chemiczną, w tym rozpuszczenie lignin. Wspomniane wyżej efekty mają związek z dostępnością powierzchni celulozy. Dzieje się tak dlatego, ponieważ w procesie fermentacji celuloza jest rozkładana przez cellulosomy, mulit-enzymatyczne kompleksy rozkładające cząstki celulozy będąc do nich

przytwierdzone. Można zatem założyć, że cząstka po skolonizowaniu przez mikroorganizmy i po zsyntezowaniu cellulosomów jest hydrolizowana we wszystkich dostępnych miejscach. Założenie nasycenia powierzchni pozwala przyjąć, że na powierzchni cząstki reakcja hydrolizy przebiega zgodnie z równaniem kinetyki rzędu I. Zatem prawdziwe jest równanie:

$$\frac{dM}{dt} = -k_s \cdot S, \tag{4}$$

gdzie: M to masa cząstki (g), t oznacza czas (h), S to hydrolizowana powierzchnia (cm^2) oraz k_s oznacza stałą kinetyki pierwszego rzędu zależną od powierzchni ($g \cdot cm^{-2} \cdot h^{-1}$).

Możliwe jest zapisanie równania celem uwzględnienia uwalnianej objętości cząstki uzyskując:

$$\frac{dV}{dt} = \frac{-k_s \cdot S}{\rho} \tag{5}$$

gdzie V to objętość cząstki (cm^3) oraz ρ oznacza gęstość cząstki ($g \cdot cm^{-3}$).

Zakładając sferyczny kształt cząstki, uwalniana objętość materiału może być zapisana w następujący sposób:

$$\frac{dV}{dt} = \frac{-k_s \cdot 4 \cdot \pi \cdot R^2}{\rho}, \tag{6}$$

gdzie R oznacza promień cząstki (cm).

Można zauważyć, że:

$$\frac{dV}{dt} = \frac{dV}{dR} \cdot \frac{dR}{dt} = 4 \cdot \pi \cdot R^2 \cdot \frac{dR}{dt}, \tag{7}$$

dlatego:

$$4 \cdot \pi \cdot R^2 \cdot \frac{dR}{dt} = \frac{-k_s \cdot 4 \cdot \pi \cdot R^2}{\rho}, \tag{8}$$

a po uproszczeniach uzyskano:

$$\frac{dR}{dt} = \frac{-k_s}{\rho}. \tag{9}$$

Możliwe jest zatem zbudowanie modelu izotropowego materiału zakładającego stały ubytek cząstki w kierunku promieniowym. W takim przypadku można również stwierdzić, że kinetyka reakcji jest proporcjonalna do dostępnej powierzchni materiału. Prezentowane założenie jest również prawdziwe dla cząstek cylindrycznych, zakładając wyłącznie promieniowy rozkład cząstek. Na podstawie prezentowanych założeń opracowano uproszczone modele przedstawione poniżej.

Model zakładający kształt walca:

$$B(t) = \begin{cases} BP \cdot (1 - (1 - k \cdot (t - \lambda))^2), & \begin{cases} k \cdot (t - \lambda) < 1 \\ t - \lambda > 0 \end{cases} \\ BP, & k \cdot (t - \lambda) \geq 1 \\ 0, & t - \lambda \leq 0 \end{cases}, \tag{10}$$

oraz model zakładający kulisty kształt cząstki:

$$B(t) = \begin{cases} BP \cdot (1 - (1 - k \cdot (t - \lambda))^3), & \begin{cases} k \cdot (t - \lambda) < 1 \\ t - \lambda > 0 \end{cases} \\ BP, & k \cdot (t - \lambda) \geq 1 \\ 0, & t - \lambda \leq 0 \end{cases} \tag{11}$$

gdzie: *BP* to potencjał produkcji biogazu [ml/g], *k* to stała kinetyki pierwszego rzędu [1/h], λ to opóźnienie reakcji [h].

Należy zwrócić uwagę na fakt, że zależność kinetyki reakcji wyraża się w strukturze równania, a stała *k* to typowa stała kinetyki rzędu I, co potwierdza jednostka. Szczegółowe wyprowadzenie powyższych równań znajduje się w załączonej publikacji nr 1.

Zaprezentowane modele porównano z modelem kinetyki pierwszego rzędu, który jest często stosowany do opisu hydrolizy materiału lignocelulozowego:

$$B(t) = \begin{cases} BP \cdot (1 - exp(-k \cdot (t - \lambda))), & t - \lambda > 0 \\ 0, & t - \lambda \leq 0 \end{cases} \tag{12}$$

4.11 Dopasowanie modeli

Modele parametryczne dopasowano z wykorzystaniem metody ważonych najmniejszych kwadratów (z wyjątkiem dopasowania modelu do stałych *k* w funkcji średniego wymiaru cząstek, gdzie wykorzystano metodę najmniejszych kwadratów bez wag). Do dopasowania wykorzystano algorytm Levenberga-Marquardta poprzedzony algorytmem uogólnionego symulowanego wyżarzania (Xiang et al., 2013). W obu algorytmach zastosowano parametry domyślne. Współczynnik wag obliczono jako lokalne nachylenie krzywej produkcji biogazu (Vavilin et al., 2004) wg wzoru:

$$w_i = B_i - B_{i-1}, \tag{13}$$

gdzie w_i to współczynnik wagowy ($ml \cdot g^{-1}$), B_i to wartość krzywej produkcji biogazu w danym czasie pomiaru i ($ml \cdot g^{-1}$), a B_{i-1} to poprzednio zmierzona wartość krzywej produkcji biogazu ($ml \cdot g^{-1}$).

Ocenę dopasowania wykonano za pomocą globalnego błędu względnego:

$$\delta = 100\sqrt{\sum_{i=1}^{n}(z_i - p_i)^2 / \sum_{i=1}^{n} z_i{}^2}, \quad (14)$$

gdzie n jest liczbą pomiarów, a z i p są odpowiednio wartościami rzeczywistymi oraz uzyskanymi z modelu.

Oszacowano błąd dla krzywych, reprezentujących pełny przebieg produkcji biogazu oraz tylko dla ostatniego dnia próby, co nazwano błędem końcowym.

Model nieparametryczny „smoothing spline" dopasowano do krzywych produkcji biometanu za pomocą metody uogólnionej walidacji krzyżowej (ang. Generalized Cross Validation, GCV), aby uniknąć „przeuczenia" modelu. Wszystkie punkty pomiarowe użyto jako węzły modelu. W procesie aproksymacji zastosowano wagi, obliczane jako odwrotność zmierzonych, skumulowanych wartości produkcji biometanu. Podejście to wybrano na podstawie własnych doświadczeń autora. Pozostałe parametry ustawiono jako domyślne. Zastosowana funkcja „smooth.spline" pozwoliła na obliczenie pochodnych skumulowanych krzywych produkcji. Wszystkie obliczenia przeprowadzono przy użyciu pakietu „R" (wersja 3.5.1).

4.12 Wyznaczanie inhibicji

Inhibicję wyznaczono za pomocą wzoru:

$$I = \left(1 - \frac{T_R}{T_L}\right) \cdot 100\% \quad (15)$$

gdzie I oznacza względną inhibicję, rozumianą jako wydłużenie czasu trwania danego etapu procesu w odniesieniu do próby referencyjnej (%); T_R czas trwania etapu procesu dla próby referencyjnej (h); i T_L czas trwania etapu procesu dla próby inhibitowanej (h).

4.13 Analiza statystyczna

Do porównania krzywych produkcji biogazu/biometanu wykorzystano test Kruskala–Wallisa. Wartości końcowej, skumulowanej produkcji biogazu/biometanu, wilgotności, oraz gęstości właściwej przeanalizowano za pomocą analizy wariancji. Do zweryfikowania

poprawności założeń analizy wariancji wykorzystano test Levene'a na jednorodność wariancji oraz test normalności rozkładu Shapiro-Wilka. Relacje zmiennych analizowano za pomocą metody regresji liniowej. Różnice uznano za istotne statystycznie przy $p \leq 0,05$. Analizę statystyczną przeprowadzono przy użyciu pakietu „R” (wersja 3.5.1).

5. Wyniki i dyskusja

Próbki MCC zbadano za pomocą mikroskopu SEM. Zdjęcia wybranych próbek przedstawiono na rys. 3. Z obserwacji wynika, że cząstki mają kształt zbliżony do walca lub kuli, co jest zbieżne z założeniami nowych modeli. Warto zauważyć, że największe cząstki są aglomeratami mniejszych cząstek. Pozostałe właściwości badanych próbek przedstawiono w tab. 1. Analiza wariancji wykazała, że brak jest podstaw do stwierdzenia, że poszczególne frakcje celulozy istotnie różnią się między sobą pod kątem zawartości wilgoci ($p>>0,05$). Wykazano istotne różnice w gęstości właściwej ($p = 0,0008$), niemniej różnice te zawierały się w bardzo wąskim zakresie 1,581-1,603 $g \cdot ml^{-3}$. Należy zatem stwierdzić, że próbki były homogeniczne pod względem gęstości właściwej, a stwierdzone różnice, istotne statystycznie były wynikiem bardzo precyzyjnego pomiaru. W przypadku stopnia polimeryzacji i krystaliczności wartości również zmieniały się w bardzo wąskim zakresie. W przypadku stopnia polimeryzacji 328-336 a w przypadku stopnie krystaliczności 56-60%, co skłania do stwierdzenia, że pod względem tych parametrów próbki były homogeniczne. Oznacza to, że podstawową różnicą między badanymi próbkami jest wymiar cząstek, a pozostałe właściwości, potencjalnie wpływające na kinetykę procesu pozostają niezmienne. Z tego względu badany zbiór próbek ma charakter unikatowy. Wyniki badań na tego typu zbiorze nie były do tej pory publikowane.

Przygotowane próbki MCC poddano procesowi fermentacji anaerobowej celem uzyskania krzywych produkcji biogazu, które rys. 4. W tym przypadku do modelowania wykorzystano krzywe produkcji biogazu zamiast krzywych produkcji metanu, ponieważ krzywe produkcji biogazu uwzględniają dwutlenek węgla wytworzony podczas fazy hydrolizy. Analiza statystyczna wykazała, że nie ma podstaw do stwierdzenia istotnych różnic w końcowym uzysku biogazu (analiza wariancji, $p = 0.0622$), jednak krzywe różniły się kinetyką procesu (dla testu Kruskala–Wallisa $p=0.0105$), co daje podstawę do dalszego modelowania.

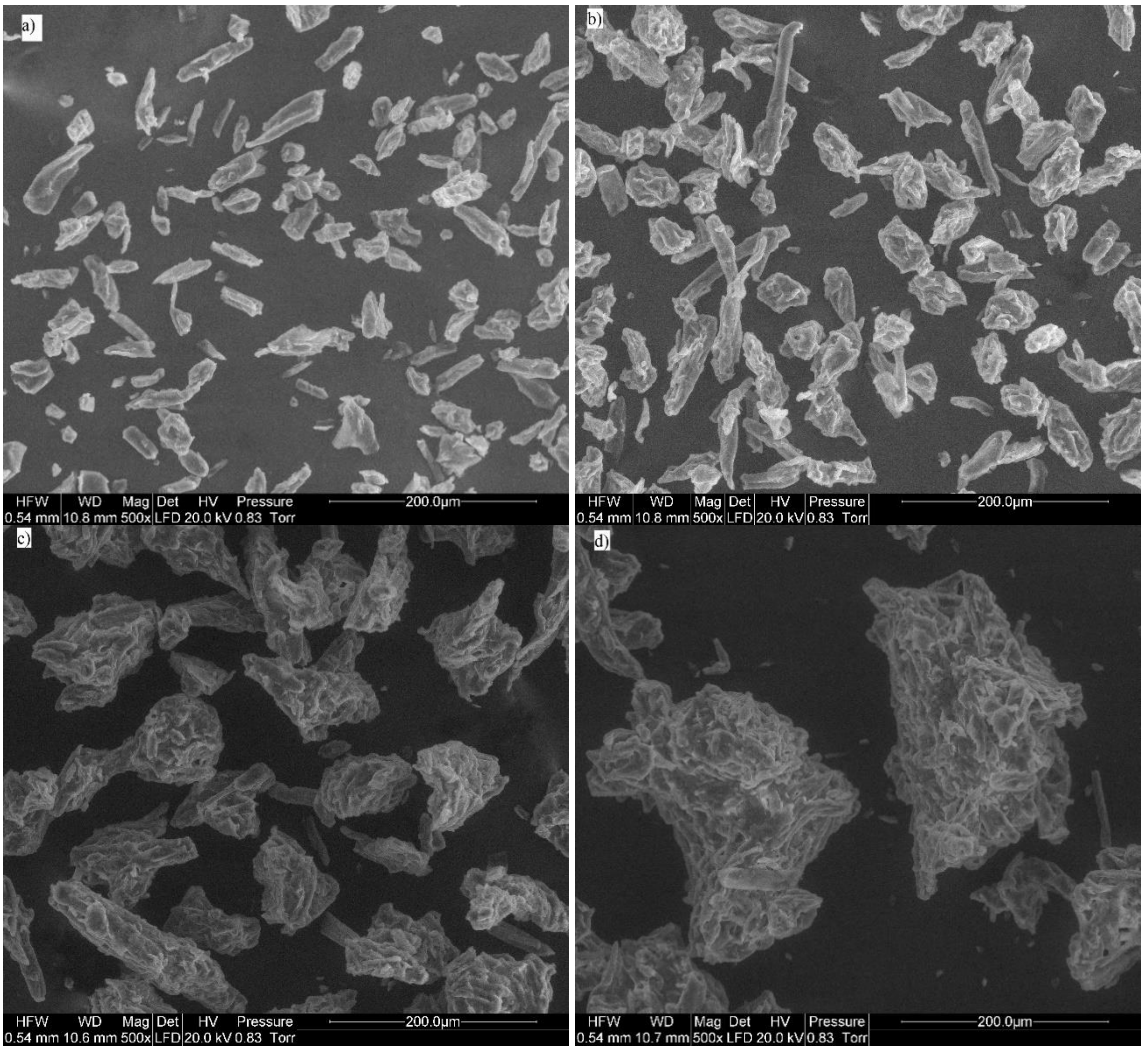

Rys. 3. Zdjęcia celulozy mikrokrystalicznej o wymiarach: a) 20–32 µm; b) 32–45 µm; c) 56–100 µm; d) 150–212 µm.

Tab. 1. Podstawowe właściwości frakcji celulozy mikrokrystalicznej. SD oznacza odchylenie standardowe

Frakcja [µm]	Średnia geometryczna cząstek [µm]	Zawartość wilgoci w.m.*		Gęstość właściwa		Stopień polimeryzacji	Krystaliczność
		Średnia n = 3 [%]	SD [%]	Średnia n = 3 [g·ml^{-3}]	SD [g·ml^{-3}]	Wartość n = 1 [–]	Wartość n = 1 [%]
20<32	25	5,20	0,28	1,597	0,001	328	56
32<45	38	4,89	0,16	1,600	0,001	336	58
45<56	*50*	*5,09*	*0,13*	*1,595*	*0,001*	*330*	*60*
56<100	75	4,97	0,32	1,589	0,005	333	58
100<150	122	4,90	0,35	1,581	0,009	335	59
150<212	178	5,05	0,08	1,603	0,001	333	57
212<300	252	4,95	0,29	1,593	0,006	333	57

* w.m. – względem wilgotnej stubstancji.

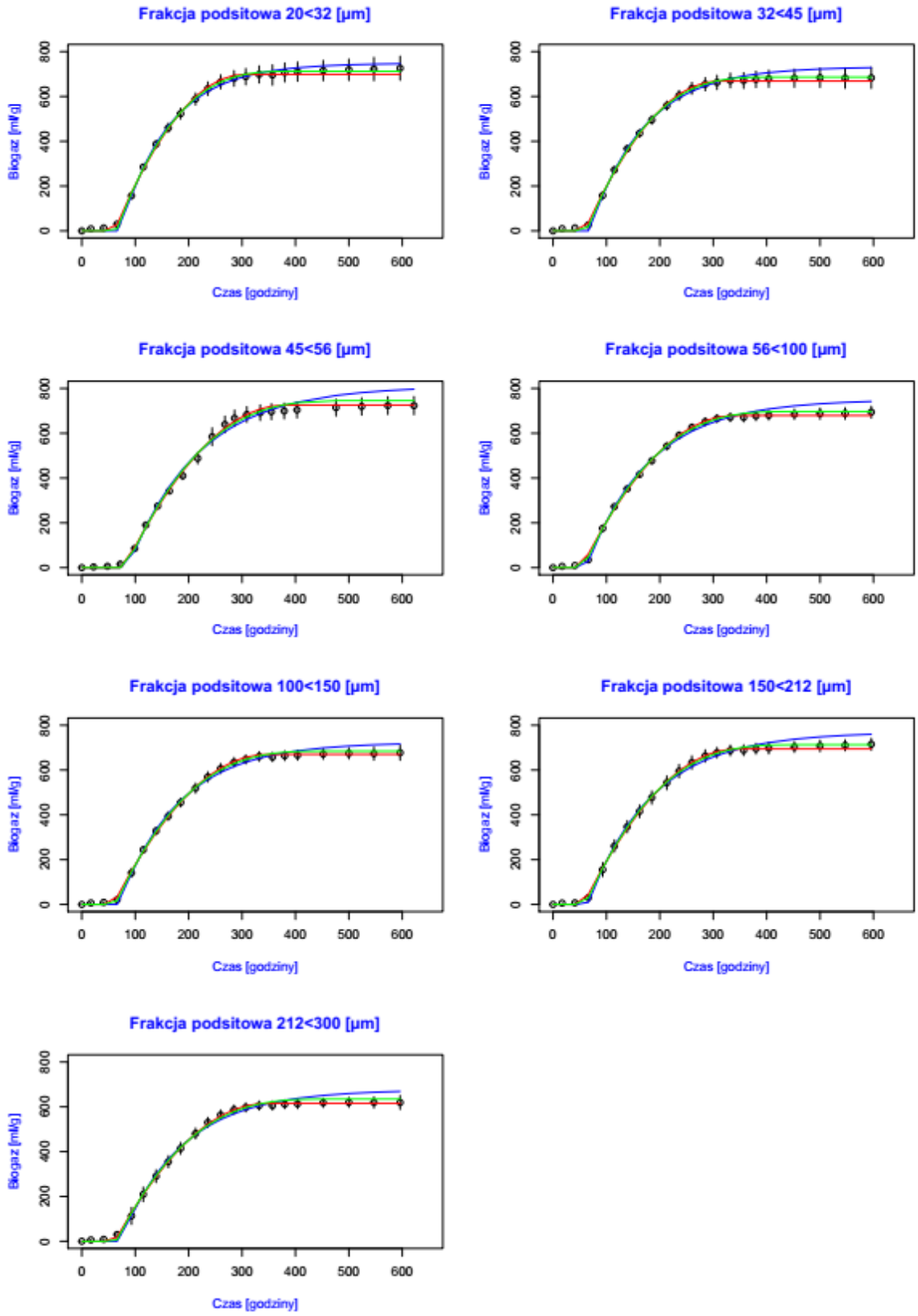

Rys. 4. Krzywe produkcji biogazu dla każdej z badanych próbek. Kółka oznaczają średnią z trzech prób pomiarowych, pionowe kreski oznaczają odchylenie standardowe. Niebieskie, czerwone i zielone linie oznaczają dopasowania odpowiednio dla modelu kinetyki rzędu I, modelu cząstek cylindrycznych oraz sferycznych

Wyniki porównania modeli przedstawia rys. 4. Nowo opracowane modele zaprezentowane w niniejszej pracy są bardziej adekwatne, w porównaniu do modelu kinetyki rzędu I, do opisu procesu fermentacji anaerobowej celulozy mikrokrystalicznej. Potwierdza to, że reakcja hydrolizy celulozy jest zależna od dostępnej powierzchni, co jest zgodne w poprzednimi badaniami dotyczącymi cellulosomów (Fierobe et al., 2002). W większości przypadków, w przeciwieństwie do modelu cząstki sferycznej oraz walcowej model kinetyki rzędu I zawyża uzysk biogazu. Szczegółowe dane dotyczące dopasowania modeli zestawiono w tab. 2. Nowe modele wykazują lepsze dopasowanie mierzone globalnym błędem względnym, które wynoszą 5,31% i 5,59%, odpowiednio dla modelu cząstek kulistych oraz sferycznych w porównaniu do 7,49% dla modelu kinetyki rzędu I. Największe różnice są widoczne dla końcowych wartości uzysku biogazu, dla których błąd względny nie przekracza 2,4% oraz 2,1%, odpowiednio dla modelu cząstek kulistych oraz sferycznych, podczas gdy dla modelu kinetyki rzędu I błąd ten sięga 11%.

Tab. 2. Porównanie dopasowania analizowanych modeli

Frakcja [μm]	Model kinetyki pierwszego rzędu		Model cząstek cylindrycznych		Model cząstek kulistych	
	Globalny błąd względny [%]	Błąd końcowy [%]	Globalny błąd względny [%]	Błąd końcowy [%]	Globalny błąd względny [%]	Błąd końcowy [%]
20<32	5,41	6,60	5,31	2,37	5,06	2,10
32<45	5,87	8,70	4,66	2,00	4,52	1,88
45<56	*7,49*	*11,09*	*5,05*	*1,53*	*5,59*	*1,84*
56<100	4,92	7,55	3,04	1,26	3,10	1,05
100<150	4,75	7,05	3,44	1,40	3,59	1,40
150<212	5,31	6,92	4,00	1,40	3,90	1,02
212<300	6,03	8,94	4,10	1,38	4,66	1,59

Krzywa modelu kinetyki rzędu pierwszego wykracza poza dopuszczalne granice wyznaczone przez odchylenie standardowe obliczone na podstawie ostatniej wartości pomiarowej. Warto zwrócić uwagę, że obserwacja ta nie dotyczy przypadku najmniejszej frakcji cząstek 20<32 μm. W tym przypadku wszystkie modele mieszczą się w granicach odchylenia standardowego z trzech prób. Wskazuje to, że im mniejsze cząstki, tym rola wymiaru cząstek zanika, ze względu na coraz lepsze wykorzystanie powierzchni, co zbliża właściwości cząstek celulozy do właściwości materiału rozpuszczalnego w wodzie. Na tej podstawie można stwierdzić, że zastosowanie nowych modeli może mieć istotne znaczenie dla opisu fermentacji lignocelulozy, ponieważ jej cząstki z reguły są większe niż badane w niniejszej publikacji.

Związek wymiaru cząstki celulozy z kinetyką procesu, którą opisują stałe kinetyczne modelu przedstawiono na rys. 5. Stała kinetyki wzrasta dla cząstek mniejszych niż 120 µm; wzrost szybko przyspiesza ze zmniejszaniem się wymiarów cząstek. Do opisu wspomnianej zależności zaproponowano następujący wzór empiryczny inspirowany równaniem Michaelisa-Menten:

$$k = 1 - \frac{k_{max} \cdot d}{K_s + d} \quad , \tag{16}$$

gdzie k oznacza zmierzona stałą kinetyki (h^{-1}), k_{max} oznacza maksymalną wartość stałej kinetyki (h^{-1}), K_s stałą połowy nasycenia (µm) i d średnią średnicę cząstek (µm).

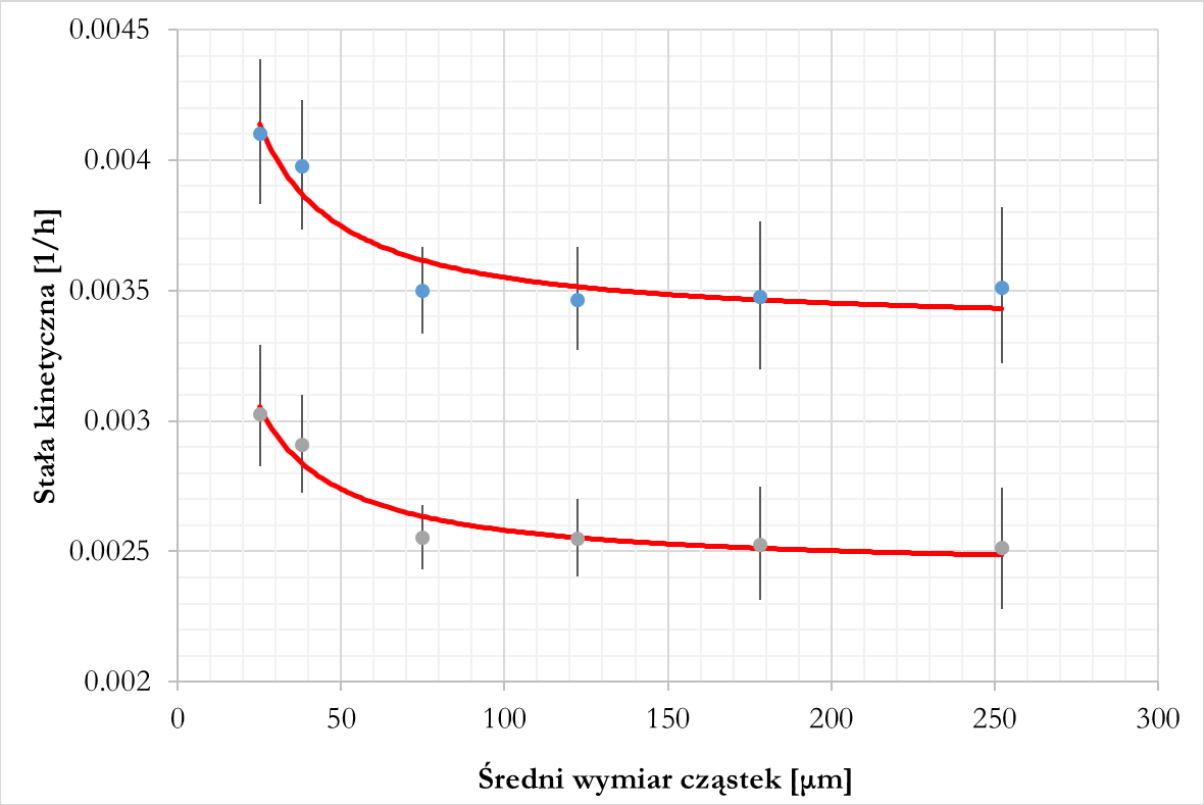

Rys. 5. Stałe k wyznaczone dla modelu cząstek cylindrycznych (krzywa górna) oraz sferycznych (krzywa dolna). Punkty oznaczają wyznaczone wartości, pionowe kreski oznaczają 95% przedział ufności. Czerwone linie oznaczają dopasowanie modelu.

Globalny błąd względny dopasowania wynosił 2,08% i 1,71%, odpowiednio dla modelu cząstek cylindrycznych i sferycznych. Interpretacja modelu jest następująca: jeśli średnica cząstki jest ≈0, to większość miejsc adsorpcji enzymów jest dostępna, więc proces może przebiegać szybko (duża wartość stałej k). Wraz ze zwiększaniem się średnicy, część powierzchni nie jest dostępna na początku procesu, a zostaje odsłonięta dopiero w trakcie jego trwania, dlatego proces przebiega wolniej (mała wartość stałej k). Przedstawione obserwacje,

które graficznie są zaprezentowane na rys. 5 są spójne z najnowszymi badaniami dotyczącymi celulosomów, według których celulosomy wykazują dużą aktywność dla małych cząstek celulozy (długość ≤ ~70 nm) (Eibinger et al., 2020).

Uzyskane wartości stałych kinetyki porównano z bezpośrednimi pomiarami powierzchni właściwej metodą BET (rys. 6), często stosowaną do opisu efektów obróbki wstępnej materiału (Gao et al., 2017; Mustafa et al., 2016). Szczegółowe dane pomiarowe zamieszczono w załączonej publikacji. Wartości pomiarowe wahały się w zakresie od 0,73 do 0.87 $m^2 \cdot g^{-1}$. Co zaskakujące, powierzchnia właściwa cząstek frakcji 20–32 µm (0,80 $m^2 \cdot g^{-1}$) była mniejsza niż powierzchnia właściwa cząstek 32–45 µm (0,87 $m^2 \cdot g^{-1}$). Można to przypisać strukturze cząstek, ponieważ cząstki 20–32 µm są w większości pojedynczymi cząstkami, podczas gdy cząstki frakcji 32–45 µm są aglomeratami mniejszych cząstek (rys. 3). Niektóre wyniki badań wskazują, że powierzchnia właściwa jest najważniejszym wskaźnikiem skuteczności hydrolizy (Lu et al., 2019). Wniosek ten oparto na próbkach celulozy zmielonej w młynie kulowym, w których powierzchnię właściwą zmieniono jednocześnie z innymi parametrami substratu, przede wszystkim ze stopniem krystaliczności.

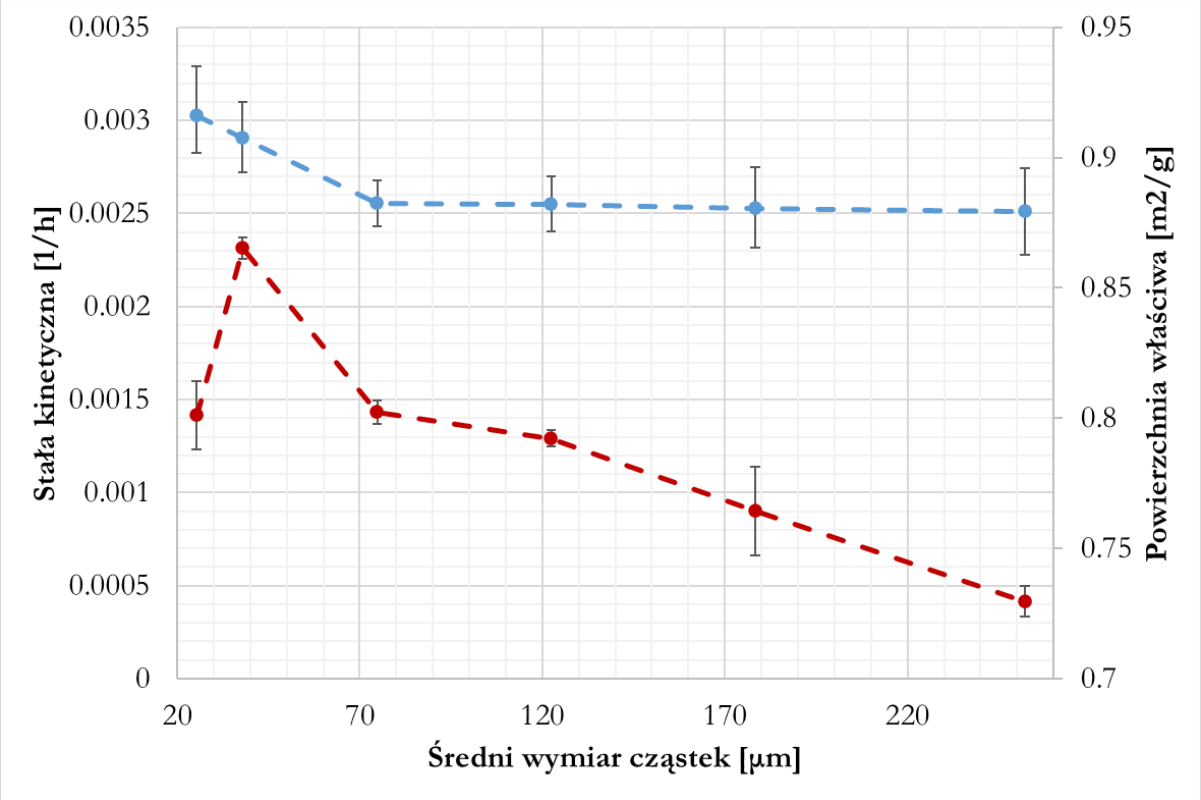

Rys. 6. Powierzchnia właściwa próbek porównana z stałymi k modelu cząstek sferycznych. Dla stałych k (łamana górna) pionowe linie oznaczają 95% przedział ufności, dla powierzchni właściwej (łamana dolna) pionowe linie oznaczają odchylenie standardowe.

W analizowanym badaniu powierzchnia nie opisuje dokładnie zmian kinetyki procesu. W szczególności cząstki 20–32 μm wykazują odwrotną tendencję, ponieważ powierzchnia cząstek zmniejsza się, podczas gdy stała *k* rośnie. Ostatnie badania pokazują, że enzymy przestrzennie zorganizowane w celulosomie mogą dostosowywać swój kształt do nanokryształów celulozy. Powierzchnię celulosomu oszacowano na 1500 nm^2 (Eibinger et al., 2020). Powierzchnia właściwa mierzona metodą BET uwzględnia powierzchnię mezoporów, które definiuje się jako pory o szerokościach z zakresu 2–50 nm (Thommes et al., 2015). Pory te mogą być mniejsze niż proponowana powierzchnia celulosomu, stąd na podstawie przedstawionych danych można postawić hipotezę, że celulosomy nie wykorzystują powierzchni mezoporów.

Koleją metodą używaną do oszacowania dostępnej powierzchni adsorpcji jest metoda pozwalająca na wyznaczenie wskaźnika *WRV*. Typowo, większa wartość wskaźnika *WRV* wiąże się z lepszą ekspozycją powierzchni i większą porowatością (Zhang et al., 2015), jednak w przypadku MCC kluczowa jest hydrofobowość powierzchni (Lu et al., 2019), stąd jeśli krystaliczność pozostaje stała, mniejsze wartości wskaźnika *WRV* należy interpretować jako korzystne. Na rys. 7 przedstawiono porównanie wartości wskaźnika *WRV* ze stałymi *k* modelu cząstek kulistych. Wskaźnik *WRV* zwiększa się wraz z wymiarem cząstek i są to zmienne skorelowane na poziomie r = 0,822. Jednocześnie *WRV* nie odzwierciedla zmian stałej *k*. Wyniki *WRV* nie mogą być zatem interpretowane jako samodzielny wskaźnik dostępności powierzchni. Należy zaznaczyć, że w niniejszym badaniu wyniki *WRV* zmieniają się w wąskim zakresie (2,52–3,39 g $H_2O \cdot g^{-1}$).

Przedstawiona wyżej dyskusja potwierdza, że powierzchnia cząstek jest kluczowa dla procesu hydrolizy celulozy. Wykorzystana w badaniach celuloza stanowiła jednak substrat modelowy. W warunkach przemysłowych procesowi fermentacji poddawana jest lignoceluloza. Zasadne jest zatem zbadanie potencjalnego wpływu lignin na kinetykę procesu. Należy jednak zaznaczyć, że w wyniku obróbki mechanicznej całość lignin pozostaje w formie stałej. Warto wziąć pod uwagę potencjalny wpływ lignin w formie stałej nie tylko na fazę hydrolizy, ale i metanogenezy. W tym celu przeprowadzono badanie z wykorzystaniem tzw. inokulum niezbalansowanego. Jest to pojęcie wprowadzone na potrzeby tej pracy naukowej. Krzywą produkcji metanu z MCC z wykorzystaniem inokulum niezbalansowanego zaprezentowano na rys. 8.

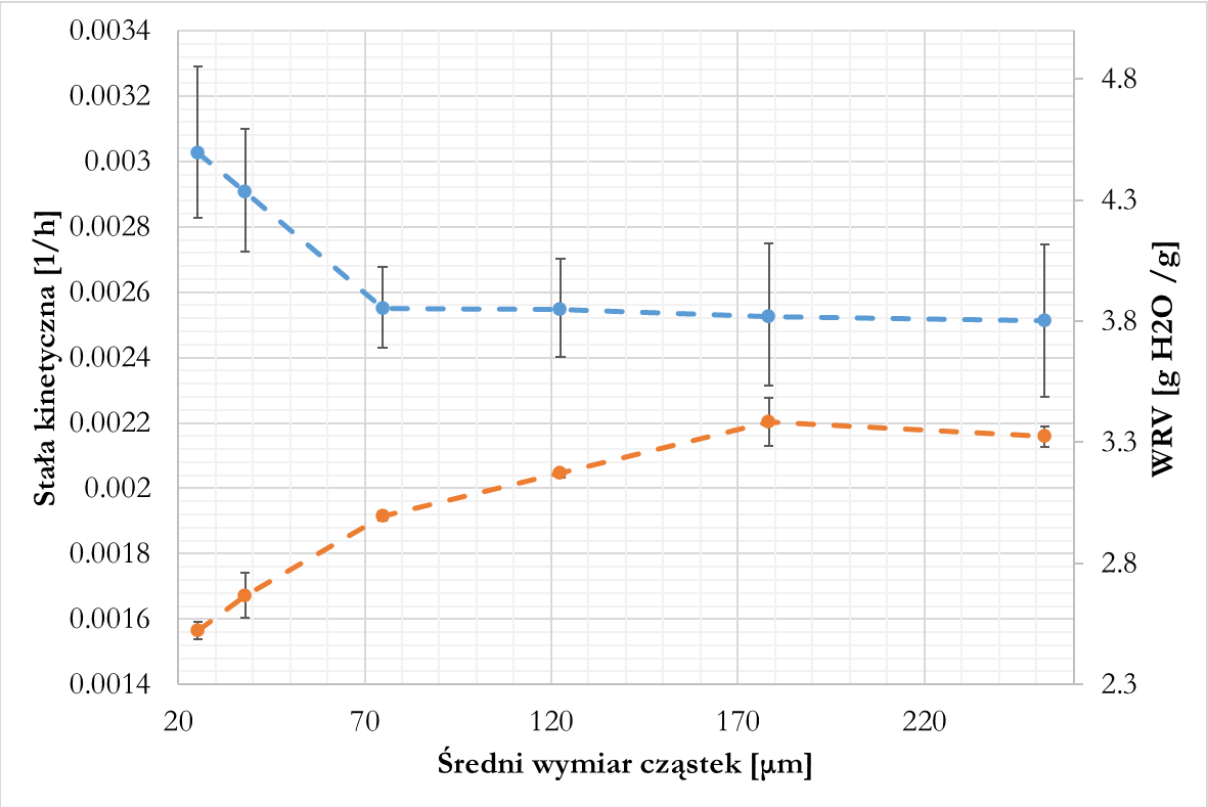

Rys. 7. Wskaźnik WRV porównany ze stałymi k modelu cząstek sferycznych. Dla stałych k (łamana górna) pionowe linie oznaczają 95% przedział ufności, dla WRV (łamana dolna) pionowe linie oznaczają odchylenie standardowe.

W porównaniu do krzywych o prawidłowym przebiegu (rys. 4) można zaobserwować zaburzenia polegające na spowolnieniu procesu wynikające z akumulacji lotnych kwasów tłuszczowych (LKT). Należy zatem stwierdzić, że fazą limitującą proces stała się metanogeneza, a nie hydroliza. Celem dokładnego zbadania wpływu lignin w formie stałej na to zjawisko wykonano eksperyment, w którym poddano fermentacji MCC z dodatkiem lignin.

W tym eksperymencie nie zaobserwowano produkcji gazu z próby zerowej (bez dodatku MCC ani lignin) oraz z próby, w której wykorzystane były wyłącznie ligniny bez dodatku MCC. Wskazuje to na brak rozpuszczalnych związków, pochodnych lignin w reaktorach, ponieważ niektóre związki, takie jak aldehyd syryngowy, w przeciwieństwie do lignin stałych, mogą być wykorzystywane przez mikroorganizmy jako substraty (Barakat et al., 2012). Produkcję gazu zaobserwowano we wszystkich reaktorach, do których dodano MCC. Analiza wariancji nie dała podstaw do stwierdzenia istotnych różnic w uzysku gazu, między próbkami z MCC (krytyczny poziom istotności $p = 0{,}313$). Co zaskakujące obserwacja ta nie jest zgodna z wynikami zawartymi w literaturze (Li et al., 2018). Wykorzystano pełen, teoretyczny potencjał produkcji metanu z MCC ($355{,}7 \pm 13{,}4$ ml), co wskazuje, że nie wystąpił mechanizm

inhibicji kompetycyjnej. Potwierdza to hipotezę, że ligniny zawarte w lignocelulozie pełnią funkcję bariery fizycznej, a nie inhibitora kompetycyjnego (Djajadi et al., 2018).

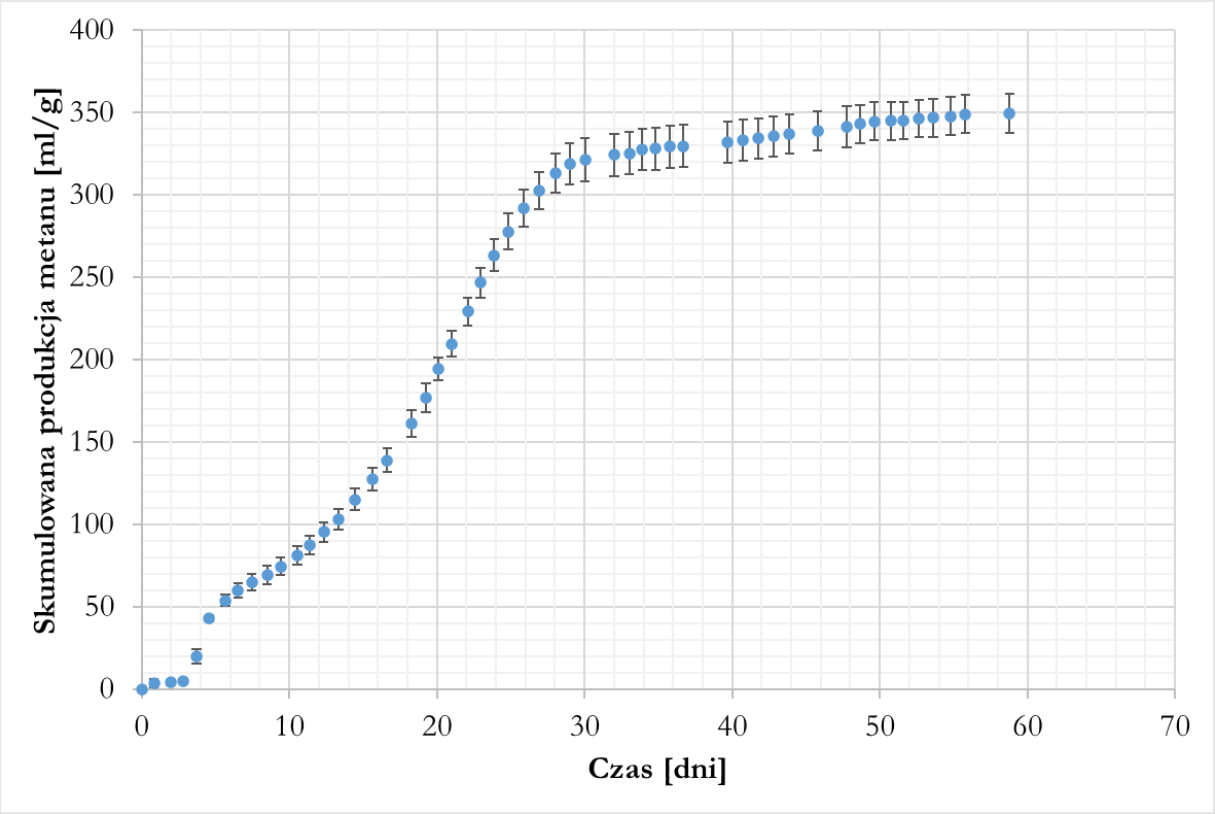

Rys. 8. Krzywa produkcji biometanu z materiału referencyjnego przez kultury niezbalansowane. Pionowe słupki oznaczają odchylenie standardowe

Uzyskane krzywe produkcji metanu modelowano z wykorzystaniem krzywych „smoothing spline", celem odfiltrowania szumów informacyjnych powstających w trakcie pomiarów oraz uzyskania możliwości wyznaczenia pochodnej modelowanego przebiegu. Wyniki aproksymacji przebiegu, który przedstawia rys. 8 pokazuje rys. 9. Wyznaczono również pochodną modelu z dokładnością do jednej godziny. Oznacza to, że pochodna odzwierciedla godzinową produkcję metanu. Wyznaczono charakterystyczne punkty procesu, które oznaczono strzałkami. Analogicznie postąpiono z krzywymi uzyskanymi w procesie fermentacji celulozy z dodatkiem lignin. Patrząc od lewej strony wykresu strzałki oznaczają: początek spadku wydajności procesu spowodowany akumulacją LKT (1), druga strzałka (2) oznacza maksymalną inhibicję, a trzecia (3) koniec inhibicji i powrót do niezaburzonej kinetyki procesu. Punkty te pozwalają na wyznaczenie etapów procesu (tab. 3). Szczegółowe dane dotyczące wpływu lignin na wydłużenie czasu trwania poszczególnych etapów zawarto w tab. 4.

Tab. 3. Etapy inhibitowanego procesu fermentacji oraz zakres ich występowania

Etap procesu	Nazwa	Czas wystąpienia	Opis
I	Etap początkowy	Od początku eksperymentu do punktu 1	Po początkowym opóźnieniu procesu następuje wzrost produkcji metanu. LKT nie wywołują jeszcze negatywnych skutków
II	Etap narastającej inhibicji	Od punktu 1 do punktu 2	Metanogeneza zwalnia w wyniku akumulacji LKT. Na koniec etapu osiąga maksymalny poziom
III	Etap malejącej inhibicji	Od punktu 2 do punktu 3	Maleje stężenie LKT, negatywne skutki akumulacji powoli ustępują
IV	Etap końcowy	Od punktu 3 do końca eksperymentu	Proces spowalnia w wyniku ubytku substratu. Inhibicja LKT nie występuje

Tab. 4. Inhibicja poszczególnych etapów procesu w zależności od ilości dodanych lignin

Dodatek lignin [g]	Inhibicja etapu I [%]	Inhibicja etapu II [%]	Inhibicja etapu III [%]
0	0,00	0,00	0,00
3	-8,79	11,32	-26,11
7	9,17	22,95	-59,86
10	21,43	25,98	-17,62
13	30,28	33,33	49,56
17	35,29	65,06	39,95
20	47,34	75,26	39,14

Na rys. 10 przedstawiono wpływ dodatku lignin na czas trwania pierwszego etapu procesu oraz dopasowaną linię regresji, której wynikowe parametry zestawiono w tab. 5. Wykazano statystycznie istotną liniową zależność między stopniem inhibicji a dodatkiem lignin ($p = 0{,}0004$). Wyniki wskazują na dodatni wskaźnik inhibicji; oznacza to spowolnienie procesu hydrolizy MCC w wyniku dodania lignin kraft, co jest całkowicie zgodne z dotychczasową wiedzą zawartą w literaturze (Li et al., 2018). W przypadku dodatku 3 g lignin inhibicja nie wystąpiła; może to oznaczać, że istnieje pewna wartość progowa, od której zaczynają występować negatywne skutki dodatku lignin.

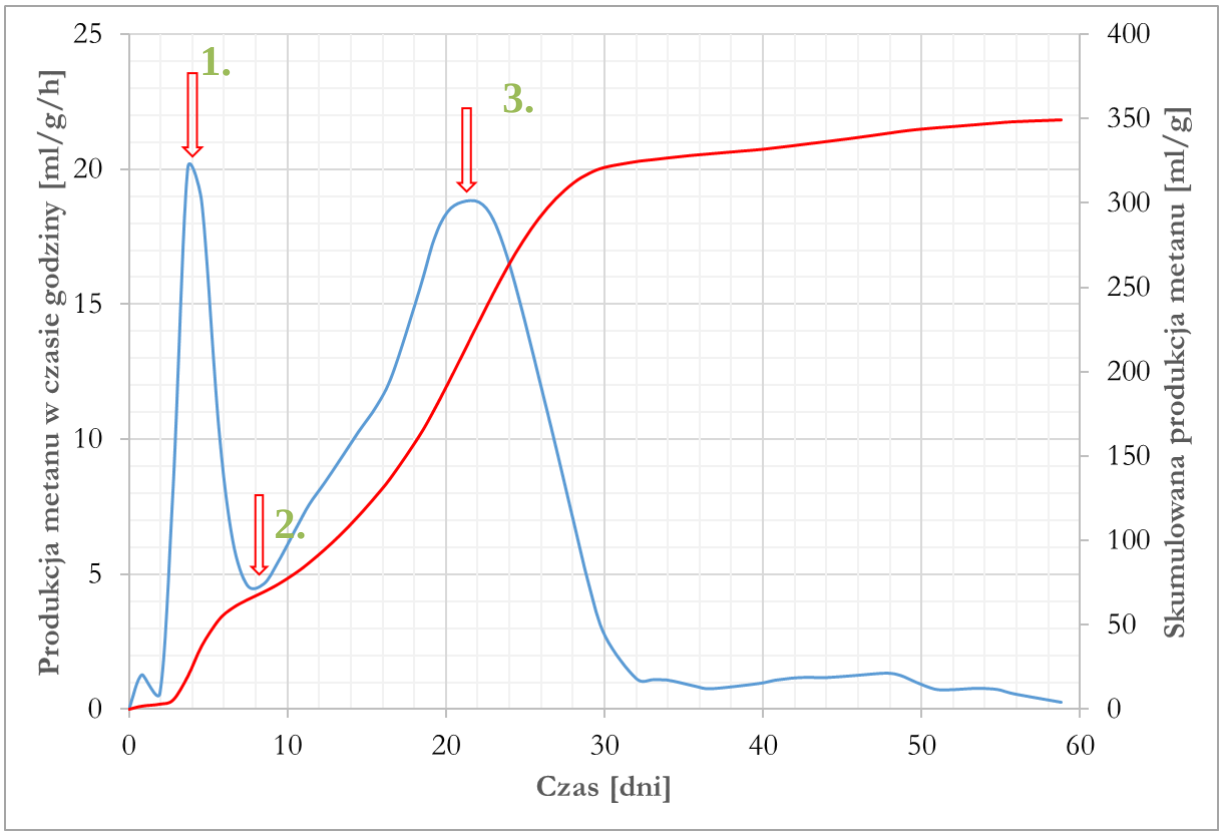

Rys. 9. Krzywa produkcji metanu (kolor czerwony) z celulozy mikrokrystalicznej aproksymowana modelem „smoothing spline". Niebieska krzywa oznacza pierwszą pochodną modelu, która odpowiada godzinowej produkcji metanu. Strzałkami 1, 2 oraz 3 (patrząc od lewej) zaznaczono charakterystyczne punkty procesu.

Tab. 5. Dopasowanie modelu liniowego odzwierciedlającego wpływ lignin na czas trwania etapów procesu

Etap	Stała [%]		Współczynnik kierunkowy [%·g^{-1}]		Krytyczny poziom istotności p	R^2
	Wartość	Błąd standardowy	Wartość	Błąd standardowy		
I	-7,50	3,95	2,68	0,33	0,0004	0,920
II	-3,29	4,93	3,67	0,41	0,0003	0,930
III	-33,83	22,78	3,74	1,89	0,1048	0,327

Rys. 11 przedstawia wpływ dodatku lignin na czas trwania drugiego etapu procesu. Zaobserwowano statystycznie istotną liniową zależność (p = 0,003). Dodatek lignin spowodował wyraźne wydłużenie czasu trwania tego etapu. Biorąc pod uwagę fakt, że w wyniku dodatku lignin zmniejszyła się kinetyka reakcji hydrolizy i związana z tym produkcja LKT, to można stwierdzić, że dodatek lignin spowodował również zmniejszenie kinetyki metanogenezy. Gdyby ligniny nie miałby wpływu na fazę produkcji metanu, relacja przedstawiona na wykresie powinna być odwrotna. Jest to bezpośredni dowód uzasadniający słuszności postawionej hipotezy badawczej. Biorąc pod uwagę, że istnieje techniczna możliwość prowadzenia procesu fermentacji anaerobowej z rozdziałem faz hydrolizy

i metanogenezy, zasadne jest rozważenie wykonania separacji frakcji stałej hydrolizatu lignocelulozowego przed wprowadzeniem go do reaktora metanogenezy.

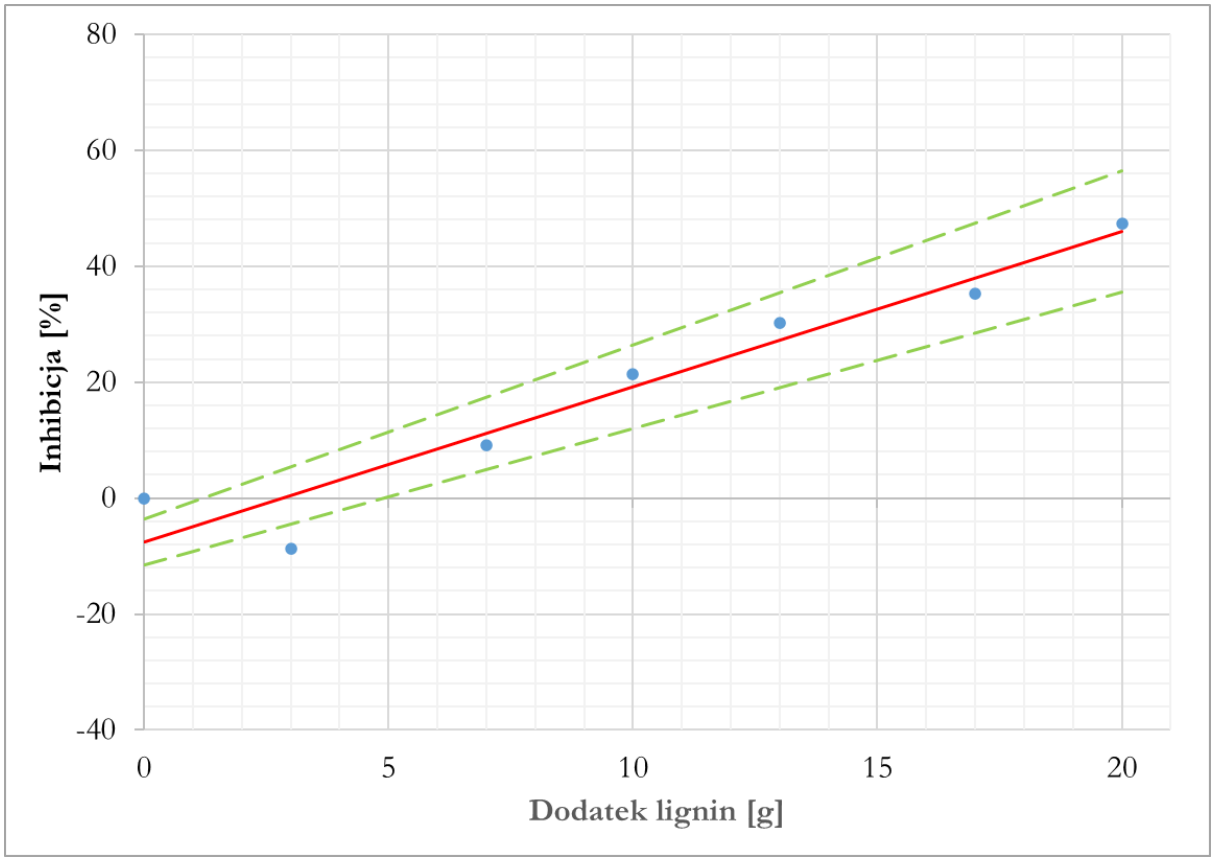

Rys. 10. Efekt dodatku lignin na czas zapoczątkowania inhibicji wywołanej LKT

Rys. 12 przedstawia wpływ lignin na etap wychodzenia z inhibicji. Wpływ ten nie jest jednoznaczny. W tym przypadku dodatek lignin w ilości 13 g, 17 g oraz 20 g spowodował dodatnią inhibicję, podczas gdy dodatek w ilości 3 g, 7 g oraz 10 g spowodował ujemną inhibicją (stymulację). Pozytywne skutki dodatku niewielkich ilości lignin można tłumaczyć możliwością neutralizacji inhibitora i stymulacją wzrostu metanogenów, dzięki obecności większej ilości cząstek stałych w reaktorach. Wcześniejsze badania raportowały wpływ lignin na stymulacje wzrostu (Pilarska et al., 2019, 2018). Stwierdzono jednak, że większe dawki ligniny tłumią jej pozytywne skutki. Stwierdzenie istnienia wspomnianego efektu ma charakter hipotetyczny, gdyż niniejsze badania nie dostarczyły na to dowodów.

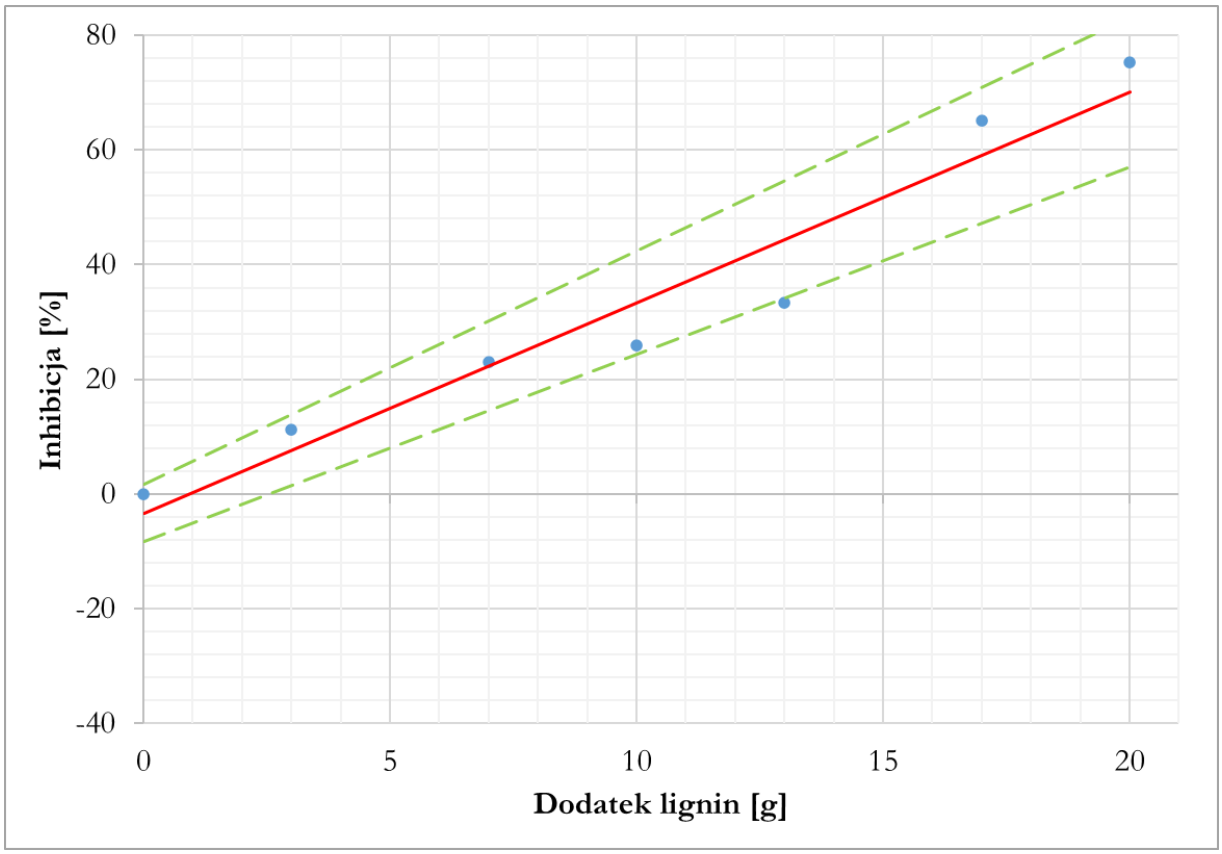

Rys. 11. Efekt dodatku lignin na czas osiągnięcia maksymalnej inhibicji wywołanej LKT

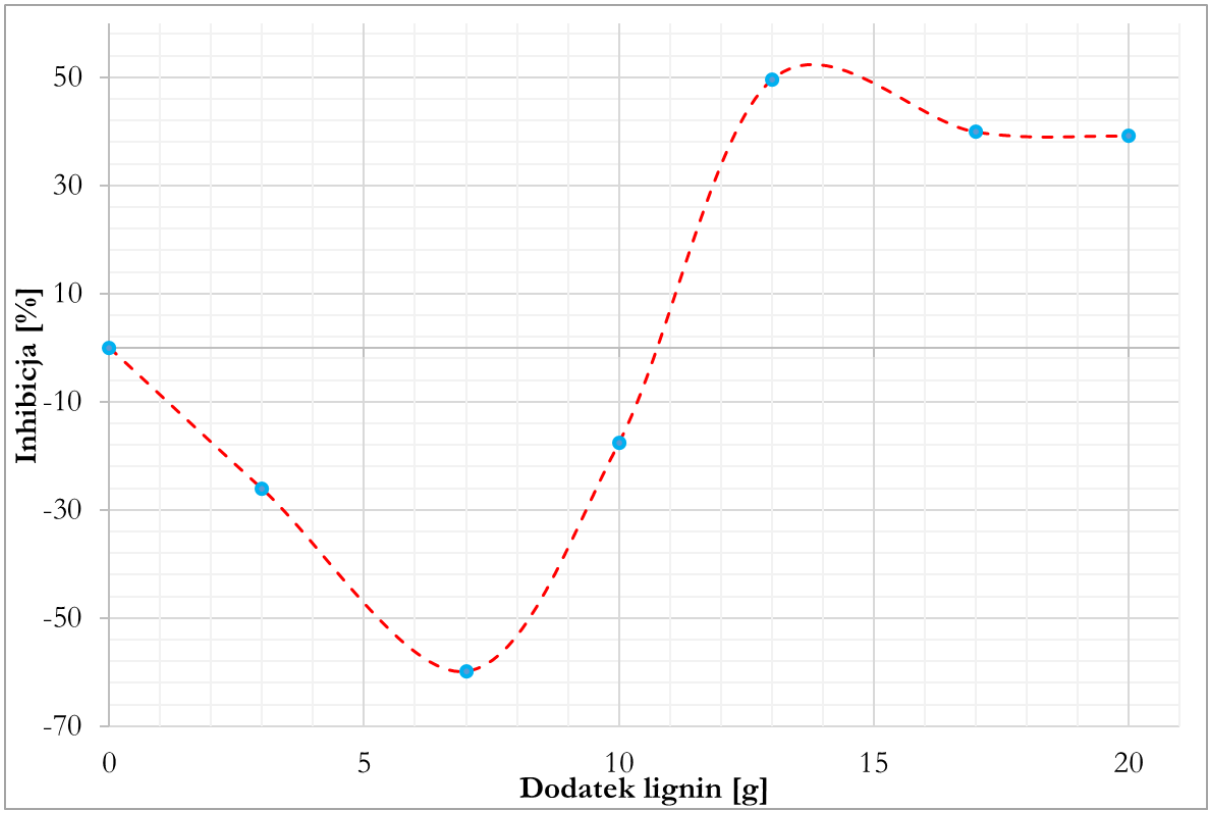

Rys. 12. Efekt dodatku lignin na trwanie etapu wychodzenia z inhibicji wywołanej LKT

6. Wnioski

Wnioski o charakterze naukowym

- Modele uwzględniające ubytek powierzchni materiału hydrolizowanego w procesie fermentacji anaerobowej lepiej opisują badane zjawisko od modelu kinetyki rzędu pierwszego.

- Nierozpuszczalne ligniny są inhibitorem zarówno hydrolizy, jak i metanogenezy. Negatywny wpływ nierozpuszczalnych lignin na metanogenezę ujawnia się dla kultur niezbalansowanych

Wniosek o charakterze utylitarnym

- W przypadku procesu prowadzonego z rozdziałem faz należy rozważyć separację frakcji przed podaniem materiału do reaktora fazy metanogenezy.

7. Literatura

Adams, J.J., Currie, M.A., Ali, S., Bayer, E.A., Jia, Z., Smith, S.P., 2010. Insights into higher-order organization of the cellulosome revealed by a dissect-and-build approach: Crystal structure of interacting Clostridium thermocellum multimodular components. J. Mol. Biol. 396, 833–839. https://doi.org/10.1016/j.jmb.2010.01.015

Atelge, M.R., Atabani, A.E., Banu, J.R., Krisa, D., Kaya, M., Eskicioglu, C., Kumar, G., Lee, C., Yildiz, Y., Unalan, S., Mohanasundaram, R., Duman, F., 2020. A critical review of pretreatment technologies to enhance anaerobic digestion and energy recovery. Fuel 270, 117494. https://doi.org/10.1016/j.fuel.2020.117494

Barakat, A., Monlau, F., Steyer, J.P., Carrere, H., 2012. Effect of lignin-derived and furan compounds found in lignocellulosic hydrolysates on biomethane production. Bioresour. Technol. 104, 90–99. https://doi.org/10.1016/j.biortech.2011.10.060

Bayer, E.A., Lamed, R., 1986. Ultrastructure of the cell surface cellulosome of clostridium thermocellum and its interaction with cellulose. J. Bacteriol. 167, 828–836. https://doi.org/10.1128/jb.167.3.828-836.1986

Bochmann, G., Montgomery, L.F.R., 2013. Storage and pre-treatment of substrates for biogas production. Biogas Handb. Sci. Prod. Appl. 85–103. https://doi.org/10.1533/9780857097415.1.85

da Rocha, D., Paetzold, E., Kanswohl, N., 2013. The shrinking core model applied on anaerobic digestion. Chem. Eng. Process. Process Intensif. 70, 294–300. https://doi.org/10.1016/j.cep.2013.05.003

De Sanctis, M., Chimienti, S., Pastore, C., Piergrossi, V., Di Iaconi, C., 2019. Energy efficiency improvement of thermal hydrolysis and anaerobic digestion of Posidonia oceanica residues. Appl. Energy 252, 113457. https://doi.org/10.1016/j.apenergy.2019.113457

Djajadi, D.T., Jensen, M.M., Oliveira, M., Jensen, A., Thygesen, L.G., Pinelo, M., Glasius, M., Jørgensen, H., Meyer, A.S., 2018. Lignin from hydrothermally pretreated grass biomass retards enzymatic cellulose degradation by acting as a physical barrier rather than by inducing nonproductive adsorption of enzymes. Biotechnol. Biofuels 11, 1–13. https://doi.org/10.1186/s13068-018-1085-0

Eibinger, M., Ganner, T., Plank, H., Nidetzky, B., 2020. A Biological Nanomachine at Work: Watching the Cellulosome Degrade Crystalline Cellulose. ACS Cent. Sci. 0–7. https://doi.org/10.1021/acscentsci.0c00050

Evans, R., Wallis, A.F.A., 1989. Cellulose molecular weights determined by viscometry. J. Appl. Polym. Sci. 37, 2331–2340. https://doi.org/10.1002/app.1989.070370822

Fierobe, H.-P., Bayer, E.A., Tardif, C., Czjzek, M., Mechaly, A., Bélaïch, A., Lamed, R., Shoham, Y., Bélaïch, J.-P., 2002. Degradation of Cellulose Substrates by Cellulosome Chimeras. J. Biol. Chem. 277, 49621–49630. https://doi.org/10.1074/jbc.M207672200

Gao, C., Xiao, W., Ji, G., Zhang, Y., Cao, Y., Han, L., 2017. Regularity and mechanism of wheat straw properties change in ball milling process at cellular scale. Bioresour. Technol. 241, 214–219. https://doi.org/10.1016/j.biortech.2017.04.115

Gilvari, H., de Jong, W., Schott, D.L., 2019. Quality parameters relevant for densification of bio-materials: Measuring methods and affecting factors - A review. Biomass and Bioenergy 120, 117–134. https://doi.org/10.1016/j.biombioe.2018.11.013

Hindeleh, A.M., Johnson, D.J., 1971. The resolution of multipeak data in fibre science. J. Phys. D. Appl. Phys. 4, 259–263. https://doi.org/10.1088/0022-3727/4/2/311

Karimi, K., Taherzadeh, M.J., 2016. A critical review on analysis in pretreatment of lignocelluloses: Degree of polymerization, adsorption/desorption, and accessibility. Bioresour. Technol. 203, 348–356. https://doi.org/10.1016/j.biortech.2015.12.035

Koyama, M., Yamamoto, S., Ishikawa, K., Ban, S., Toda, T., 2017. Inhibition of anaerobic digestion by dissolved lignin derived from alkaline pre-treatment of an aquatic macrophyte. Chem. Eng. J. 311, 55–62. https://doi.org/10.1016/j.cej.2016.11.076

Kratky, L., Jirout, T., 2011. Biomass Size Reduction Machines for Enhancing Biogas Production. Chem. Eng. Technol. 34, 391–399. https://doi.org/10.1002/ceat.201000357

Kumar, R., Wyman, C.E., 2009. Access of cellulase to cellulose and lignin for poplar solids produced by leading pretreatment technologies. Biotechnol. Prog. 25, 807–819. https://doi.org/10.1002/btpr.153

Li, W., Khalid, H., Zhu, Z., Zhang, R., Liu, G., Chen, C., Thorin, E., 2018. Methane production through anaerobic digestion: Participation and digestion characteristics of cellulose, hemicellulose and lignin. Appl. Energy 226, 1219–1228. https://doi.org/10.1016/j.apenergy.2018.05.055

Li, Y., Chen, Y., Wu, J., 2019. Enhancement of methane production in anaerobic digestion process: A review. Appl. Energy 240, 120–137. https://doi.org/10.1016/j.apenergy.2019.01.243

Li, Y., Sun, Z., Ge, X., Zhang, J., 2016. Effects of lignin and surfactant on adsorption and hydrolysis of cellulases on cellulose. Biotechnol. Biofuels 9, 1–9. https://doi.org/10.1186/s13068-016-0434-0

Lorenci Woiciechowski, A., Dalmas Neto, C.J., Porto de Souza Vandenberghe, L., de Carvalho Neto, D.P., Novak Sydney, A.C., Letti, L.A.J., Karp, S.G., Zevallos Torres, L.A., Soccol, C.R., 2020. Lignocellulosic biomass: Acid and alkaline pretreatments and their effects on biomass recalcitrance – Conventional processing and recent advances. Bioresour. Technol. 304, 122848. https://doi.org/10.1016/j.biortech.2020.122848

Lu, M., Li, J., Han, L., Xiao, W., 2019. An aggregated understanding of cellulase adsorption and hydrolysis for ball-milled cellulose. Bioresour. Technol. 273, 1–7. https://doi.org/10.1016/j.biortech.2018.10.037

Ma, J., Frear, C., Wang, Z.W., Yu, L., Zhao, Q., Li, X., Chen, S., 2013. A simple methodology for rate-limiting step determination for anaerobic digestion of complex substrates and effect of microbial community ratio. Bioresour. Technol. 134, 391–395. https://doi.org/10.1016/j.biortech.2013.02.014

Manyi-Loh, C.E., Mamphweli, S.N., Meyer, E.L., Okoh, A.I., Makaka, G., Simon, M., 2013. Microbial anaerobic digestion (bio-digesters) as an approach to the decontamination of animal wastes in pollution control and the generation of renewable energy. Int. J. Environ. Res. Public Health 10, 4390–4417. https://doi.org/10.3390/ijerph10094390

Monschein, M., Reisinger, C., Nidetzky, B., 2013. Enzymatic hydrolysis of microcrystalline cellulose and pretreated wheat straw: A detailed comparison using convenient kinetic analysis. Bioresour. Technol. 128, 679–687. https://doi.org/10.1016/j.biortech.2012.10.129

Mustafa, A.M., Poulsen, T.G., Sheng, K., 2016. Fungal pretreatment of rice straw with Pleurotus ostreatus and Trichoderma reesei to enhance methane production under solid-state anaerobic digestion. Appl. Energy 180, 661–671. https://doi.org/10.1016/j.apenergy.2016.07.135

Nguyen, D., Wu, Z., Shrestha, S., Lee, P.H., Raskin, L., Khanal, S.K., 2019. Intermittent micro-aeration: New strategy to control volatile fatty acid accumulation in high organic loading anaerobic digestion. Water Res. 166, 115080. https://doi.org/10.1016/j.watres.2019.115080

Park, S., Baker, J.O., Himmel, M.E., Parilla, P.A., Johnson, D.K., 2010. Cellulose crystallinity index: Measurement techniques and their impact on interpreting cellulase performance. Biotechnol. Biofuels 3, 1–10. https://doi.org/10.1186/1754-6834-3-10

Pilarska, A.A., Wolna-Maruwka, A., Pilarski, K., 2018. Kraft lignin grafted with polyvinylpyrrolidone as a novel microbial carrier in biogas production. Energies 11. https://doi.org/10.3390/en11123246

Pilarska, A.A., Wolna-Maruwka, A., Pilarski, K., Janczak, D., Przybył, K., Gawrysiak-Witulska, M., 2019. The use of lignin as a microbial carrier in the co-digestion of cheese and wafer waste. Polymers (Basel). 11. https://doi.org/10.3390/polym11122073

Ran, G., Li, D., Zheng, T., Liu, X., Chen, L., Cao, Q., Yan, Z., 2018. Hydrothermal pretreatment on the anaerobic digestion of washed vinegar residue. Bioresour. Technol. 248, 265–271. https://doi.org/10.1016/j.biortech.2017.06.068

Sakimoto, K., Kanna, M., Matsumura, Y., 2017. Kinetic model of cellulose degradation using simultaneous saccharification and fermentation. Biomass and Bioenergy 99, 116–121. https://doi.org/10.1016/j.biombioe.2017.02.016

Solé-Bundó, M., Eskicioglu, C., Garfí, M., Carrère, H., Ferrer, I., 2017. Anaerobic co-digestion of microalgal biomass and wheat straw with and without thermo-alkaline pretreatment. Bioresour. Technol. 237, 89–98. https://doi.org/10.1016/j.biortech.2017.03.151

Sołowski, G., Konkol, I., Cenian, A., 2020. Production of hydrogen and methane from lignocellulose waste by fermentation. A review of chemical pretreatment for enhancing the efficiency of the digestion process. J. Clean. Prod. 267. https://doi.org/10.1016/j.jclepro.2020.121721

Thommes, M., Kaneko, K., Neimark, A. V., Olivier, J.P., Rodriguez-Reinoso, F., Rouquerol, J., Sing, K.S.W., 2015. Physisorption of gases, with special reference to the evaluation of surface area and pore size distribution (IUPAC Technical Report). Pure Appl. Chem. 87, 1051–1069. https://doi.org/10.1515/pac-2014-1117

Vavilin, V.A., Lokshina, L.Y., Jokela, J.P.Y., Rintala, J.A., 2004. Modeling solid waste decomposition. Bioresour. Technol. 94, 69–81. https://doi.org/10.1016/j.biortech.2003.10.034

Vavilin, V.A., Rytov, S. V., Lokshina, L.Y., 1996. A description of hydrolysis kinetics in anaerobic degradation of particulate organic matter. Bioresour. Technol. 56, 229–237. https://doi.org/10.1016/0960-8524(96)00034-X

Venturin, B., Frumi Camargo, A., Scapini, T., Mulinari, J., Bonatto, C., Bazoti, S., Pereira Siqueira, D., Maria Colla, L., Alves, S.L., Paulo Bender, J., Luís Radis Steinmetz, R., Kunz, A., Fongaro, G., Treichel, H., 2018. Effect of pretreatments on corn stalk chemical properties for biogas production purposes. Bioresour. Technol. 266, 116–124. https://doi.org/10.1016/j.biortech.2018.06.069

Verein Deutscher Ingenieure, 2014. VDI 4630 - Gärsubstrate.

Wintsche, B., Jehmlich, N., Popp, D., Harms, H., Kleinsteuber, S., 2018. Metabolic adaptation of methanogens in anaerobic digesters upon trace element limitation. Front. Microbiol. 9,

1–10. https://doi.org/10.3389/fmicb.2018.00405

Xiang, Y., Gubian, S., Suomela, B., Hoeng, J., 2013. Generalized simulated annealing for global optimization: the GenSA Package. R J. 5, 13–28. https://doi.org/10.1007/s10792-010-9404-x

Xin, L., Guo, Z., Xiao, X., Xu, W., Geng, R., Wang, W., 2018. Feasibility of anaerobic digestion for contaminated rice straw inoculated with waste activated sludge. Bioresour. Technol. 266, 45–50. https://doi.org/10.1016/j.biortech.2018.06.048

Yu, L., Chen, Z.X., Tong, X., Li, K., Li, W.W., 2012. Anaerobic degradation of microcrystalline cellulose: Kinetics and micro-scale structure evolution. Chemosphere 86, 348–353. https://doi.org/10.1016/j.chemosphere.2011.09.049

Yuan, X., Wen, B., Ma, X., Zhu, W., Wang, X., Chen, S., Cui, Z., 2014. Enhancing the anaerobic digestion of lignocellulose of municipal solid waste using a microbial pretreatment method. Bioresour. Technol. 154, 1–9. https://doi.org/10.1016/j.biortech.2013.11.090

Zhang, Y., Chen, X., Gu, Y., Zhou, X., 2015. A physicochemical method for increasing methane production from rice straw: Extrusion combined with alkali pretreatment. Appl. Energy 160, 39–48. https://doi.org/10.1016/j.apenergy.2015.09.011

8. Załączniki

Załącznik nr 1:

Publikacja nr 1: Piątek M., Lisowski A., Dąbrowska M., 2021. Surface-Related Kinetic Models for Anaerobic Digestion of Microcrystalline Cellulose: The Role of Particle Size. Materials 14, 487. (140 pkt., IF = 3.057)

Załącznik nr 2:

Publikacja nr 2: Piątek M., Lisowski A., Dąbrowska M., 2021. The effects of solid lignin on the anaerobic digestion of microcrystalline cellulose and application of smoothing splines for extended data analysis of its inhibitory effects. Bioresource Technology 320, 124262. (140 pkt. IF= 7.539)

Załącznik nr 3:

Suplement publikacji nr 2: „Supplementary data 1”

materials

MDPI

Article

Surface-Related Kinetic Models for Anaerobic Digestion of Mi-crocrystalline Cellulose: The Role of Particle Size

Michał Piątek *, Aleksander Lisowski and Magdalena Dąbrowska

Department of Biosystems Engineering, Institute of Mechanical Engineering, Warsaw University of Life Sciences, Nowoursynowska 166, 02-787 Warsaw, Poland; aleksander_lisowski@sggw.edu.pl (A.L.); magdalena_dabrowska@sggw.edu.pl (M.D.)

* Correspondence: michal_piatek@sggw.edu.pl

Abstract: In this work, for modelling the anaerobic digestion of microcrystalline cellulose, two surface-related models based on cylindrical and spherical particles were developed and compared with the first-order kinetics model. A unique dataset consisting of particles with different sizes, the same crystallinity and polymerisation degree was used to validate the models. Both newly developed models outperformed the first-order kinetics model. Analysis of the kinetic constant data revealed that particle size is a key factor determining the anaerobic digestion kinetics of crystalline cellulose. Hence, crystalline cellulose particle size should be considered in the development and optimization of lignocellulose pre-treatment methods. Further research is necessary for the assessment of impact of the crystalline cellulose particle size and surface properties on the microbial cellulose hydrolysis rate.

Keywords: surface-related kinetics; anaerobic digestion; microcrystalline cellulose; modelling

Citation: Piątek, M.; Lisowski, A.; Dąbrowska, M. Surface-Related Kinetic Models for Anaerobic Digestion of Microcrystalline Cellulose: The Role of Particle Size. *Materials* **2021**, *14*, 487. https://doi.org/10.3390/ma14030487

Received: 18 December 2020
Accepted: 12 January 2021
Published: 20 January 2021

1. Introduction

Lignocellulose materials are abundant substrates for biogas and renewable energy production [1–3]. A better understanding of the key factors in the degradation process is required to increase the use of these materials for biogas production. Lignocellulose is a unique, recalcitrant structure of material plant cell walls. Its complex structure hinders microbial degradation. Further, cellulose is water insoluble and forms highly stable hydrogen-bonded crystalline fibers. These characteristics prevents its efficient utilisation in the anaerobic digestion process [4–9].

It is necessary to better understand the relationships between lignocellulose composition, degree of degradation, and degradation kinetics [10,11]. Moreover, there is still little information regarding the relationship between the kinetics of lignocellulose degradation and the structure of cellulose itself [12], particularly regarding the impact of crystallinity and enzyme adsorption sites [13]. The crystalline structure of lignocellulose hinders its degradation, and thus, the hydrolysis of these insoluble compounds is slow. However, the mechanisms behind the reduced hydrolysis rate are not fully understood; the low hydrolysis rate may be attributed to enzyme-associated factors such as enzyme inactivation, jamming due to enzyme overfilling on the cellulose surface, and inhibition of the enzymes. In addition, substrate-related factors, such as multiphase cellulose composition, changes in the degree of polymerization, crystallinity, reduction in reactivity, and substrate availability, as well as other physical properties may also contribute to the reduced hydrolysis rate [14].

In addition, the hydrolysis rate depends on many strongly related factors, such as the type and structure of the substrate (e.g. surface area and crystallinity), cellulose activity, and reaction conditions [15]. Some studies have shown that a decrease in crystallinity is invariably accompanied by a decrease in other substrate characteristics such as particle

size and an increase in the available surface area that results from the pre-treatment of the material (mainly achieved by grinding) [16,17].

Hydrolysis of lignocellulose is considered to be the rate-limiting step in the anaerobic digestion process [11,18,19]. It has also been shown that the hydrolysis rate is controlled by enzyme kinetics if the amount of the enzyme exceeds the amount of the adsorption sites. In this case, hydrolysis can be described by first-order kinetics that have been widely used to describe the hydrolysis kinetics of cellulose and other solid particulate materials [20–24]. It is clear from the previous studies [21,22] that all accessible surface sites were used by enzymes; however, the first-order kinetics model does not describe a decrease in the amount of adsorption sites related to the shape and size of particulate matter. Furthermore, during anaerobic digestion, cellulose is hydrolyzed by cellulosomes that are multienzyme complexes produced by cellulose-degrading anaerobic microbes and mediate cell attachment to the of particulate [25–27]. After attachment to cellulose particle, cellulosomes grow rapidly and maintain contact with bacteria [26]; thus, enzyme–particle collisions can be necklaced as process rate limiting factor. Therefore, the available particulate surface is a crucially important factor. Some surface-related models of particulate hydrolysis have been developed [28–30], but this problem requires further investigation, particularly regarding cellulosome activity. To the best of our knowledge, surface-related models for anaerobic digestion have not been developed or improved upon in recent works. In this paper, we present a newly developed surface-related approach for the modelling of particulate matter degradation during anaerobic digestion using microcrystalline cellulose (MCC) as the model substrate. Pure cellulose was used in experiment to avoid interferences with lignin such as competitive and non-competitive inhibition [31]. The goal of this study was to isolate the role of cellulose particle size, so in our data set polymerization degree and crystallinity are also constant across samples, despite the fact that it is well known that mentioned above factors have significant impact on cellulose degradation kinetics [3]. It was assumed that the cellulosome activity on the entire accessible MCC surface was constant; however, particle surface, related to particle radius, decreased; thus, change in kinetics is strictly surface related. Based on this assumption, we developed two surface-related models for the hydrolysis of cylindrical and spherical particles, respectively, and compared these models to the first-order kinetics model. A unique dataset comprising of data for the particles with the same crystallinity and degree of polymerisation but with different sizes was used to validate the model. Such a dataset has not been used in previous studies. This constitutes an additional novelty in this paper. Due to a lack of reliable lag-phase-duration data pertaining to cellulosome formation as well as for the simplest possible modelling of the hydrolysis process activation, all of the tested models incorporated lag-phase modelling with the assumption of sudden hydrolysis process activation after the lag time.

2. Materials and Methods

2.1. Experimental Data

2.1.1. Material Preparation

MCC Flocel 102 was purchased from a local market (ITC, Piastów, Poland) and was separated according to the ANSI/ASAE S319.4 standard using a LAB-11-200/UP sieve separator (Eko-Lab, Brzesko, Poland) with oscillatory motion in the vertical plane [32,33]. The set of sieves had dimensions of the opening screens in the following sequence from the bottom to the top: 20, 32, 45, 56, 100, 150, 212, and 300 μm. A pan was located at the bottom. The sieve set was selected based on the initial test such that approximately half of the material passed through the middle mesh size. The mass of a single sample of cellulose subjected to separation was 50 g. The duration of sieving was 300 s and was controlled using a stopwatch. The end-point was determined based on preliminary experiments. For time durations between 300 and 600 s, the mass on the pan did not change by 0.1%; therefore, for economic reasons, it was decided to set the duration as 300 s. Seven samples

of particle fractions between 20 and 300 μm were obtained. Mean geometric size of particles were calculated as geometric mean of top and bottom sieve size of given pair of sieves.

2.1.2. Anaerobic Digestion

The samples were processed by anaerobic digestion. The inoculum was obtained from a mesophilic, agricultural biogas plant post-digester. Inoculum contained 3.1% ± 0.05% total solids and 63.2% ± 0.05% volatile solids. Each fraction (10 g) was weighed on a WPS 600/C electronic scale (Radwag, Radom, Poland) with an accuracy of 0.01 g and placed into 2 dm^3 bottles. Following this, inoculum (1800 ml) was added. Bottles with inoculum only (1800 ml) were also prepared as blank. The inoculum-to-substrate ratio in the reactor was 3.5:1 based on organic dry matter in order to eliminate a possible negative effect of a high substrate dose on the process [34,35]. The bottles were flushed with nitrogen and placed in a water bath at 37 C, and the reactor contents were manually mixed once a day. The amount of gas was measured by the brine displacement method [36]. Displaced brine was weighed on electronic scales with an accuracy of 0.01 g, as frequently as is necessary to fully recognize the course of gas formation (once a day or every second day at the end of process) [37]. Batch trials were simultaneously conducted in triplicate, and the obtained biogas volume was converted to the volume at standard conditions (1013 hPa, 273 K). The anaerobic digestion process was conducted for 25 days. Anaerobic digestion of the particle fraction in the 45–56 μm range was repeated because of trial failure on the first approach. Inoculum from the same biogas plant was used, but it was collected at a different time. Test results for particle fraction in the 45–56 μm range are given herein; however, as they were not obtained under the same conditions, they are not included in the overall analysis.

2.1.3. SEM Imaging

Images of randomly chosen microcrystalline cellulose samples were obtained by scanning electron microscopy (SEM, FEI Quanta 200 with microanalyser model EDS and digital image record; FEI Company, Hillsboro, OR, USA; merged with Philips Electron Optics) at the Analytical Centre of WULS. To obtain SEM images, a few cellulose particles were taken from each fraction and placed into a vacuum chamber.

2.1.4. True Density Measurement

Particle density was measured via gas stereopycnometry (Quantachrome Instruments, Boynton Beach, FL, USA). A mass sample m of MCC was placed in the measuring cell with a capacity of V_C = 100 cm^3. For this state, the pressure p_1 of the helium gas in the measuring cell was recorded. Then, the valve through which the gas was directed to the reference cell with the volume V_A was opened, and its pressure p_2 was measured [38]. The true density of the MCC was determined as

$$\rho = \frac{m}{V_C - V_A/(\frac{p_1}{p_2} - 1)}, \quad (1)$$

where ρ is the true density (g·cm^{-3}), m is the mass of the MCC sample (g), V_C is the volume of the measuring cell (cm^3), V_A is the reference cell volume (cm^3), p_1 is the pressure in the measuring cell (MPa), and p_2 is the reference cell pressure (MPa).

2.1.5. Measurement of the Polymerization Degree

The polymerization degree was measured according to the PN-90/E-04421 and PN-92/P-50101/01 standards. Solution viscosity was assessed using an Ubbelohde viscometer (Schott Instruments GmbH, Mainz, Germany) with a capillary diameter of 0.84 mm. The cellulose solution outflow time was recorded every 10 min for 2 h for each sample weighing approximately 0.4 g. The capillary temperature was 25 ± 0.1 C, and the error of the limiting viscosity number did not exceed 2%. The polymerization degree was

calculated using the Immergut equation, $DP^{\alpha} = K[\eta]$, where DP is the average degree of viscosity polymerization (–), [η] is the weight average intrinsic viscosity (–), and K and α are the empirical constants equal to 1.65 g·cm^{-3} and 0.9, respectively [39]. To minimize the deleterious effect of the copper (II) ethylenediamine (CUEN) solution, the polymerization degree for zero retention time was calculated by extrapolation.

2.1.6. Crystallinity Index Measurement

The crystallinity of the MCC samples (approximately 0.5 g) was evaluated by X-ray diffractometry (Tur M62 with a horizontal goniometer HZG-4, Carl Zeiss AG, Jena, Germany) with a Cu Kα radiation source (wavelength λ = 1.5418 Å) at a voltage of 30 kV and current of 25 mA. The scanning scope was 2θ = 5–30° with a step size of 0.04°, and the impulse counting time was 3 s. The crystalline structure of MCC gives rise to distinct peaks at 15°, 16.4°, and 22.5°. The cellulose crystallinity was calculated by the XRD deconvolution method [40,41]. From the peak deconvolution method, the amorphous peak (2θ) was predicted to be located at approximately 21°.

2.1.7. Specific Surface Measurement

Specific surface area (SSA) was measured using the Brunauer–Emmett–Teller (BET) method [42]. Samples were degassed in vacuum for 24 h in 105 °C prior to measurement in order to remove water and other contaminations. Measurements were performed using a QUADRASORB SI surface area analyzer (Quantachrome Instruments, Boynton Beach, FL, USA). Nitrogen gas was used as an adsorbate. All the necessary calculations were made using the 3 Flex analyzer software (v. 3.01, Micromeritics Instr., Norcross, GA, USA).

2.1.8. Water Retention Value Measurement

Water retention value (*WRV*) was measured according to the previously used protocol [43,44]. A precisely weighted sample (MA 50/1R electronic scale, Radwag, Radom, Poland with an accuracy of 0.1 mg) of cellulose (1 g) was placed in a centrifuge tube containing deionised water (10 ml), mixed, and left for 24 h. Then, the samples were centrifuged (3000 g for 20 min), and the supernatant was decanted. The remaining wet MCC samples were weighted and dried in an oven for 10 h in 105 °C. Then, the water retention value (*WRV*) was calculated as

$$WRV = \frac{W_{wet} - W_{dried}}{W_{dried}}, \quad (2)$$

where *WRV* is the water retention value (g $H_2O \cdot g^{-1}$), W_{wet} is the weight of the wet centrifuged sample (g), and W_{dried} is the sample weight after drying (g).

2.2. Kinetics Models

2.2.1. The First-Order Kinetics Model

In this study, three types of kinetic models were compared. The first was the first-order kinetics model with a lag phase [45] given by

$$B(t) = BP \cdot (1 - exp(-k \cdot (t - \lambda))), \quad (3)$$

where $B(t)$ is the biogas production at time t (ml·g^{-1}), BP is the potential ultimate biogas production (ml·g^{-1}), t is the time (h), k is the first-order kinetics constant, and λ is the duration of the lag phase (h).

Sudden process activation after the lag phase was assumed. Thus, the lag during the lag time kinetics constant k is 0; the model is first deactivated, and then activated when t-λ is higher than 0. For the first-order kinetics model, the half hydrolysis time is expressed as

$$t_{0.5} = ln(2)/k, \quad (4)$$

where $ln()$ denotes natural logarithm.

As mentioned above, this model focuses on the kinetics of substrate degradation with a kinetic constant k. It was found that the kinetic constant has different values for different substrate sizes even though this process occurs under the same pH and temperature conditions [21].

The SEM micrographs are presented in Figure 1. The SEM analysis of the shape of the MCC particles indicates that particle shape depends on the size of the mixture fraction separated by the sieves. Omitting surface irregularities and crystal roughness, it was assumed that the finer particles in the size range of 20–45 μm have a cylindrical shape and can be approximated as cylinders. In contrast, the particles with the sizes in the range of 56–212 μm form agglomerates in which the particle geometry can be approximated as spherical. These observations inspired the development of two mathematical models in which the access of enzymes to particles depends on the shape of the latter. Mathematical descriptions of the kinetics of the surface-related hydrolysis for the cylindrical and spherical particle shapes are presented below.

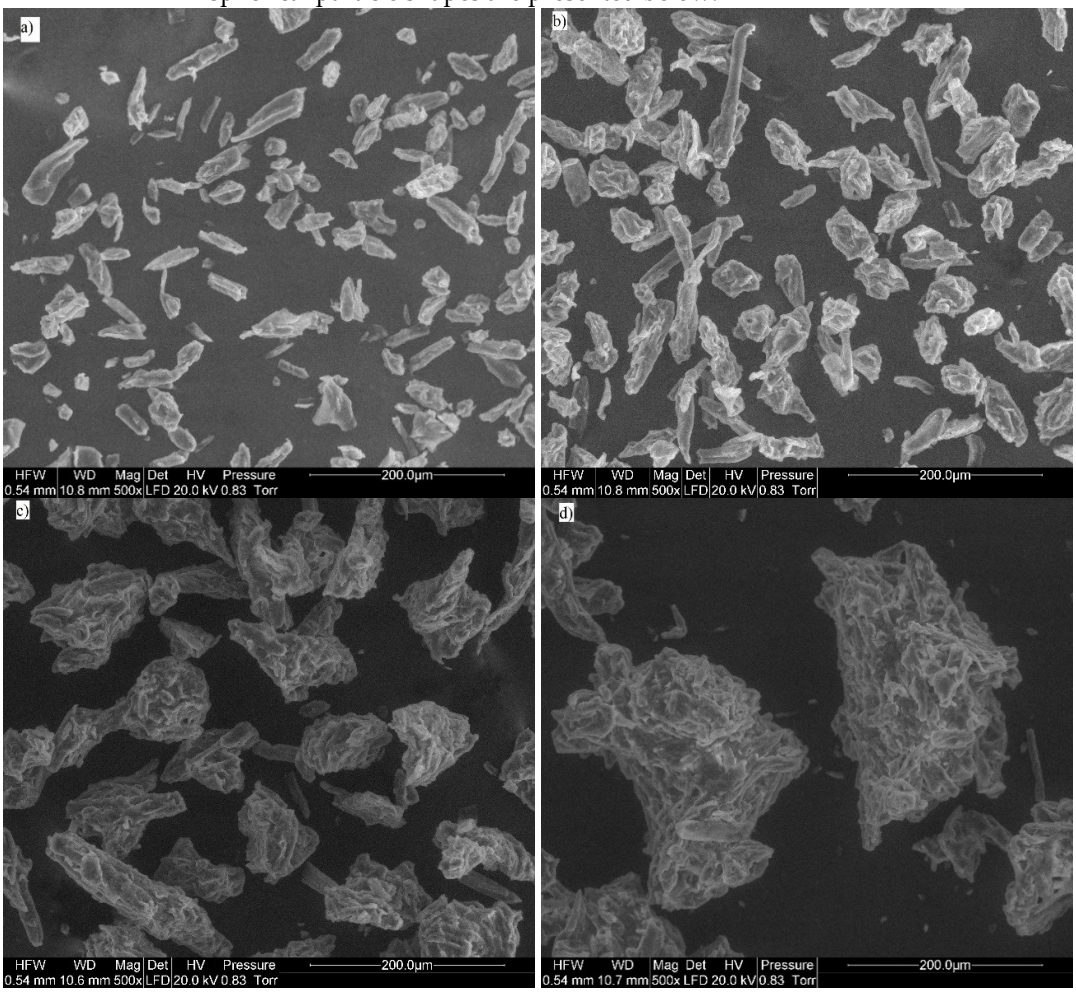

Figure 1. SEM micrographs of MCC particles with sizes of (**a**) 20–32 μm; (**b**) 32–45 μm; (**c**) 56–100 μm; (**d**) 150–212 μm.

2.2.2. Derivation of Surface-Related Models

A basic surface-related model equation was previously presented in the literature [46] as

$$\frac{dM}{dt} = -k_s \cdot S \quad (5)$$

where M is the mass of the substrate (g), t is the time (h), S is the surface susceptible to hydrolysis (cm^2), and k_s is the surface-related hydrolysis constant ($g \cdot cm^{-2} \cdot h^{-1}$); however,

detail derivation of model assumptions was not presented there. Step by step derivation is as follows.

It is possible to rewrite the above equation in terms of the released volume of the substrate, obtaining

$$\frac{dV}{dt} = \frac{-k_s \cdot S}{\rho} \quad (6)$$

where V is the substrate volume (cm^3), and ρ is the substrate density ($g \cdot cm^{-3}$).

Considering the degradation of spherical particles, the change in the volume can be expressed as

$$\frac{dV}{dt} = \frac{-k_s \cdot 4 \cdot \pi \cdot R^2}{\rho}, \quad (7)$$

where R is the particle radius (cm).

We note that

$$\frac{dV}{dt} = \frac{dV}{dR} \cdot \frac{dR}{dt} = 4 \cdot \pi \cdot R^2 \cdot \frac{dR}{dt}, \quad (8)$$

Thus,

$$4 \cdot \pi \cdot R^2 \cdot \frac{dR}{dt} = \frac{-k_s \cdot 4 \cdot \pi \cdot R^2}{\rho}, \quad (9)$$

This simplifies to

$$\frac{dR}{dt} = \frac{-k_s}{\rho}. \quad (10)$$

Thus, for spherical particles, it is possible to construct a model assuming an isotropic substrate and a constant decrease in the radius. It can be concluded that the rate of reaction is proportional to the particle surface area; thus, the decrease in the particle radius is constant. It was assumed that for cellulose, only the external layer of material is hydrolyzed at a given time. This approach is in line with the approach used for modelling the surface-related degradation of starch [46]. The present assumption for spherical particles is also valid for cylindrical particles with the assumption of radial particle degradation. Models sharing presented assumptions, adapted for biogas production curves, were not presented in literature before. In next sections full derivation of models adapted for biogas production curves are presented.

2.2.3. Model for Cylindrical Particles

Based on the presented assumptions for degradation kinetics, the model for cylindrical particles is expressed as

$$B(t) = BP \cdot \rho \cdot n \cdot \pi \cdot L \cdot (R^2 - (R - \frac{k_s}{\rho} \cdot t)^2), \quad (11)$$

where $B(t)$ is the cumulative biogas yield at time t ($ml \cdot g^{-1}$), BP is the ultimate biogas production ($ml \cdot g^{-1}$), n is the number of particles, L is the average particle length (cm), and R is the initial average particle radius (cm). In this model, measured particle radius and length can be introduced; however, knowledge about particles number is then necessary.

The introduced lag phase model takes the following form

$$B(t) = BP \cdot \rho \cdot n \cdot \pi \cdot L \cdot (R^2 - (R - \frac{k_s}{\rho} \cdot (t - \lambda))^2). \quad (12)$$

The model shares lag-phase assumptions with the first-order kinetics model. If biogas or biomethane production curves are available without any additional information about the substrate specific surface or density, the only viable approach for modelling using surface-related models is relative modelling conducted with the assumption that the volume of the particle integrates to one. Additionally, assuming particles homogeneity, density is equal across particles. This allows the omission of the substrate density and the number of particles in the models. This makes models more clear in interpretation. Therefore, the model for the relative modelling of degradation for cylindrical particles is expressed as

$$B(t) = BP \cdot \pi \cdot L \cdot (R^2 - (R - r_s \cdot t)^2) \quad (13)$$

and

$$B(t) = BP \cdot \pi \cdot L \cdot R^2 \cdot (1 - (1 - \frac{r_s}{R} \cdot t)^2), \quad (14)$$

where r_s is the kinetic constant for relative modelling that considers the decrease in the particle radius. The unit of r_s is cm·h^{-1}. It can be assumed that the total particle volume is equal to 1, ensuring that the most common structure of empirical equations is used for biogas or methane cumulative production curve modelling. Here, the constant related to the gas production potential is multiplied by an expression related to process dynamics. The dynamics-related expression integrates to 1 in its domain in nearly all cases [47]. It is assumed that the volume of a cylinder is equal to 1

$$\pi \cdot L \cdot R^2 = 1. \quad (15)$$

Hence, Eq. 14 can be transformed and simplified to

$$B(t) = BP \cdot (1 - (1 - k \cdot t)^2), \quad (16)$$

where k is the first-order kinetic constant (h^{-1}). Next, λ for lag-phase modelling is introduced, so that the final equation form is

$$B(t) = BP \cdot (1 - (1 - k \cdot (t - \lambda))^2). \quad (17)$$

For Eq. 17, the reciprocal of the constant k is the time required to complete the conversion after the lag phase. After this time, the constant k is assumed to be 0, as during the lag phase. The half decay time ($t_{0.5}$) is given by

$$t_{0.5} = (1 - \sqrt{0.5})/k. \quad (18)$$

2.2.4. Model for Spherical Particles

The model for spherical particles is based on the same assumptions as the previous model, with the exception that the particles are spherical; therefore, the basic equation is

$$B(t) = BP \cdot \rho \cdot n \cdot \frac{4}{3} \cdot \pi \cdot (R^3 - \left(R - \frac{k_s}{\rho} \cdot t\right)^3). \quad (19)$$

Introducing a lag phase, the model takes the following form

$$B(t) = BP \cdot \rho \cdot n \cdot \tfrac{4}{3} \cdot \pi \cdot (R^3 - (R - \tfrac{k_s}{\rho} \cdot (t - \lambda))^3). \quad (20)$$

For relative modelling, the model takes the following form

$$B(t) = BP \cdot \frac{4}{3} \cdot \pi \cdot (R^3 - (R - r_s \cdot t)^3) \quad (21)$$

and

$$B(t) = BP \cdot \frac{4}{3} \cdot \pi \cdot R^3 \cdot (1 - \left(1 - \frac{r_s}{R} \cdot t\right)^3). \quad (22)$$

By analogizing to the model of cylindrical particles, it is possible to assume that volume of a sphere is equal to 1. Thus,

$$\frac{4}{3} \cdot \pi \cdot R^3 = 1, \quad (23)$$

$$B(t) = BP \cdot (1 - (1 - k \cdot t)^3). \quad (24)$$

Next, we include λ for lag-phase modelling; therefore, the final equation form is

$$B(t) = BP \cdot (1 - (1 - k \cdot (t - \lambda))^3). \quad (25)$$

The reciprocal of the constant k is the time required to complete the conversion after the lag phase. The half decay time ($t_{0.5}$) is given by

$$t_{0.5} = (1 - \sqrt[3]{0.5})/k. \quad (26)$$

2.3. Model Fitting

All of the calculations were performed using the R package (version 3.5.1). The functions implemented in the "GenSA", "minpac.lm" libraries were used to model biogas production. The models were fitted with the weighted least-squares method. The weights were calculated as a local slope of the biogas production curve [48]

$$w_i = B_i - B_{i-1}, \quad (27)$$

where w_i is the weight factor (ml·g^{-1}), B_i (ml·g^{-1}) is the biogas production curve value at a given measurement time i, and B_{i-1} (ml·g^{-1}) is the previously measured value of the biogas production curve.

Two algorithms were used during the approximation process. The Levenberg-Marquardt ("nlsLM" function from "minpac.lm" library) algorithm was preceded by a

generalised simulated annealing algorithm ("GenSA" function from "GenSA" library) to initiate parameter estimation [49]. The default algorithm parameters were used for both algorithms. The global relative error was used to evaluate the fit [50]

$$\delta = 100 \sqrt{\sum_{i=1}^{n} (z_i - p_i)^2 / \sum_{i=1}^{n} z_i^2}, \quad (28)$$

where n is the number of measurements, and z and p are the actual values and values obtained from the model, respectively. Error was estimated for the whole curves and alternatively for the last day of the trial only, to emphasize error on biogas yield. .

Because all the models used in this study had the same number of parameters, additional informational criteria (such as the Akaike criterion) were not determined.

2.4. Statistical Analysis

The Kruskal–Wallis test ("kruskal.test" form "stats" library) was used to compare the whole biogas production curves. The values of cumulative biogas production, cellulose moisture, and true density were compared using analysis of variance ("aov" function from "stats" library). Levene's test for the homogeneity of variance ("leveneTest" function from "car" library) and the Shapiro–Wilk normality test ("shapiro.test" function from "stats" library) were used to check the validity of the analysis of variance assumptions. Differences were considered statistically significant at $p \leq 0.05$ for the statistical test.

3. Results and Discussion

3.1. Material Characterisation

The SEM images of MCC are shown in Figure 1, and it can be concluded that this material is characterized by irregular shape and polydispersity [51]. However, there are significant differences between the shapes of the small particles and large particles, with the geometric mean particle sizes of 25–38 and 75–178 μm, respectively. These particle shapes resemble cylinders and spheres, respectively. The smallest particles of MCC were mostly independent, while large particles formed spontaneous agglomerates due to the aggregation of single, fine crystals. Individual MCC particles from kenaf bast and wood pulp [52] and from cellulose filter papers [53] were determined to be rod-shaped. The particle shape of Flocel MCC with a mean volume diameter of 153 μm was determined to be generally fibrous with a few plate-like structures [54]. The physicochemical properties of the material are presented in Table 1.

Table 1. Basic material characteristics.

Fractions [μm]	Geometric Mean Particle Size [μm]	Moisture Content w.b.		True Density		Polymerisation Degree	Crystallinity
		Mean n = 3 [%]	SD [%]	Mean n = 3 [g·ml^{-3}]	SD [g·ml^{-3}]	Value n = 1 [–]	Value n = 1 [%]
20 < 32	25	5.20	0.28	1.597	0.001	328	56
32 < 45	38	4.89	0.16	1.600	0.001	336	58
45 < 56	*50*	*5.09*	*0.13*	*1.595*	*0.001*	*330*	*60*
56 < 100	75	4.97	0.32	1.589	0.005	333	58
100 < 150	122	4.90	0.35	1.581	0.009	335	59
150 < 212	178	5.05	0.08	1.603	0.001	333	57
212 < 300	252	4.95	0.29	1.593	0.006	333	57

SD—standard deviation.

Significant differences were found for the true density of MCC particles ($p = 0.0008$), but the values varied in a very narrow range of 1.581–1.603 g·ml^{-3}. There was no evidence regarding differences in moisture ($p >> 0.05$). The MCC moisture content was in the narrow range of 4.89–5.20% w.b., and is comparable to the values of 3.96–5.06% w.b. obtained for other types of MCC (Avicel, Flocel, fine powder, Ranq, fibres from sisal) [54]. The values of sample crystallinity can be compared when the moisture contents of the samples do not differ significantly [55]. XRD showed comparable results for crystallinity in the range of 56–59% (without the 45–56 μm particle fraction). In addition, the results for the polymerisation degree were comparable in a range of 328–336 (Table 1). Four types of MCC, namely, Avicel, Flocel, fine powder, and fibres from sisal, were obtained and had similar values of 60% for the crystallinity index (calculated by the Segal formula) [54]. The lack of correlation ($r = –0.028$) between the crystallinity and particle size differs from other findings in the literature [56]. However, it should be emphasized that the split of the mixture into fractions is not caused by the grinding of the material during which particle crushing occurs [56]. In this study, the finer particles merged into spontaneous agglomerates, and during this process, the fine particles did not undergo substantial physical changes. This indicates that the polymerization degree and material crystallinity do not impact the sample kinetics comparison. This conclusion is in line with previous studies that indicated that crystallinity is only one of several parameters that should be taken into account when assessing the enzymatic rate of cellulose degradation [57]. Further, relatively small changes in the crystallinity index should not be correlated with the changes in cellulose digestibility [41]. The results of the specific surface and *WRV* measurements are presented in Table 2.

Statistically important differences in *WRV* were observed ($p << 0.05$). While the *WRV* values for the samples varied in a narrow range of 2.5–3.4 g $H_2O \cdot g^{-1}$, the differences were distributed across the whole range of particle diameter. Similarly, specific surface results varied only in the 0.73–0.87 $m^2 \cdot g^{-1}$ range (Table 2) and were distributed across a range of diameters. In Section 3.3., the results presented in this section are analyzed in detail along with modelled data described in Section 3.2.

Table 2. Results of specific surface and *WRV* measurements.

Sample	Specific Surface Area		*WRV*	
	Mean n=1 [$m^2 \cdot g^{-1}$]	**Standard Deviation [$m^2 \cdot g^{-1}$]**	**Mean n=5 [g $H_2O \cdot g^{-1}$]**	**Standard Deviation [g $H_2O \cdot g^{-1}$]**
20 < 32	0.801	0.013	2.52	0.04
32 < 45	0.865	0.004	2.67	0.09
45 < 56	*0.834*	*0.002*	*2.72*	*0.05*
56 < 100	0.802	0.004	3.00	0.02
100 < 150	0.792	0.003	3.17	0.02
150 < 212	0.765	0.017	3.39	0.10
212 < 300	0.730	0.006	3.32	0.04

3.2. Results of Anaerobic Digestion and Model Comparison

Biogas production potential values are summarized in Table 3. Obtained biogas yield allowed to conclude that hydrolysis was completed, and theoretical biogas production potential was recovered [37]. Based on the Kruskal–Wallis test, significant differences ($p = 0.0105$) were found between the biogas production curves. Therefore, the curves were modelled separately. Biogas production curves are depicted in Figure 2, along with the model approximations for each MCC fractional sample.

Table 3. Comparison of measured and estimated biogas production potential.

Fractions [μm]	Measured Biogas Production Potential		First-Order Kinetic Model Estimates [ml·g^{-1}]	Cylindrical Particle Model Estimates [ml·g^{-1}]	Spherical Particle Model Estimates [ml·g^{-1}]
	Mean [ml·g^{-1}]	Standard Deviation [ml·g^{-1}]			
20 < 32	726	54	748	698	712
32 < 45	683	47	732	668	686
45 <56	*723*	*41*	*810*	*726*	*746*
56 < 100	694	27	750	679	697
100 < 150	677	34	723	670	684
150 < 212	715	26	769	694	713
212 < 300	619	31	676	615	635

However, analysis of variance did not provide statistically significant evidence for the differences in cumulative biogas production ($p = 0.0622$). A comparison of the results of these two tests indicated that the differences between the biogas production curves can be attributed to different process kinetics.

Comparison of lag-phase duration, half decay time, and complete decay time is presented in Table 4. All models approximated the biogas production curves well. The obtained values for the lag-phase duration, half hydrolysis time, and complete hydrolysis time are presented. Lag-phase duration can be considered as an effect of whole population or single cell growth [58]. As previously mentioned, during the batch tests, the inoculum-to-substrate ratio was 3.5:1 (based on organic dry matter); thus, the system was saturated with microorganisms. Therefore, the observed lag phase cannot be related to microbial population growth. The apparent lag should be considered as the time required for the synthesis of cellulosomes by individual cells and subsequent hydrolysis start-up. For the particles with the size in the 45–56 μm range, the lag-phase duration and half decay time were the longest, which was consistent for all of the tested models (Table 4).

Table 4. Comparison of lag-phase duration, half decay time, and complete decay time. Complete decay time compared for surface related models only.

Fractions [μm]	First-Order Kinetic Model			Cylindrical Particle Model			Spherical Particle Model		
	Lag Phase [d]	Half Decay Time [d]	Complete Decay Time [d]	Lag Phase [d]	Half Decay Time [d]	Complete Decay Time [d]	Lag Phase [d]	Half Decay Time [d]	Complete Decay Time [d]
20 < 32	2.97	2.66	–	2.54	2.98	10.16	2.69	2.84	13.77
32 < 45	2.86	2.90	–	2.47	3.07	10.48	2.62	2.96	14.33
45 < 56	*3.59*	*3.79*	–	*3.32*	*3.68*	*12.57*	*3.45*	*3.60*	*17.44*
56 < 100	2.56	3.44	–	2.21	3.49	11.91	2.37	3.37	16.33
100 < 150	2.87	3.27	–	2.45	3.52	12.02	2.62	3.37	16.35
150 < 212	2.69	3.51	–	2.36	3.51	11.99	2.52	3.40	16.50
212 < 300	2.98	3.34	–	2.57	3.47	11.86	2.70	3.42	16.58

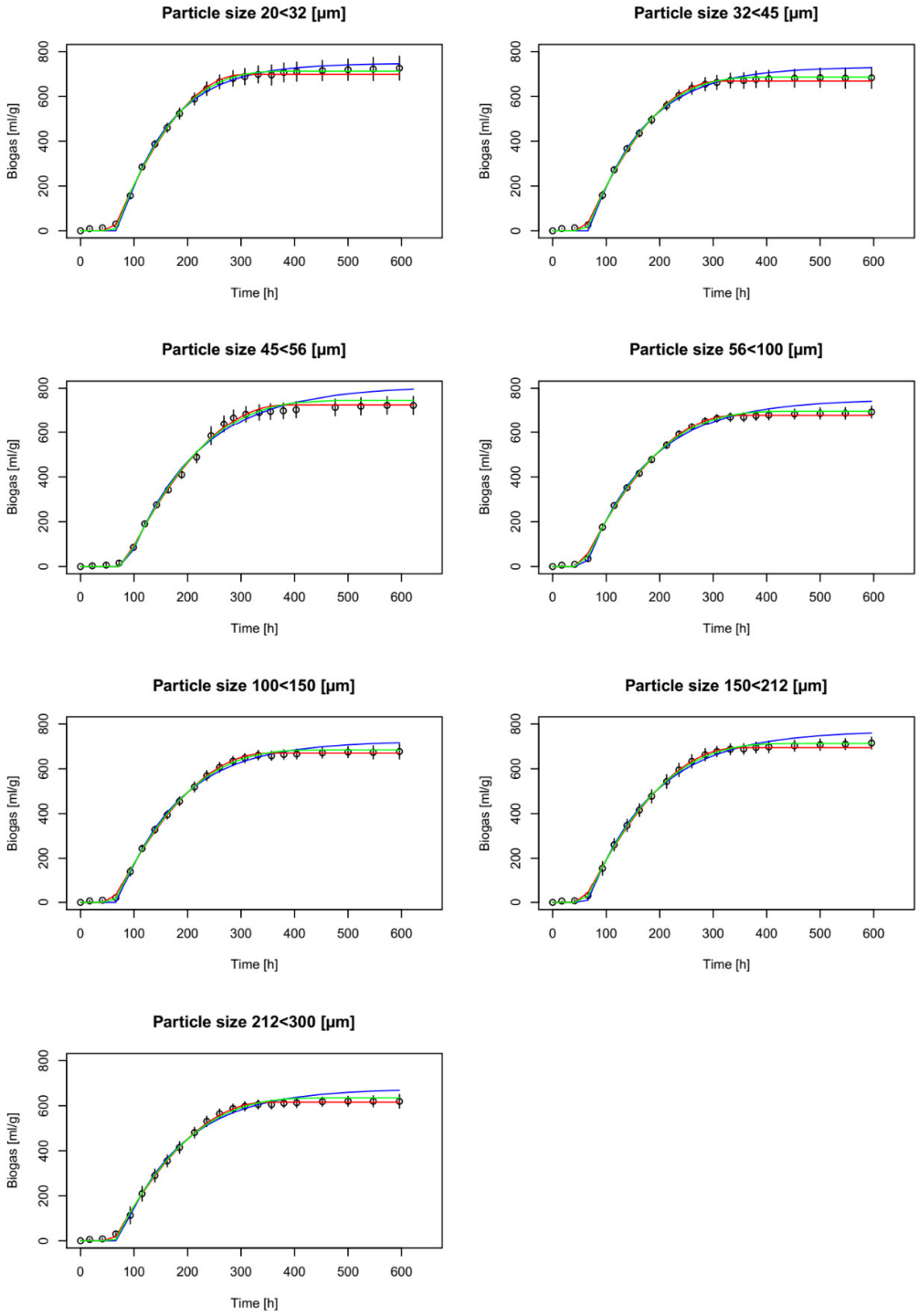

Figure 2. Biogas production experimental and model data for each sample. Circles denote the means of three samples, and vertical bars denote standard deviations. Blue, red, and green lines denote the first-order kinetic model and the approximations for the cylindrical and spherical particles, respectively.

This indicates that the inoculum used for anaerobic digestion of this sample, which was collected at a different time and had a lower activity, cannot be directly compared to

the rest of the data. For this reason, the results for the particles with sizes in the 45–56 μm range were excluded from the further analysis of the lag phase, decay time, and overall kinetics. The experimental and model values of lag-phase duration were consistent for the rest of the particles and on average were 2.93, 2.56, and 2.71 d for first-order, cylindrical, and spherical particle models, respectively. This confirms the assumption of sudden hydrolysis process activation after the lag phase. This approach enables the calculation of the complete process time by adding the lag-phase duration and the time for the completion of decay/hydrolysis. Only surface-related models enable the calculation of the time to complete hydrolysis.

Comparison of model performance has shown that process kinetics are surface related, which is in line with previous research on cellulose hydrolysis by cellulosomes [13]. The spherical particle model estimated a longer hydrolysis time than the cylindrical particle model, and the average times were 15.64 and 11.40 d (excluding particles with the sizes in the 45–56 μm range), respectively. The smallest and largest differences were found for the particle fractions in the 20–32 and 212–300 μm size ranges (excluding particles with the sizes in the 45–56 μm range), respectively, and were 3.61 and 4.72 d, respectively (Table 4). The half decay times were similar for all tested models, with the values in the narrow range of 2.43–2.98 d; thus, differences between the surface-related models were observed at the end of the process.

The results shown in Figure 2 and the data presented in Table 3 show that the first-order kinetics model overestimates real biogas production, with the exception of the curve for the 20–32 μm particle fraction, and the first-order kinetics estimates do not fit into the area marked by the curve and its standard deviation (Figure 2), in contrast to both surface-related models. This demonstrates the better prediction of anaerobic fermentation by these two models; however, it is not possible to clearly distinguish if the cylindrical or spherical model is better. The first-order kinetics model also exhibited the largest global relative error (6.03%) and the end-of-trial relative error (8.94%) for the 212–300 μm particle fraction. In comparison, the largest end-of-trial errors were observed for the 20–32 μm particle fraction, and were 2.37% and 2.10% for the cylindrical and spherical particle models, respectively (Table 5).

Table 5. Comparison of model performance.

Fractions [μm]	First-order Kinetics Model		Cylindrical PParticle Model		Spherical Particle Model	
	Global Relative Error [%]	End-of-Trial Relative Error [%]	Global Relative Error [%]	End-of-Trial Relative Error [%]	Global Relative Error [%]	End-of-Trial Relative Error [%]
20 < 32	5.41	6.60	5.31	2.37	5.06	2.10
32 < 45	5.87	8.70	4.66	2.00	4.52	1.88
45 < 56	*7.49*	*11.09*	*5.05*	*1.53*	*5.59*	*1.84*
56 < 100	4.92	7.55	3.04	1.26	3.10	1.05
100 < 150	4.75	7.05	3.44	1.40	3.59	1.40
150 < 212	5.31	6.92	4.00	1.40	3.90	1.02
212 < 300	6.03	8.94	4.10	1.38	4.66	1.59

In most cases, the end-of-trial relative errors were slightly lower for the spherical particle model in than those obtained by the cylindrical particle model; the obtained values were 1.51% and 1.64% (excluding the fraction with the particle sizes in the 45–56 μm range), respectively, and can be attributed to the improved lag-phase modelling by the spherical particle model.

3.3. Analysis of Relations between Kinetic Constants, WRV and SSA

In this study, cellulose crystallinity and polymerization degree remained constant across samples; thus, k values were influenced by available adsorption sites related to substrate surface. For better analysis of k values, we proposed an empirical equation, which is the opposite Michaelis–Menten saturation equation

$$k = 1 - \frac{k_{max} \cdot d}{K_s + d}, \quad (29)$$

where k is measured kinetic constant value (h^{-1}), k_{max} is the maximum kinetic constant value (h^{-1}), K_s is the half saturation constant (μm), and d is the mean particle diameter (μm).

The obtained global relative errors were 2.08% and 1.71% for cylinder and spherical shaped particles model, respectively. The results obtained using this approximation are presented in Figure 3.

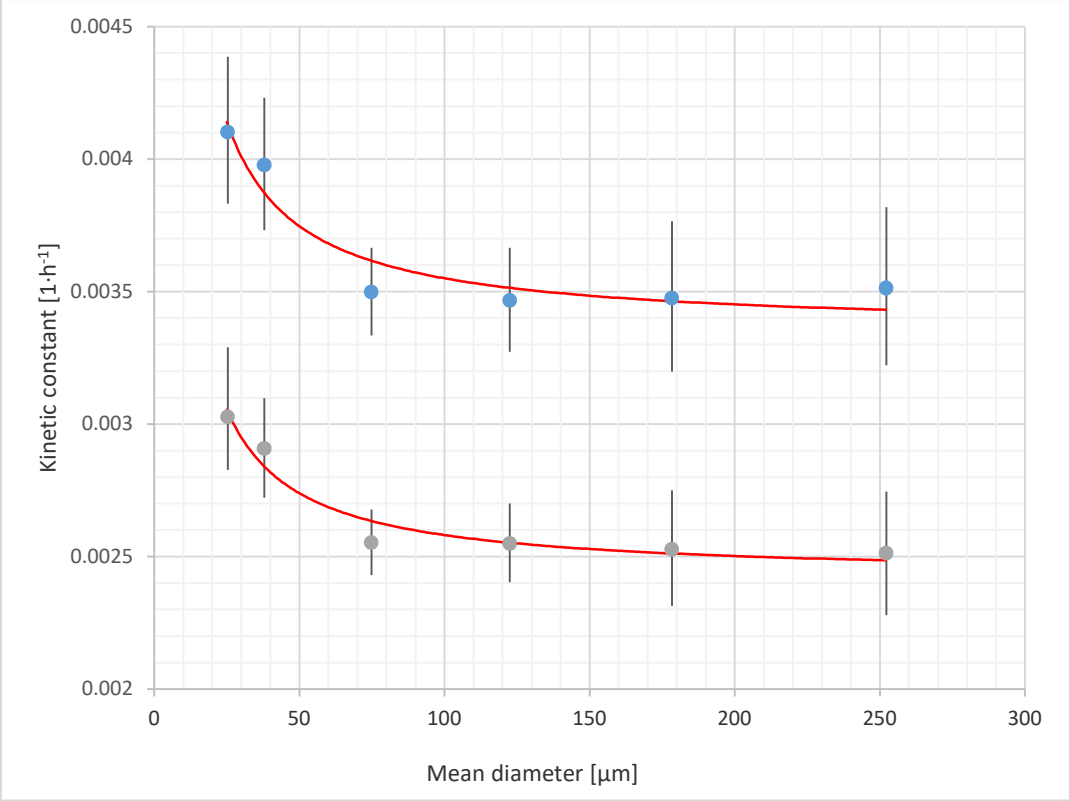

Figure 3. Measured k constants for the cylinder (top) and spherical (bottom) shaped particles models. Points represent measured values and lines represent model approximations.

The proposed model interpretation refers only to process initialization and is as follows: when particle diameter is ≈ 0, nearly all adsorption sites are exposed. Then, with the increase in the particle diameter, the initial exposure of the enzyme adsorption sites decreases, so that the process requires more time based on the model assumptions (lower k constant). In this particular case, it can be stated that the difference in the particle size was the sole reason for better exposure of adsorption sites. During pre-treatment, both cellulose crystallinity and particle size usually change [16,17]. This is also true for ball milling of MCC [59]. A previous study on cellulose sonication has indicated the possibility of substantial hydrolysis enhancement due to considerable particle size reduction (from 38 μm to < 0.40 μm) with only slight changes in crystallinity (12% decrease) and degree of polymerization (no change), thus proving that recrystallisation is not inevitable [60]. Another study showed a considerable particle size decrease (from 300–500 to 20 μm in

length and from 10–20 to 2 μm in diameter) after 120 h of enzymatic hydrolysis, while cellulose crystallinity decreased by only 12% [12]. Additionally, 400–500 nm channels were observed on the particles' surfaces after 48 h. Moreover, acid hydrolysis can lead to production of cellulose nanoparticles (size reduction from 45–53 μm to 53.5 ± 5.3 nm) with only 1.84% decrease in crystallinity, but a substantial decrease in the polymerization degree (from 466 to 215) [61]. Enzymatic hydrolysis can also lead to similar results, obtaining a size reduction from 45–53 μm to 36.5 ± 1.9 nm, polymerization degree decrease from 466 to 293, and 9.87% decrease in crystallinity [61]. Hence, it can be concluded that enzymatic hydrolysis causes only a 10–12% decrease in cellulose crystallinity, and a substantial decrease in the particle size. These observations are in line with our research, proving that change in the particle size only can enhance cellulose hydrolysis kinetics. This is confirmed by the recent studies on cellulosome activity that concluded that cellulosomes are particularly active for the smallest cellulose crystals (length ≤ ~70 nm) [62]. Such small particles are hardly attacked by free enzymes, possibly due to enzyme jamming [62,63]. However, for anaerobic digestion of lignocellulose, the influence of the particle size can be observed for much larger particles (0.15–1.70 mm) [64]. This can be attributed to the modification of the lignocellulosic matrix rather than the cellulose itself.

The *WRV* methods can be applied in order to measure the adsorption surface area. Typically, larger *WRVs* are associated with better surface exposure [65], larger inner pore volume, and lower crystallinity [43,44]. In MCC hydrolysis, hydrophobicity can be considered to be the key factor [44], and hence lower *WRVs* can be interpreted to be more beneficial if the crystallinity remains constant, which is true for this study. Figure 4 shows a comparison of *WRV* and *k* constant data, and it is observed that *WRV* increases with increasing particle size. Differences in uncertainty measures used on Figures 4 and 5 are the effect of different calculation software used. *WRV* changes can be attributed to the higher pore volume. However, *WRV* is correlated with the particle size (r = 0.822), and thus the *WRV* data cannot be interpreted without the knowledge of the particle size; however, it changes in a relatively narrow range (2.52–3.39 g $H_2O \cdot g^{-1}$).

The BET specific surface area is frequently used to characterize lignocellulosic materials [43,66]. In this study, absolute SSA values do not differ substantially across samples, while kinetic constants show greater absolute differences, especially for the smallest particles. In this study, the surface area ranges from 0.73 to 0.87 $m^2 \cdot g^{-1}$ (Table 2). Surprisingly, the specific surface area of the 20–32 μm particles (0.80 $m^2 \cdot g^{-1}$) is lower than that of the 32–45 μm particles (0.87 $m^2 \cdot g^{-1}$). This can be attributed to the particle structure, because the 20–32 μm particles are rather individual particles, while the 32–45 μm particles are agglomerates of smaller particles (Figure 1). While some studies have indicated that SSA is the most important indicator of hydrolysis effectiveness [44], this conclusion was based on ball-milled cellulose samples, where SSA was altered simultaneously with other properties such as a substantial crystallinity change. Additionally, during hydrolysis by free enzymes, not only the surface area, but also the surface properties, such as roughness, are important and can cause enzyme jamming [67]. Comparison of SSA with *k* constants is presented in Figure 5. In this study, the SSA does not accurately describe the changes in process kinetics. In particular, the 20–32 μm particles show an opposite trend, because SSA decreases while *k* constant increases. Recent studies show that spatially organized enzymes in cellulosome can adapt their shape to cellulose nanocrystals. The individual cellulosome surface was calculated as approximately 1500 nm^2 [62]. SSA measured using the BET method is due to the areas of mesopores that are defined as the pores with the widths in the 2–50 nm range [68]. These pores are likely to be smaller than the proposed cellulosome area; hence, according to presented data, it can be hypothesized that cellulosomes do not necessarily utilize the mesopore surface. Additionally, the formation of agglomerates leads to decreased adsorption sites accessibility [69].

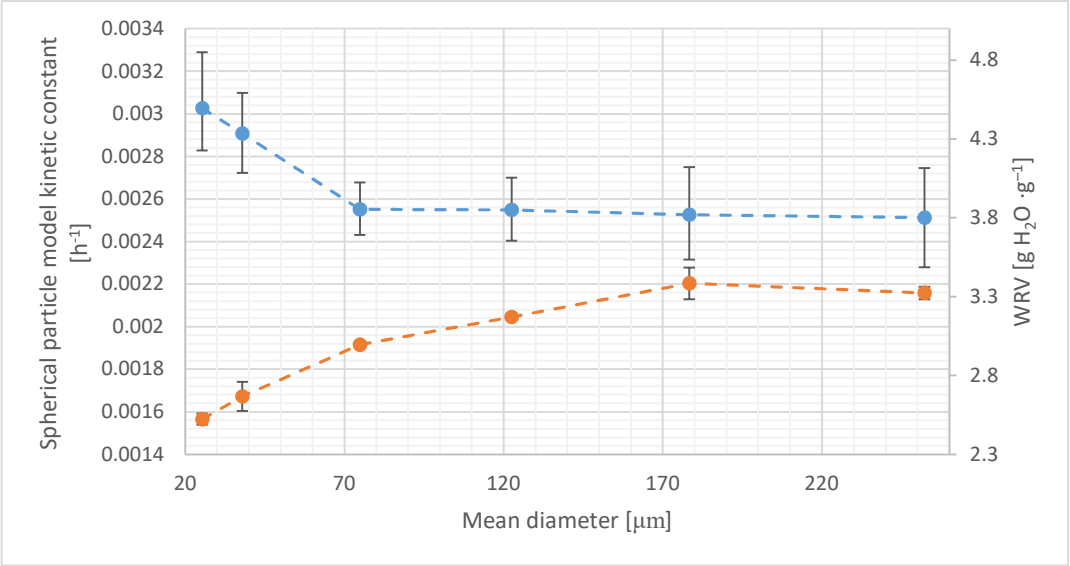

Figure 4. *WRV* compared to spherical shaped particle model kinetic constant values. For *k* constant (top) and *WRV* (bottom) points, the error bars represent the 95% confidence interval and standard error, respectively.

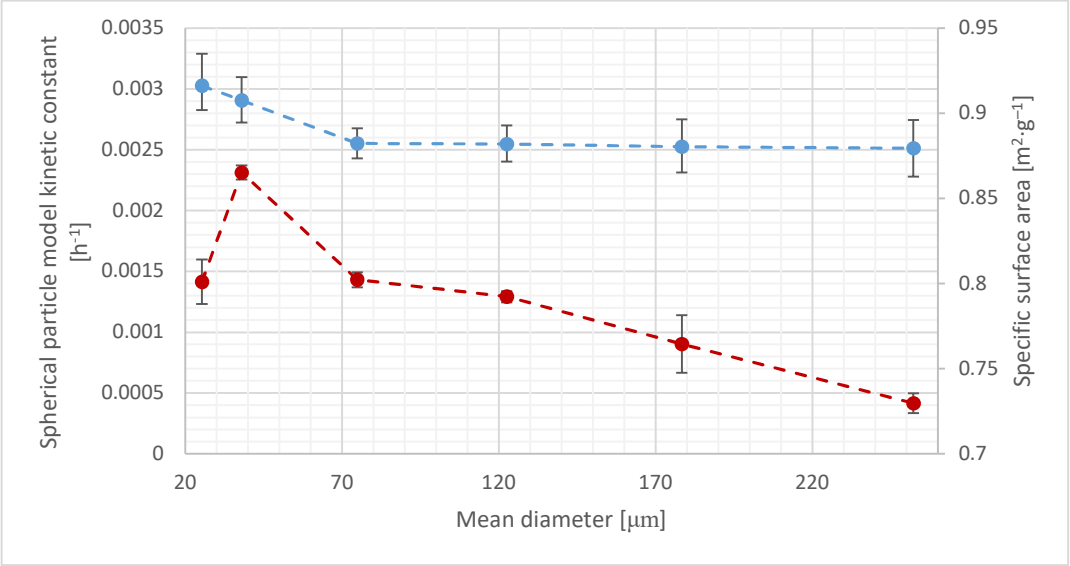

Figure 5. Specific surface area compared to the spherical shaped kinetic constant values. For the *k* constant (top) and SSA (bottom) data points, the error bars represent the 95% confidence interval and the standard error, respectively.

4. Conclusions

All the tested models provide a good approximation of the hydrolysis process. However, the surface-related models outperform the first-order kinetics model that overestimates the true biogas production potential. The simple models presented in this work can be used as part of extended models in the evaluation of lignocellulose pretreatment methods. It is clear that the generation of amorphous cellulose during pretreatment is desirable because of its lower free energy demand for hydrolysis [44]. However, the unique data set presented in this paper and the newly developed surface-related modelling approach revealed that particle size is a key factor determining the kinetics of crystalline hydrolysis. Hence, crystalline cellulose particle size should be an important target property in the development and optimization of lignocellulose pre-

treatment methods. Further research for the evaluation of the impact of the crystalline cellulose particle size and surface properties on the microbial cellulose hydrolysis rate is required.

Author Contributions: conceptualization: M.P., A.L., and M.D.; methods: M.P., A.L., and M.D.; software: M.P.; formal analysis: M.P.; investigation: M.P.; resources: M.P.; data curation: M.P.; writing–original draft preparation: M.P.; writing–review and editing: A.L. and M.D.; visualization: M.P., A.L., and M.D.; project administration: A.L.; supervision: A.L. and M.D. All authors have read and agreed to the published version of the manuscript.

Funding: This research was partially supported by the Ministry of Science and Higher Education of Poland.

Data Availability Statement: The data presented in this study are available on request from the corresponding author.

Conflicts of Interest: The authors declare that there are no financial or commercial conflicts of interest.

References

1. Liu, T.; Zhou, X.; Li, Z.; Wang, X.; Sun, J. Effects of liquid digestate pretreatment on biogas production for anaerobic digestion of wheat straw. *Bioresour. Technol.* **2019**, *280*, 345–351.
2. Akyol, Ç.; Ince, O.; Bozan, M.; Ozbayram, E.G.; Ince, B. Fungal bioaugmentation of anaerobic digesters fed with lignocellulosic biomass: What to expect from anaerobic fungus *Orpinomyces* sp. *Bioresour. Technol.* **2019**, *277*, 1–10.
3. Bahmani, M.A.; Shafiei, M.; Karimi, K. Anaerobic digestion as a pretreatment to enhance ethanol yield from lignocelluloses. *Process Biochem.* **2016**, *51*, 1256–1263.
4. Rouches, E.; Escudié, R.; Latrille, E.; Carrère, H. Solid-state anaerobic digestion of wheat straw: Impact of S/I ratio and pilot-scale fungal pretreatment. *Waste Manag.* **2019**, *85*, 464–476.
5. Rahman, M.A.; Møller, H.B.; Saha, C.K.; Alam, M.M.; Wahid, R.; Feng, L. Anaerobic co-digestion of poultry droppings and briquetted wheat straw at mesophilic and thermophilic conditions: Influence of alkali pretreatment. *Renew. Energy* **2018**, *128*, 241–249.
6. Solé-Bundó, M.; Eskicioglu, C.; Garfí, M.; Carrère, H.; Ferrer, I. Anaerobic co-digestion of microalgal biomass and wheat straw with and without thermo-alkaline pretreatment. *Bioresour. Technol.* **2017**, *237*, 89–98.
7. Dumas, C.; Silva Ghizzi Damasceno, G.; Abdellatif, B.; Carrère, H.; Steyer, J.P.; Rouau, X. Effects of grinding processes on anaerobic digestion of wheat straw. *Ind. Crops Prod.* **2015**, *74*, 450–456.
8. Yao, Y.; Bergeron, A.D.; Davaritouchaee, M. Methane recovery from anaerobic digestion of urea-pretreated wheat straw. *Renew. Energy* **2018**, *115*, 139–148.
9. Kainthola, J.; Shariq, M.; Kalamdhad, A.S.; Goud, V.V. Enhanced methane potential of rice straw with microwave assisted pretreatment and its kinetic analysis. *J. Environ. Manag.* **2019**, *232*, 188–196.
10. Li, Y.; Sun, Z.; Ge, X.; Zhang, J. Effects of lignin and surfactant on adsorption and hydrolysis of cellulases on cellulose. *Biotechnol. Biofuels* **2016**, *9*, 20.
11. Koyama, M.; Yamamoto, S.; Ishikawa, K.; Ban, S.; Toda, T. Inhibition of anaerobic digestion by dissolved lignin derived from alkaline pre-treatment of an aquatic macrophyte. *Chem. Eng. J.* **2017**, *311*, 55–62.
12. Yu, L.; Chen, Z.X.; Tong, X.; Li, K.; Li, W.W. Anaerobic degradation of microcrystalline cellulose: Kinetics and micro-scale structure evolution. *Chemosphere* **2012**, *86*, 348–353.
13. Fierobe, H.-P.; Bayer, E.A.; Tardif, C.; Czjzek, M.; Mechaly, A.; Bélaïch, A.; Lamed, R.; Shoham, Y.; Bélaïch, J.-P. Degradation of Cellulose Substrates by Cellulosome Chimeras. *J. Biol. Chem.* **2002**, *277*, 49621–49630.
14. Monschein, M.; Reisinger, C.; Nidetzky, B. Enzymatic hydrolysis of microcrystalline cellulose and pretreated wheat straw: A detailed comparison using convenient kinetic analysis. *Bioresour. Technol.* **2013**, *128*, 679–687.
15. Kumar, R.; Wyman, C.E. Access of cellulase to cellulose and lignin for poplar solids produced by leading pretreatment technologies. *Biotechnol. Prog.* **2009**, *25*, 807–819.
16. Yu, Q.; Liu, R.; Li, K.; Ma, R. A review of crop straw pretreatment methods for biogas production by anaerobic digestion in China. *Renew. Sustain. Energy Rev.* **2019**, *107*, 51–58.
17. Yuan, X.; Wen, B.; Ma, X.; Zhu, W.; Wang, X.; Chen, S.; Cui, Z. Enhancing the anaerobic digestion of lignocellulose of municipal solid waste using a microbial pretreatment method. *Bioresour. Technol.* **2014**, *154*, 1–9.
18. Antwi, E.; Engler, N.; Nelles, M.; Schüch, A. Anaerobic digestion and the effect of hydrothermal pretreatment on the biogas yield of cocoa pods residues. *Waste Manag.* **2019**, *88*, 131–140.
19. Shrestha, S.; Fonoll, X.; Khanal, S.K.; Raskin, L. Biological strategies for enhanced hydrolysis of lignocellulosic biomass during anaerobic digestion: Current status and future perspectives. *Bioresour. Technol.* **2017**, *245*, 1245–1257.
20. Batstone, D.J.; Keller, J.; Angelidaki, I.; Kalyuzhnyi, S.V.; Pavlostathis, S.G.; Rozzi, A.; Sanders, W.T.; Siegrist, H.; Vavilin, V.A. The IWA Anaerobic Digestion Model No 1 (ADM1). *Water Sci. Technol.* **2002**, *45*, 65–73.

21. Vavilin, V.A.; Fernandez, B.; Palatsi, J.; Flotats, X. Hydrolysis kinetics in anaerobic degradation of particulate organic material: An overview. *Waste Manag.* **2008**, *28*, 939–951.
22. South, C.R.; Hogsett, D.A.L.; Lynd, L.R. Modeling simultaneous saccharifi cation and fermentation of continuous reactors. *Enzym. Microb. Technol.* **1995**, *17*, 797–803.
23. García-Gen, S.; Sousbie, P.; Rangaraj, G.; Lema, J.M.; Rodríguez, J.; Steyer, J.P.; Torrijos, M. Kinetic modelling of anaerobic hydrolysis of solid wastes, including disintegration processes. *Waste Manag.* **2015**, *35*, 96–104.
24. Liew, L.N.; Shi, J.; Li, Y. Methane production from solid-state anaerobic digestion of lignocellulosic biomass. *Biomass Bioenergy* **2012**, *46*, 125–132.
25. Artzi, L.; Bayer, E.A.; Moraïs, S. Cellulosomes: Bacterial nanomachines for dismantling plant polysaccharides. *Nat. Rev. Microbiol.* **2017**, *15*, 83–95.
26. Bayer, E.A.; Lamed, R. Ultrastructure of the cell surface cellulosome of clostridium thermocellum and its interaction with cellulose. *J. Bacteriol.* **1986**, *167*, 828–836.
27. Adams, J.J.; Currie, M.A.; Ali, S.; Bayer, E.A.; Jia, Z.; Smith, S.P. Insights into higher-order organization of the cellulosome revealed by a dissect-and-build approach: Crystal structure of interacting Clostridium thermocellum multimodular components. *J. Mol. Biol.* **2010**, *396*, 833–839.
28. Vavilin, V.A.; Rytov, S.V.; Lokshina, L.Y. A description of hydrolysis kinetics in anaerobic degradation of particulate organic matter. *Bioresour. Technol.* **1996**, *56*, 229–237.
29. da Rocha, D.; Paetzold, E.; Kanswohl, N. The shrinking core model applied on anaerobic digestion. *Chem. Eng. Process. Process Intensif.* **2013**, *70*, 294–300.
30. Sakimoto, K.; Kanna, M.; Matsumura, Y. Kinetic model of cellulose degradation using simultaneous saccharification and fermentation. *Biomass Bioenergy* **2017**, *99*, 116–121.
31. Zhu, Z.; Li, W.; Zhang, R.; Thorin, E.; Khalid, H.; Chen, C.; Liu, G. Methane production through anaerobic digestion: Participation and digestion characteristics of cellulose, hemicellulose and lignin. *Appl. Energy* **2018**, *226*, 1219–1228.
32. Wilcox, R.A.; Deyoe, C.W.; Pfost, H.B. A Method for Determining and Expressing the Size of Feed Particles by Sieving. *Poult. Sci.* **1970**, *49*, 9–13.
33. Lisowski, A.; Kostrubiec, M.; Dąbrowska-Salwin, M.; Świętochowski, A. The Characteristics of Shredded Straw and Hay Biomass: Part 2—The Finest Particles. *Waste Biomass Valorization* **2018**, *9*, 115–121.
34. Piatek, M.; Lisowski, A.; Kasprzycka, A.; Lisowska, B. The dynamics of an anaerobic digestion of crop substrates with an unfavourable carbon to nitrogen ratio. *Bioresour. Technol.* **2016**, *216*, 607–612.
35. Piątek, M.; Lisowski, A.; Lisowska, B. Application of titration methods for measuring the contents of ammonium nitrogen and volatile fatty acids in agricultural biogas plants. *J. Biotechnol.* **2017**, *264*, 38–42.
36. Das, A.; Mondal, C. Comparative Kinetic Study of Anaerobic Treatment of Thermally Pretreated Source-Sorted Organic Market Refuse. *J. Eng.* **2015**, *2015*, 684749.
37. Verein Deutscher Ingenieure. *VDI 4630—Gärsubstrate*; Verein Deutscher Ingenieure: Düsseldorf, Germany, 2014; ISBN 8488637001201.
38. Gilvari, H.; de Jong, W.; Schott, D.L. Quality parameters relevant for densification of bio-materials: Measuring methods and affecting factors—A review. *Biomass Bioenergy* **2019**, *120*, 117–134.
39. Evans, R.; Wallis, A.F.A. Cellulose molecular weights determined by viscometry. *J. Appl. Polym. Sci.* **1989**, *37*, 2331–2340.
40. Hindeleh, A.M.; Johnson, D.J. The resolution of multipeak data in fibre science. *J. Phys. D Appl. Phys.* **1971**, *4*, 259–263.
41. Park, S.; Baker, J.O.; Himmel, M.E.; Parilla, P.A.; Johnson, D.K. Cellulose crystallinity index: Measurement techniques and their impact on interpreting cellulase performance. *Biotechnol. Biofuels* **2010**, *3*, 10.
42. Brunauer, S.; Emmett, P.H.; Teller, E. Adsorption of Gases in Multimolecular Layers. *J. Am. Chem. Soc.* **1938**, *60*, 309–319.
43. Gao, C.; Xiao, W.; Ji, G.; Zhang, Y.; Cao, Y.; Han, L. Regularity and mechanism of wheat straw properties change in ball milling process at cellular scale. *Bioresour. Technol.* **2017**, *241*, 214–219.
44. Lu, M.; Li, J.; Han, L.; Xiao, W. An aggregated understanding of cellulase adsorption and hydrolysis for ball-milled cellulose. *Bioresour. Technol.* **2019**, *273*, 1–7.
45. Mochizuki, M.; Hattori, T. Kinetic study of growth throughout the lag phase and the exponential phase of Escherichia coli. *FEMS Microbiol. Lett.* **1987**, *45*, 291–296.
46. Sanders, W.T.M.; Geerink, M.; Zeeman, G.; Lettinga, G. Anaerobic hydrolysis kinetics of particulate substrates. *Water Sci. Technol.* **2000**, *41*, 17–24.
47. Strömberg, S.; Nistor, M.; Liu, J. Early prediction of Biochemical Methane Potential through statistical and kinetic modelling of initial gas production. *Bioresour. Technol.* **2015**, *176*, 233–241.
48. Vavilin, V.A.; Lokshina, L.Y.; Jokela, J.P.Y.; Rintala, J.A. Modeling solid waste decomposition. *Bioresour. Technol.* **2004**, *94*, 69–81.
49. Xiang, Y.; Gubian, S.; Suomela, B.; Hoeng, J. Generalized simulated annealing for global optimization: The GenSA Package. *R. J.* **2013**, *5*, 13–28.
50. Lisowski, A.; Wójcik, J.; Klonowski, J.; Sypuła, M.; Chlebowski, J.; Kostyra, K.; Nowakowski, T.; Strużyk, A.; Świętochowski, A.; Dąbrowska, M.; et al. Compaction of chopped material in a mini silo. *Biomass Bioenergy* **2020**, *139*, 105631.
51. Gaudreault, R.; Van De Ven, T.G.M.; Whitehead, M.A. Mechanisms of flocculation with poly(ethylene oxide) and novel cofactors. *Colloids Surfaces A Physicochem. Eng. Asp.* **2005**, *268*, 131–146.

52. Wang, D.; Shang, S. bin; Song, Z. qian; Lee, M.K. Evaluation of microcrystalline cellulose prepared from kenaf fibers. *J. Ind. Eng. Chem.* **2010**, *16*, 152–156.
53. Ahmadi, M.; Madadlou, A.; Sabouri, A.A. Isolation of micro- and nano-crystalline cellulose particles and fabrication of crystalline particles-loaded whey protein cold-set gel. *Food Chem.* **2015**, *174*, 97–103.
54. Bhimte, N.A.; Tayade, P.T. Evaluation of microcrystalline cellulose prepared from sisal fibers as a tablet excipient: A technical note. *AAPS PharmSciTech* **2007**, *8*, E56–E62.
55. Agarwal, U.P.; Ralph, S.A.; Baez, C.; Reiner, R.S.; Verrill, S.P. Effect of sample moisture content on XRD-estimated cellulose crystallinity index and crystallite size. *Cellulose* **2017**, *24*, 1971–1984.
56. Awa, K.; Shinzawa, H.; Ozaki, Y. The Effect of Microcrystalline Cellulose Crystallinity on the Hydrophilic Property of Tablets and the Hydrolysis of Acetylsalicylic Acid as Active Pharmaceutical Ingredient Inside Tablets. *AAPS PharmSciTech* **2015**, *16*, 865–870.
57. Karimi, K.; Taherzadeh, M.J. A critical review on analysis in pretreatment of lignocelluloses: Degree of polymerization, adsorption/desorption, and accessibility. *Bioresour. Technol.* **2016**, *203*, 348–356.
58. Swinnen, I.A.M.; Bernaerts, K.; Dens, E.J.J.; Geeraerd, A.H.; Van Impe, J.F. Predictive modelling of the microbial lag phase: A review. *Int. J. Food Microbiol.* **2004**, *94*, 137–159.
59. Zheng, Y.; Fu, Z.; Li, D.; Wu, M. Effects of ball milling processes on the microstructure and rheological properties of microcrystalline cellulose as a sustainable polymer additive. *Materials* **2018**, *11*, 1057.
60. Zhang, Q.; Benoit, M.; De Oliveira Vigier, K.; Barrault, J.; Jégou, G.; Philippe, M.; Jérôme, F. Pretreatment of microcrystalline cellulose by ultrasounds: Effect of particle size in the heterogeneously-catalyzed hydrolysis of cellulose to glucose. *Green Chem.* **2013**, *15*, 963–969.
61. Satyamurthy, P.; Jain, P.; Balasubramanya, R.H.; Vigneshwaran, N. Preparation and characterization of cellulose nanowhiskers from cotton fibres by controlled microbial hydrolysis. *Carbohydr. Polym.* **2011**, *83*, 122–129.
62. Eibinger, M.; Ganner, T.; Plank, H.; Nidetzky, B. A Biological Nanomachine at Work: Watching the Cellulosome Degrade Crystalline Cellulose. *ACS Cent. Sci.* **2020**, *6*, 739–746.
63. Bommarius, A.S.; Katona, A.; Cheben, S.E.; Patel, A.S.; Ragauskas, A.J.; Knudson, K.; Pu, Y. Cellulase kinetics as a function of cellulose pretreatment. *Metab. Eng.* **2008**, *10*, 370–381.
64. Momoh, O.L.Y.; Ouki, S. Development of a novel fractal-like kinetic model for elucidating the effect of particle size on the mechanism of hydrolysis and biogas yield from ligno-cellulosic biomass. *Renew. Energy* **2018**, *118*, 71–83.
65. Zhang, Y.; Chen, X.; Gu, Y.; Zhou, X. A physicochemical method for increasing methane production from rice straw: Extrusion combined with alkali pretreatment. *Appl. Energy* **2015**, *160*, 39–48.
66. Mustafa, A.M.; Poulsen, T.G.; Sheng, K. Fungal pretreatment of rice straw with Pleurotus ostreatus and Trichoderma reesei to enhance methane production under solid-state anaerobic digestion. *Appl. Energy* **2016**, *180*, 661–671.
67. Igarashi, K. Traffic jams reduce hydrolytic efficiency of cellulase on cellulose surface. *Science* **2011**, *334*, 1279–1282.
68. Thommes, M.; Kaneko, K.; Neimark, A.V.; Olivier, J.P.; Rodriguez-Reinoso, F.; Rouquerol, J.; Sing, K.S.W. Physisorption of gases, with special reference to the evaluation of surface area and pore size distribution (IUPAC Technical Report). *Pure Appl. Chem.* **2015**, *87*, 1051–1069.
69. Eibinger, M.; Ganner, T.; Bubner, P.; Rošker, S.; Kracher, D.; Haltrich, D.; Ludwig, R.; Plank, H.; Nidetzky, B. Cellulose surface degradation by a lytic polysaccharide monooxygenase and its effect on cellulase hydrolytic efficiency. *J. Biol. Chem.* **2014**, *289*, 35929–35938.

Bioresource Technology 320 (2021) 124262

Contents lists available at ScienceDirect

Bioresource Technology

journal homepage: www.elsevier.com/locate/biortech

The effects of solid lignin on the anaerobic digestion of microcrystalline cellulose and application of smoothing splines for extended data analysis of its inhibitory effects

Michał Piątek *, Aleksander Lisowski, Magdalena Dąbrowska

Department of Biosystems Engineering, Institute of Mechanical Engineering, Warsaw University of Life Sciences, Nowoursynowska 166, 02-787 Warsaw, Poland

HIGHLIGHTS

- A new approach of modelling inhibited anaerobic digestion was presented.
- Developed approach described the long-term inhibitory effects in the batch mode.
- A knowledge gap regarding the impact of solid lignin on methanogens was addressed.
- Solid lignin caused mild inhibition of methanogens.
- Volatile fatty acids accumulation can be induced by high dosages of solid lignin.

ARTICLE INFO

Keywords:
Anaerobic digestion
Cellulose
Lignin
Inhibition
Modelling

ABSTRACT

Lignocellulose is an abundant substrate for biogas production; however, for efficient utilization, proper pre-treatment is required to enhance the biomethane yield and hydrolysis rate significantly. Phenolic compounds from dissolved lignin, produced during alkali pre-treatment, have inhibitory effects on the anaerobic digestion; however, the possible inhibitory effects of solid lignin have not gathered enough interest. Especially, the effect of solid lignin on methanogenesis remains a knowledge gap. In this study, kraft lignin was used as a model solid lignin substrate for its co-digestion with microcrystalline cellulose. A new approach of modelling biomethane production curves using smoothing splines was developed to describe the long-term inhibitory effects of solid lignin on hydrolysis and methanogenesis. The method gives possibility to describe long-term inhibitory effects by using batch instead of continuous test data. Results revealed that kraft lignin showed mild inhibitory effects on methanogens. However lignin impact combined with volatile fatty accumulation can prolong hydrolysis and reactor recovery start-up by 47.3% and 75.3%, respectively. For small dosages of solid lignin adaptation of methanogens is possible.

1. Introduction

Lignocellulose is an abundant source of substrate for biogas production (Mustafa et al., 2016). However, a proper pre-treatment of lignocellulose for its efficient utilization during anaerobic digestion is required to enhance the biogas and biomethane yield significantly (Li et al., 2019). Moreover, a hydrolysis is typically the limiting step of the anaerobic digestion of lignocellulose, and the pre-treatment aims to enhance the hydrolysis rate (De Sanctis et al., 2019; Karimi and Taherzadeh, 2016). The pre-treatment drawback is the formation of inhibitory by-products such as hydroxymethyl furfural (HMF) and furfural (Atelge et al., 2020). It is also known that phenolic compounds from dissolved lignin, produced during alkali pre-treatment, (Lorenci Woiciechowski et al., 2020; Venturin et al., 2018) have inhibitory effects on the anaerobic digestion phases: hydrolysis, acidogenesis, and methanogenesis (Koyama et al., 2017). However, the possible inhibitory effects of the solid lignin that remains after pre-treatment have not gathered enough interest. Especially, the effect of solid lignin on methanogenesis remains a knowledge gap. Uneven inhibition of the anaerobic digestion phases can lead to various imbalances in the process and volatile fatty acid (VFA) accumulation (Ma et al., 2013a; Nguyen et al., 2019), in turn leading to process failure (Nguyen et al., 2019;

* Corresponding author.
E-mail address: michal_piatek@sggw.edu.pl (M. Piątek).

https://doi.org/10.1016/j.biortech.2020.124262
Received 1 August 2020; Received in revised form 7 October 2020; Accepted 10 October 2020
Available online 16 October 2020

Zhang et al., 2018). For this reason, these inhibitory effects must be assessed. Generally, two main methods, the biomethane potential test (BMP) and anaerobic toxicity assay (ATA), are applied to assess such inhibition. ATA is a simple method based on the comparison of biomethane produced from the reference and inhibited samples at a fixed time point (Li et al., 2017). It provides generalized information on the possible inhibition at a chosen time point, which is usually a few days, but not on the microbial community acclimation and biomass growth (Chen et al., 2016). Rapid methods, such as resazurin reduction assay (Chen et al., 2016) and those that utilize luminescent bacteria (Ji et al., 2013), have the same drawbacks as those of ATA. The BMP method used for inhibition assessment is the typical BPM method, according to VDI 4630 (Verein Deutscher Ingenieure, 2014), that has been modified with the presence of an inhibitor in the reactor. Mathematical modelling, frequently using a Modified Gompertz model, is then performed (Li et al., 2018). The drawback of this approach is the inability to model the biphasic process with the curve plateau. Hence, this constitutes a knowledge gap, and modifications of these methods were required (Ma et al., 2013a). The ADM1 model (Batstone et al., 2002) can provide a better insight into the inhibition caused by VFAs (Boubaker and Ridha, 2008). However, since it requires a sophisticated calibration procedure (Arnell et al., 2016), its application is difficult and limited.

In this study, we presented a new, easy to use, heuristic, and flexible approach of inhibition modelling by applying nonparametric modelling with smoothing splines. Presented modelling approach described inhibition based on process phases duration rather than gas production at given, fixed time point. Splines provided an adaptive fit to the data (Jang and Oh, 2011), and thus enabled the possibility of overcoming the parametric model drawbacks, which were related to the assumptions of the priori shape of the curve. They could also be used to model the effects of a chosen inhibitor on hydrolysis and methanogenesis in the presence of naturally accumulated or manually added VFAs. This is important because data on the joint negative effects of inhibitors on processes have rarely been reported (Ji et al., 2013; Tian et al., 2018). In this study, a modelling approach was proposed to investigate the inhibitory effects of solid lignin on the anaerobic digestion of microcrystalline cellulose using balanced among hydrolysis and methanogenesis and imbalanced microbial communities. This approach also allowed us to obtain information on the long-term effects of microbial performance and adaptation in the presence of solid lignin and VFAs. Microcrystalline cellulose and kraft lignin were used, because they are well known substrates, commonly used in anaerobic digestion research. This approach made the research easily reproducible. Kraft lignin is produced in kraft process which includes alkaline lignocellulose pretreatment, thus is suitable to simulate impact of alkali pretreated lignocellulose. This is solid material and can be applied to investigate noncompetitive hydrolysis inhibition (Oliveira et al., 2020). Additionally possible noncompetitive methanogenesis inhibition (Wang et al., 1992) caused by solid lignocellulose can be investigated, which is the main hypothesis for this study.

2. Materials and methods

2.1. Experimental data

This study consisted of two batch trials. In both trials, the microcrystalline cellulose Flocel 102, bought from a local market, and kraft lignin (370959, Sigma-Aldrich, USA) were used. In the first trial, the microcrystalline cellulose was blended with kraft lignin in various mass ratios, from 10:3 up to 10:20. In the second trial, sucrose was used as the additional material, to obtain better insight on direct lignin impact on methanogenesis. Each sample of the material was weighed on the WPS 600/C electronic scale (Radwag, Radom, Poland), which had an accuracy of 0.01 g. All tests were performed using 2 dm^3 glass. The inoculum was obtained from a mesophilic, agricultural biogas plant post-digester. The main substrate for the biogas plant was maize silage. Reactors, after being filled with substrates and the inoculum (1800 mL), were flushed with nitrogen and placed in a water bath, which was operated at 37 °C. The contents of the reactors were manually mixed once a day. The amount of gas produced was measured by a brine displacement method (Ran et al., 2018; Xin et al., 2018). Displaced brine was weighed on the WLC.X2 electronic scale (Radwag, Radom, Poland), which had an accuracy of 0.1 g. The batch trials were conducted in triplicate simultaneously. The volume of the obtained biogas was converted to the standard conditions (1013 hPa, 273 K). The composition of the gas was analysed using a Gas Data GFM 406 portable gas analyser (Gas Data Limited, United Kingdom). The percentages of CH_4 and CO_2 were measured with an accuracy of ±1% by pumping the displaced brine backwards into the bottle, which was directly connected to the reactor. The pH was measured using a WTW ProfiLine pH 3110 pH meter equipped with a SenTix® 41electrode (Xylem Inc.), which had an accuracy of ±0.01.

2.1.1. First batch test

The aim the first trial was to investigate kraft lignin impact, especially on methanogenesis, when methanogenesis was a process limiting step. The inoculum for the first trial was firstly used in the preceding trial, for which microcrystalline cellulose was used as sole substrate. Trial was conducted in 37 C. Then inoculum was stored for about four of months at room temperature (20 ± 2 °C). Six microcrystalline cellulose (10 g) samples were placed in reactors, and kraft lignin (3 g, 7 g, 10 g, 13 g, 17 g, and 20 g) was added as a co-substrate. Cellulose moisture content was 5.01 ± 0.23%. Samples of cellulose (10 g) and lignin (20 g) only were also prepared. An inoculum (1800 mL) sample without added substrates was used as a blank. The amount of inoculum organic dry matter in each reactor was 30 g. The cellulose to inoculum volatile solids mass ratio was 1:3. The pH of the inoculum was 8.01, and no significant differences among the samples after addition of lignin were observed. At this pH, kraft lignin was insoluble in water (Konduri and Fatehi, 2015). The tests were performed until no significant change in the biogas production was observed. The maximum duration of the first batch test was 70 d.

2.1.2. Second batch test

The second trial with sucrose was conducted to obtain better insight into kraft lignin impact on hydrolysis and methanogenesis, when fresh, balanced inoculum is used. The second trial was conducted using a fresh inoculum from the same biogas plant. An inoculum (1800 mL) sample without added substrates was used as a blank (24 g of organic dry matter was present in the inoculum in each reactor). Samples of cellulose (10 g) only and those with kraft lignin (10 g and 20 g), which was added as a co-substrate, were prepared as described for the previous trial. The cellulose to inoculum organic dry mater ratio was 1:2.4. Additionally, the sucrose hydrolysate was prepared. To hydrolyse sucrose, sucrose (50 g) was blended with the inoculum (1 dm^3) and placed in a water bath at 37 °C for 72 h. The hydrolysate (100 mL) was then poured into each hydrolysate sample in the reactors. Then, kraft lignin (10 g and 20 g) was added as a co-substrate in two or three hydrolysate samples. The reactors were filled with the inoculum (1800 mL). The pH values of the inoculum and hydrolysate were 8.25 and 7.24, respectively. The hydrolysate (100 mL) was blended with the rest of the inoculum, and the pH of the resultant mixture was 8.22. The experiment using cellulose samples was conducted for 30 d. The hydrolysate samples were tested for only 10 d because only the initial rate of the process was in the scope of this experiment.

2.2. Curve fitting

The cumulative biomethane production curves obtained in the first trial were fitted using smoothing splines ("smooth.spline" function from the "splines" library in "R" package). Curves were fitted by the generalized cross-validation method (GCV) to avoid overfitting. All distinct

points were used as spline knots. Since the values of the cumulative production curves were significantly lower at the beginning of the process, weights were used during the approximation process to underscore the importance of the first few days of production. The reciprocal of the measured cumulative biomethane production values were used to calculate the values of the weights. This approach was chosen based on the author's experience. The remaining parameters were set at default. The "smooth.spline" function allowed us to calculate the derivatives of the cumulative production curves. Since the curve was smoothed using the spline model, it was possible to interpret the dynamics of the process using derivatives, especially the points at which the first derivative changed its direction. This was consistent with the change in the production rate at the chosen time. In this study, 1 h was chosen as the time interval; therefore, the first derivative referred to the biomethane production per hour. Smoothing spline application enabled us to obtain precise data on the production rate, even when the measurements were taken at different time intervals (this can be an issue if the stand is not automated). The characteristic points of the first derivative were chosen manually for all curves and described in detail in the next section.

Cellulose samples in the second trial were modelled using the Modified Gompertz Model (Akobi et al., 2016; Li et al., 2018) by the least squares method:

$$B = B_0 exp\left\{ -exp\left[\frac{\mu e}{B_0}(\lambda - t) + 1\right]\right\} \quad (1)$$

where B is the actual measured value of cumulative biomethane production (NmL·g^{-1}); B_0 is the maximum modelled cumulative biomethane production (NmL·g^{-1}); μ is the maximum production rate (NmL·g^{-1}·d^{-1}); e is the Euler number; and λ is the duration of the lag phase (d).

2.3. Statistical analysis

The Kruskal-Wallis test was used to compare the whole biogas production curves. The cumulative biogas production values were compared using analysis of variance. Levene's test for homogeneity of variance and Shapiro-Wilk normality test were used to check the validity of the assumptions made for the analysis of variance. Linear regression was performed using the "lm" function from the "stats" library. Differences and regression parameters were considered statistically significant at $p \leq 0.05$. All analyses, including curve fitting, were conducted using the "R" package (version 3.5.1).

3. Results and discussion

3.1. Results and analysis of the first batch test

No significant gas productions were observed from the blank (reactors with sole inoculum) and reactors with inoculum and kraft lignin only (without cellulose). It could be concluded that storage of the inoculum for a long time caused complete degasification and no biomethane production. This indicated that no soluble lignin-derived compounds were present in the reactors because some compounds, such as syringaldehyde, contrary to solid lignin, could be used by the microorganisms as substrates (Barakat et al., 2012). Gas production was observed from all the cellulose samples. Analysis of variance for biomethane yield revealed no significant differences among the different lignin samples (p-value = 0.313), and this result was surprisingly not in line with previously reported results (Li et al., 2018). However, the biomethane yield could be fitted with the full cellulose potential (355.7 ± 13.4 (NmL·g^{-1}), indicating that competitive inhibition mechanism did not occur. This supported the hypothesis that lignin in lignocellulose acted as a physical barrier rather than a competitive inhibitor (Djajadi et al., 2018).

The curve of the reference sample (10 g of cellulose only) had an unusual shape (data was shown in Supplementary material). Firstly curve, looks like did not reach the plateau at end, however test was terminated according to VDI 4630 (Verein Deutscher Ingenieure, 2014). This effect was caused by low process rate ang long test duration. Secondly, after the lag phase, a rapid increase in biomethane production, followed by a slowdown in production, was observed, and a sigmoidal curve was obtained, indicating disturbances in the process. Since storage of the inoculum for a long time caused complete degasification, it could have also caused a deterioration in the microbial population, especially methanogens, which are more vulnerable to unfavourable process conditions than hydrolytic, acidogenic, and syntrophic acetogenic bacteria (Wintsche et al., 2018). Typically, the growth time of methanogens is longer than that of bacteria involved in the preceding steps of anaerobic digestion (Manyi-Loh et al., 2013). It takes 4–6 days for the microbial population to double (De Vrieze et al., 2012), and hence it is more difficult for the methanogens to recover, resulting in imbalances in the microbial population. The proper balance of microbial communities is crucial for the process to be conducted properly (Angelidaki et al., 2009; Ma et al., 2013b). This must be taken into account according to several batch test protocols, which advise using fresh inoculum or inoculum that has been degassed up to for 7 d at the test temperature (Angelidaki et al., 2009; Holliger et al., 2016; Verein Deutscher Ingenieure, 2014). The conditions for extended storage of inoculum in anaerobic conditions is one month at 35 °C (Verein Deutscher Ingenieure, 2014). Notably, the inoculum used in this trial was also used in the previous trial, for which microcrystalline cellulose was used as a sole substrate and no process disturbances were observed. Data from the above-mentioned experiment have not been published yet. Repetition of a batch test with the digestate from a preceding test is allowed according to standard protocol (Verein Deutscher Ingenieure, 2014). Usually hydrolysis is the rate limiting step of anaerobic digestion of cellulose (Jeihanipour et al., 2011). However, it is highly possible that methanogenesis was the rate limiting step in this study due to the low growth rate of methanogens, thus causing VFA accumulation and inhibition (Manyi-Loh et al., 2013; Yeh et al., 2010).

Addition of kraft lignin enhanced this phenomenon, thus prolonging the overall process time. To describe this phenomenon, modelling with smoothing splines was performed. The results are shown in. Arrows in Fig. 1 indicate the three characteristic points. This points refers to significant turning process moments, when VFA inhibition alters the process dynamics. The first point (left arrow) refers to the drop in the biomethane production rate, and can be interpreted as the point at which the accumulation of hydrolysis products begins to impact the process rate. The second point (middle arrow) indicates the maximum inhibition, which is related to the maximum VFA accumulation. This point does not occur if the microbial community is not overloaded. In that case, the initial production rate rises and then declines monotonically until the end of the process (Khalid et al., 2019). If methanogen overload does occur, VFA accumulation further causes methanogenesis depression and a drop in the production rate (Ma et al., 2013a). This can lead to process failure or recovery. In this trial, process recovery was observed because the full biomethane potential was utilized, as previously mentioned. The third point (right arrow) indicates a full recovery and the end of significant inhibition. After that point, there is a further drop in the production rate due to depletion of the substrate. The time of occurrence (Fig. 1) and cumulative biomethane production at these points are shown in Table 1. Linear regression analysis showed that there was no significant relation between biomethane production at a given point and lignin addition. p-values of the slopes at points 1, 2, and 3 were 0.0954, 0.0878, and 0.8504, respectively. This suggested that presence of lignin did not impact the VFA inhibition threshold, and this type of inhibitors exhibited additive, rather than synergetic, effects on the process.

These three points (Fig. 1) were used to construct three intervals. The first interval (0–1) extended from the beginning of the process to point 1

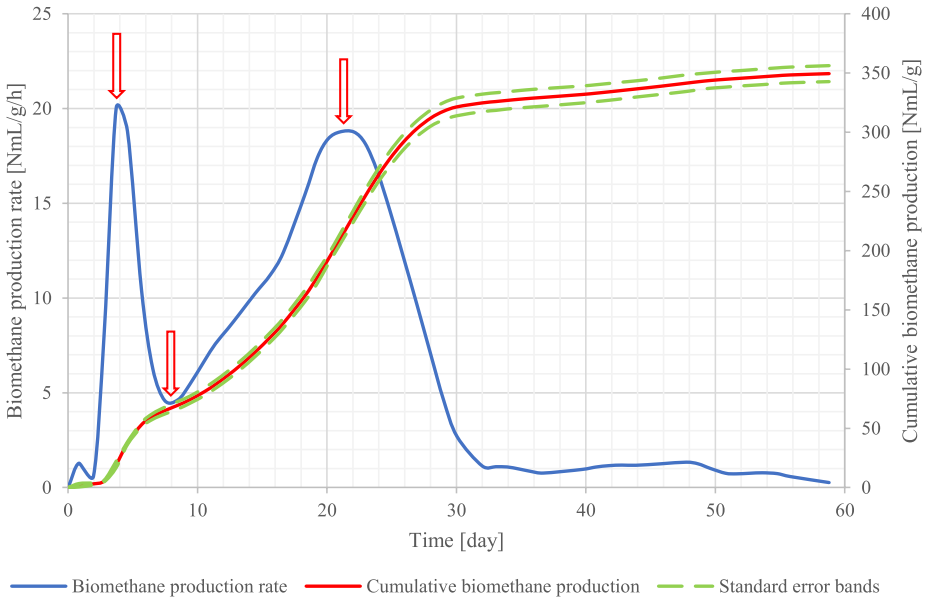

Fig. 1. Smoothing spline-modelled cumulative biomethane production and biomethane production rates of the reference sample (10 g of cellulose only). The two peaks curve is modelled using first smoothing spline model derivative and refers to hourly process rate. The red left, middle, and right arrows indicate characteristic turning points 1, 2, and 3, respectively. (For interpretation of the references to colour in this figure legend, the reader is referred to the web version of this article.)

Table 1
The time of occurrence and spline modelled cumulative biomethane production at the characteristic points.

Lignin addition [g]	Start of inhibition (point 1)		Maximum inhibition (point 2)		End of inhibition (point 3)	
	Time of occurrence [h]	Cumulative biomethane production [NmL·g^{-1}]	Time of occurrence [h]	Cumulative biomethane production [NmL·g^{-1}]	Time of occurrence [h]	Cumulative biomethane production [NmL·g^{-1}]
0	99	28.13	193	67.51	519	221.34
3	91	24.07	197	71.02	468	202.64
7	109	26.15	231	66.82	482	161.58
10	126	26.12	253	65.42	572	178.34
13	142	25.76	283	60.97	875	237.82
17	153	25.14	422	65.12	953	198.61
20	188	19.13	568	64.07	1129	211.16

(the beginning of inhibition). The second interval (1–2) extended from points 1 (the beginning of inhibition) to 2 (maximum inhibition), and the third interval (2–3) extended from points 2 (maximum inhibition) to 3 (the end of inhibition). The duration of the intervals was used to calculate relative inhibition using the equation:

$$I = \left(1 - \frac{T_R}{T_L}\right) \cdot 100\% \quad (2)$$

where I is the relative inhibition during the chosen interval (%); T_R is the duration of the interval for the reference sample (h); and T_L is the duration of the interval for the lignin inhibited sample (h).

This equation differed slightly from the equation used to calculate inhibition based on the measured gas volume at a fixed time because in this approach, time was prolonged, while in the alternative method, gas volume was decreased; therefore, the denominator in this equation was the duration of the interval for the lignin inhibited sample (Gartiser et al., 2007; Li et al., 2017). The inhibition values obtained for samples with different amounts of added lignin using the durations of the three intervals are shown in Table 2. The relative inhibition values were analysed for each interval separately using linear regression. The parameters of the regression equations are shown in Table 3. In this study, the lag phase, which occurred during anaerobic digestion of cellulose, was not analysed separately (Yu et al., 2012). This modelling approach enabled us to model the lag phase separately. However, to obtain a curve with the underlined lag phase, biomethane production must occur from

Table 2
Inhibition percentages at the characteristic points on addition of different amounts of lignin.

Lignin addition [g]	Inhibition during interval 0–1 [%]	Inhibition during interval 1–2 [%]	Inhibition during interval 2–3 [%]
0	0.00	0.00	0.00
3	−8.79	11.32	−26.11
7	9.17	22.95	−59.86
10	21.43	25.98	−17.62
13	30.28	33.33	49.56
17	35.29	65.06	39.95
20	47.34	75.26	39.14

Table 3
The parameters of linear models for inhibition percentages in function of lignin addition at the characteristic points.

Interval	Intercept [%]		Slope [%·g^{-1}]		Slope p-value	R^2
	Estimate	Standard error	Estimate	Standard error		
0–1	−7.50	3.95	2.68	0.33	0.0004	0.9200
1–2	−3.29	4.93	3.67	0.41	0.0003	0.9299
2–3	−33.83	22.78	3.74	1.89	0.1048	0.3270

the blank sample and net gas production must be calculated and modelled. In this study, the first interval jointly represented the inhibition of the lag phase and the start of VFA inhibition. During the first interval, inhibition increased significantly with the addition of lignin to the samples. Linear regression for the first interval is shown in Fig. 2. This confirmed that lignin impacted the hydrolysis inhibition linearly; however, at a higher dose of lignin, this relation can't be hold. On addition of 3 g of lignin, the inhibition was −8.79% (Table 2), indicating that a low dose of lignin did not negatively impact hydrolysis.

The duration of interval 1–2 was significantly prolonged on addition of lignin to the samples. The effects of addition of lignin on inhibition in the second interval are shown in Fig. 3. A linear relationship was observed. Interval 0–1 showed linear inhibition of hydrolysis by lignin; thus, the effects of lignin in interval 0–1 must impact interval 1–2. It can be stated that in conditions, where the hydrolysis rate is low and a long duration is required to reach maximum inhibition, methanogens are also inhibited because methanogens consume VFAs, which are provided to them by hydrolysis. Hence, in the case of no methanogens inhibition, the accumulation of hydrolysis products should be overcome faster with the increase in the amount of lignin added. A similar shape of the curve for microcrystalline cellulose was obtained in a previous study (Li et al., 2017), in which the ionic liquid was used as an inhibitor. It is known that ionic liquids inhibit cellulases (Nemestóthy et al., 2017; Summers et al., 2017) and methanogenesis (Duan et al., 2013; Li and Xu, 2017). Methanogenesis inhibition by lignin has been reported previously (Yin et al., 2000); however, it was found that the negative effects of lignin compounds on methanogens differ considerably (Sierra-Alvarez and Lettinga, 1991).

Interval 2–3 is the period from maximum inhibition to the end of inhibition. In this case, a linear relationship was not significant (for the slope, p-value = 0.327). Inhibition in interval 2–3 data was shown in Supplementary material. During this interval, samples with 13 g, 17 g, and 20 g of added lignin were 49.56%, 39.95%, and 39.14% inhibited, respectively, while samples with 3 g, 7 g, and 10 g of added lignin were stimulated by the lignin and −26.11%, −59.86%, and −17.62% inhibited, respectively (Table 2). The positive effects of addition of small amounts of lignin could be explained by mild inhibition, along with the possibility of inhibitor neutralization and growth stimulation of methanogens due to the presence of greater amounts of solid particles in the reactors. The growth promoting effects of kraft lignin have been previously reported (Pilarska et al., 2018, 2019); however, it was found that higher dosages suppress these positive effects.

3.2. Results and analysis of the second batch test

Since the curve of the reference sample in the first test exhibited a typical shape, the test was repeated with several modifications. The curve of the reference sample (10 g of cellulose only) exhibited a regular course, which data was shown in Supplementary material. After the lag phase, uninterrupted biomethane production occurred until a plateau was reached at the end of the process. The curves of samples with 10 g and 20 g of added lignin have analogous courses. All curves were modelled using the Modified Gompertz model. The results are presented in Table 4. Modelling revealed a decrease in the biomethane production caused by lignin addition, and this was confirmed by analysis of variance (p-value = 0.002). The biomethane yield from samples with 10 g and 20 g added lignin, in reference to the pure cellulose sample, was found to be decreased by 17% and 28%, respectively. It could be concluded that competitive inhibition mechanism occurred, despite the fact that the same substrates were used in both trials and only the inocula differed. The pH values of the inocula were similar in both trials (8.01 in the first trial and 8.25 in the second trial). In the second trial, fresh inoculum from a steady-state operating agricultural anaerobic digestion plant was used, and hence, we could assume that a balanced microbial population was present. Analysis of data shown in Supplementary material indicates that no significant VFA inhibition occurred. However, the maximum production rate decreased by 37% and 55% on addition of 10 g and 20 g lignin, respectively, indicating that uncompetitive hydrolysis inhibition occurred. Additionally, the lag phase was significantly prolonged from 3.8 d for the reference sample to 6.5 d and 8.0 d for the samples with 10 g and 20 g of added lignin, respectively (Table 4). Despite hydrolysis inhibition, no disturbances in the process were observed; hence, hydrolysis was the limiting step of the process.

To assess the effects of lignin on the fresh inoculum sucrose, hydrolysates with 10 g and 20 g of added lignin were fermented for 10 d. Kruskal-Wallis test indicated no significant differences between the curves (p-value = 0.9967). This result, combined with the results of the previous trial, led to the conclusion that inhibitory effects of lignin could be observed only when the proportion of the lignin dosage to the active methanogen population was high. It was also previously observed that a

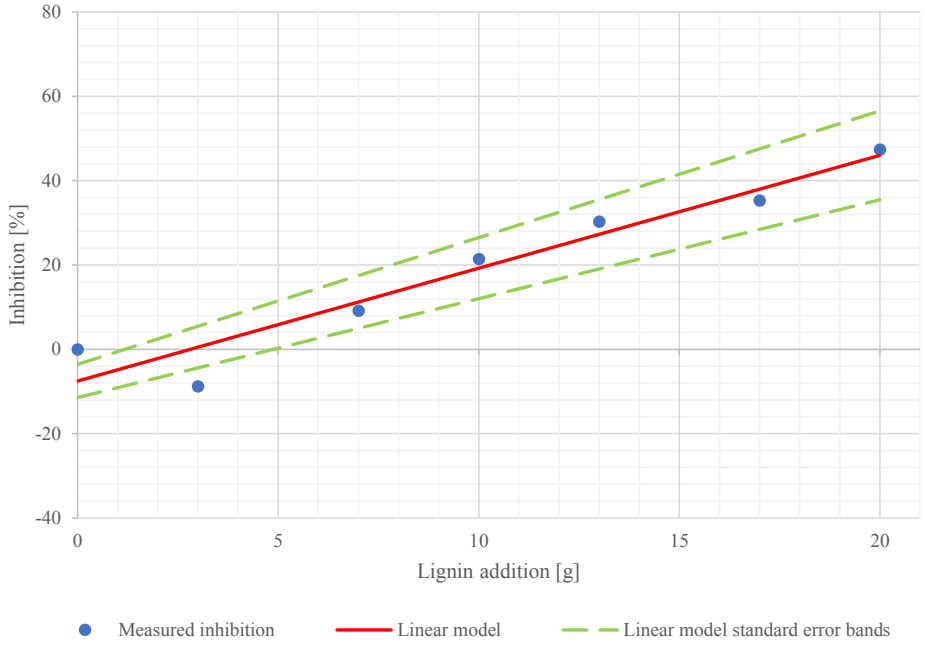

Fig. 2. The linear regression results for interval 0–1.

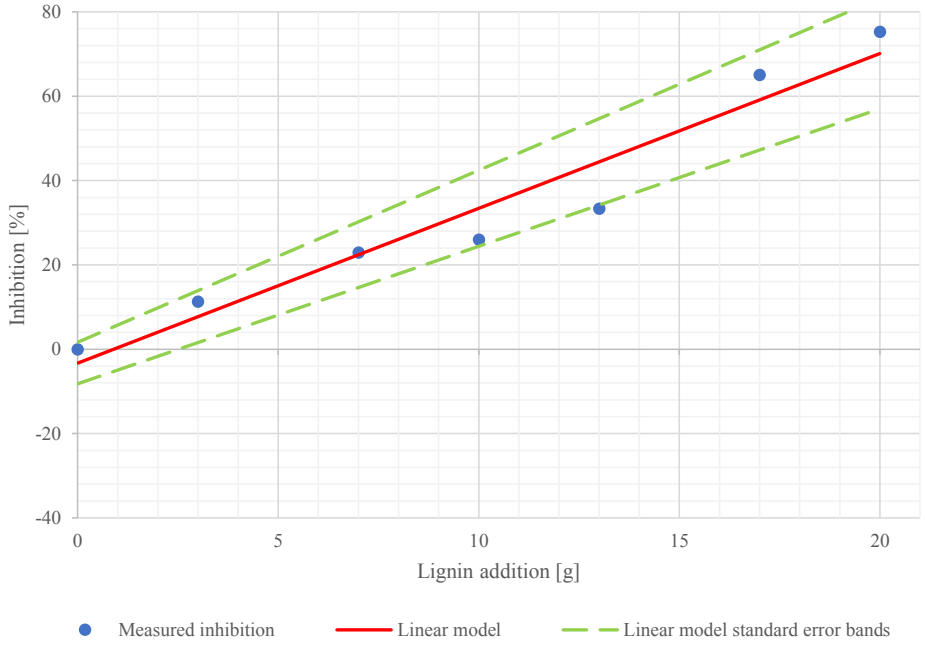

Fig. 3. The linear regression results for interval 1–2.

Table 4
The estimated parameters of the Modified Gompertz model.

Lignin addition [g]	B_0 [NmL·g^{-1}]		μ [NmL·g^{-1}·d^{-1}]		λ [d]	
	Estimate	Standard error	Estimate	Standard error	Estimate	Standard error
0	368.78	4.33	44.60	2.71	3.78	0.26
10	304.82	2.45	28.28	0.78	6.51	0.15
20	265.45	2.78	19.95	0.48	8.01	0.15

high concentration of microbial communities could overcome the inhibition (Ma et al., 2013a). This could be a problem during the dry anaerobic digestion of lignocellulose, which is a promising method for anaerobic digestion of straw (Ge et al., 2016; Zhu et al., 2010). An imbalanced microbial community is required to test mild inhibitory effects on methanogenesis. However, the use of a microbial community weakened due to long-term storage, as presented in the first trial, was definitely not time-efficient. A rapid method for the production of imbalanced cultures in different ratios was developed in a different study (Ma et al., 2013a).

4. Conclusions

In this study, anaerobic digestion of microcrystalline cellulose in the presence of kraft lignin was investigated. A new smoothing spline modelling approach was applied. This method was well suited for the estimation of inhibition by compounds, which did not directly impact cellulose yield. Additional research is required to investigate the method for other compounds. On application of the presented approach, the inhibitory effects of kraft lignin on anaerobic digestion were investigated, and it was revealed that kraft lignin showed mild inhibitory effects on methanogenesis, possibly due to noncompetitive inhibition. This approach can be applied in further research to investigate the mitigation of methanogen inhibition.

CRediT authorship contribution statement

Michał Piątek: Conceptualization, Investigation, Methodology, Software, Resources, Writing - original draft. **Aleksander Lisowski:** Writing - review & editing, Supervision. **Magdalena Dąbrowska:** Writing - review & editing.

Declaration of Competing Interest

The authors declare that they have no known competing financial interests or personal relationships that could have appeared to influence the work reported in this paper.

Appendix A. Supplementary data

Supplementary data to this article can be found online at https://doi.org/10.1016/j.biortech.2020.124262.

References

Akobi, C., Yeo, H., Hafez, H., Nakhla, G., 2016. Single-stage and two-stage anaerobic digestion of extruded lignocellulosic biomass. Appl. Energy 184, 548–559.
Angelidaki, I., Alves, M., Bolzonella, D., Borzacconi, L., Campos, J.L., Guwy, A.J., Kalyuzhnyi, S., Jenicek, P., Van Lier, J.B., 2009. Defining the biomethane potential (BMP) of solid organic wastes and energy crops: a proposed protocol for batch assays. Water Sci. Technol. 59, 927–934.
Arnell, M., Astals, S., Åmand, L., Batstone, D.J., Jensen, P.D., Jeppsson, U., 2016. Modelling anaerobic co-digestion in Benchmark Simulation Model No. 2: parameter estimation, substrate characterisation and plant-wide integration. Water Res. 98, 138–146.
Atelge, M.R., Atabani, A.E., Banu, J.R., Krisa, D., Kaya, M., Eskicioglu, C., Kumar, G., Lee, C., Yildiz, Y., Unalan, S., Mohanasundaram, R., Duman, F., 2020. A critical review of pretreatment technologies to enhance anaerobic digestion and energy recovery. Fuel 270, 117494.
Barakat, A., Monlau, F., Steyer, J.P., Carrere, H., 2012. Effect of lignin-derived and furan compounds found in lignocellulosic hydrolysates on biomethane production. Bioresour. Technol. 104, 90–99.
Batstone, D.J., Keller, J., Angelidaki, I., Kalyuzhnyi, S.V., Pavlostathis, S.G., Rozzi, A., Sanders, W.T., Siegrist, H., Vavilin, V.A., 2002. The IWA anaerobic digestion model No 1 (ADM1). Water Sci. Technol. 45, 65–73.

Boubaker, F., Ridha, B.C., 2008. Modelling of the mesophilic anaerobic co-digestion of olive mill wastewater with olive mill solid waste using anaerobic digestion model No. 1 (ADM1). Bioresour. Technol. 99, 6565–6577.
Chen, J.L., Steele, T.W.J., Stuckey, D.C., 2016. Stimulation and inhibition of anaerobic digestion by nickel and cobalt: a rapid assessment using the resazurin reduction assay. Environ. Sci. Technol. 50, 11154–11163.
De Sanctis, M., Chimienti, S., Pastore, C., Piergrossi, V., Di Iaconi, C., 2019. Energy efficiency improvement of thermal hydrolysis and anaerobic digestion of Posidonia oceanica residues. Appl. Energy 252, 113457.
De Vrieze, J., Hennebel, T., Boon, N., Verstraete, W., 2012. Methanosarcina: the rediscovered methanogen for heavy duty biomethanation. Bioresour. Technol. 112, 1–9.
Djajadi, D.T., Jensen, M.M., Oliveira, M., Jensen, A., Thygesen, L.G., Pinelo, M., Glasius, M., Jørgensen, H., Meyer, A.S., 2018. Lignin from hydrothermally pretreated grass biomass retards enzymatic cellulose degradation by acting as a physical barrier rather than by inducing nonproductive adsorption of enzymes. Biotechnol. Biofuels 11, 1–13.
Duan, E., Li, Z., Liu, J., Liu, Y., Song, Y., Guan, J., Yang, K., 2013. Anaerobic biodegradability and toxicity of caprolactam-tetrabutyl ammonium bromide ionic liquid to methanogenic gas production. RSC Adv. 3, 18817–18820.
Gartiser, S., Urich, E., Alexy, R., Kümmerer, K., 2007. Anaerobic inhibition and biodegradation of antibiotics in ISO test schemes. Chemosphere 66, 1839–1848.
Ge, X., Xu, F., Li, Y., 2016. Solid-state anaerobic digestion of lignocellulosic biomass: recent progress and perspectives. Bioresour. Technol. 205, 239–249.
Holliger, C., Alves, M., Andrade, D., Angelidaki, I., Astals, S., Baier, U., Bougrier, C., Buffière, P., Carballa, M., De Wilde, V., Ebertseder, F., Fernández, B., Ficara, E., Fotidis, I., Frigon, J.C., De Laclos, H.F., Ghasimi, D.S.M., Hack, G., Hartel, M., Heerenklage, J., Horvath, I.S., Jenicek, P., Koch, K., Krautwald, J., Lizasoain, J., Liu, J., Mosberger, L., Nistor, M., Oechsner, H., Oliveira, J.V., Paterson, M., Pauss, A., Pommier, S., Porqueddu, I., Raposo, F., Ribeiro, T., Pfund, F.R., Strömberg, S., Torrijos, M., Van Eekert, M., Van Lier, J., Wedwitschka, H., Wierinck, I., 2016. Towards a standardization of biomethane potential tests. Water Sci. Technol. 74, 2515–2522.
Jang, D., Oh, H.S., 2011. Enhancement of spatially adaptive smoothing splines via parameterization of smoothing parameters. Comput. Stat. Data Anal. 55, 1029–1040.
Jeihanipour, A., Niklasson, C., Taherzadeh, M.J., 2011. Enhancement of solubilization rate of cellulose in anaerobic digestion and its drawbacks. Process. Biochem. 46, 1509–1514.
Ji, J.Y., Xing, Y.J., Ma, Z.T., Cai, J., Zheng, P., Lu, H.F., 2013. Toxicity assessment of anaerobic digestion intermediates and antibiotics in pharmaceutical wastewater by luminescent bacterium. J. Hazard. Mater. 246–247, 319–323.
Karimi, K., Taherzadeh, M.J., 2016. A critical review on analysis in pretreatment of lignocelluloses: degree of polymerization, adsorption/desorption, and accessibility. Bioresour. Technol. 203, 348–356.
Khalid, M.J., Zeshan, Waqas, A., Nawaz, I., 2019. Synergistic effect of alkaline pretreatment and magnetite nanoparticle application on biogas production from rice straw. Bioresour. Technol. 275, 288–296.
Konduri, M.K.R., Fatehi, P., 2015. Production of water-soluble hardwood kraft lignin via sulfomethylation using formaldehyde and sodium sulfite. ACS Sustain. Chem. Eng. 3, 1172–1182.
Koyama, M., Yamamoto, S., Ishikawa, K., Ban, S., Toda, T., 2017. Inhibition of anaerobic digestion by dissolved lignin derived from alkaline pre-treatment of an aquatic macrophyte. Chem. Eng. J. 311, 55–62.
Li, W., Khalid, H., Zhu, Z., Zhang, R., Liu, G., Chen, C., Thorin, E., 2018. Methane production through anaerobic digestion: participation and digestion characteristics of cellulose, hemicellulose and lignin. Appl. Energy 226, 1219–1228.
Li, W., Xu, G., 2017. Enhancement of anaerobic digestion of grass by pretreatment with imidazolium-based ionic liquids. Environ. Technol. (United Kingdom) 38, 1843–1851.
Li, X., Schwede, S., Li, H., Yu, X., Yu, Z., Zhu, K., 2017. Toxicity of ionic liquid on anaerobic digestion. Energy Procedia 142, 938–942.
Li, Y., Chen, Y., Wu, J., 2019. Enhancement of methane production in anaerobic digestion process: A review. Appl. Energy 240, 120–137.
Lorenci Woiciechowski, A., Dalmas Neto, C.J., de Souza, Porto, Vandenberghe, L., de Carvalho Neto, D.P., Novak Sydney, A.C., Letti, L.A.J., Karp, S.G., Zevallos Torres, L. A., Soccol, C.R., 2020. Lignocellulosic biomass: Acid and alkaline pretreatments and their effects on biomass recalcitrance – conventional processing and recent advances. Bioresour. Technol. 304, 122848.
Ma, J., Frear, C., Wang, Z.W., Yu, L., Zhao, Q., Li, X., Chen, S., 2013a. A simple methodology for rate-limiting step determination for anaerobic digestion of complex substrates and effect of microbial community ratio. Bioresour. Technol. 134, 391–395.
Ma, J., Yu, L., Frear, C., Zhao, Q., Li, X., Chen, S., 2013b. Kinetics of psychrophilic anaerobic sequencing batch reactor treating flushed dairy manure. Bioresour. Technol. 131, 6–12.
Manyi-Loh, C.E., Mamphweli, S.N., Meyer, E.L., Okoh, A.I., Makaka, G., Simon, M., 2013. Microbial anaerobic digestion (bio-digesters) as an approach to the decontamination of animal wastes in pollution control and the generation of renewable energy. Int. J. Environ. Res. Public Health 10, 4390–4417.
Mustafa, A.M., Poulsen, T.G., Sheng, K., 2016. Fungal pretreatment of rice straw with Pleurotus ostreatus and Trichoderma reesei to enhance methane production under solid-state anaerobic digestion. Appl. Energy 180, 661–671.
Nemestóthy, N., Megyeri, G., Bakonyi, P., Lakatos, P., Koók, L., Polakovic, M., Gubicza, L., Bélafi-Bakó, K., 2017. Enzyme kinetics approach to assess biocatalyst inhibition and deactivation caused by [bmim][Cl] ionic liquid during cellulose hydrolysis. Bioresour. Technol. 229, 190–195.
Nguyen, D., Wu, Z., Shrestha, S., Lee, P.H., Raskin, L., Khanal, S.K., 2019. Intermittent micro-aeration: New strategy to control volatile fatty acid accumulation in high organic loading anaerobic digestion. Water Res. 166, 115080.
Oliveira, D.M., Hoshino, É.P., Mota, T.R., Marchiosi, R., Ferrarese-Filho, O., dos Santos, W.D., 2020. Modulation of cellulase activity by lignin-related compounds. Bioresour. Technol. Reports 10, 100390.
Pilarska, A.A., Wolna-Maruwka, A., Pilarski, K., 2018. Kraft lignin grafted with polyvinylpyrrolidone as a novel microbial carrier in biogas production. Energies 11.
Pilarska, A.A., Wolna-Maruwka, A., Pilarski, K., Janczak, D., Przybył, K., Gawrysiak-Witulska, M., 2019. The use of lignin as a microbial carrier in the co-digestion of cheese and wafer waste. Polymers (Basel) 11.
Ran, G., Li, D., Zheng, T., Liu, X., Chen, L., Cao, Q., Yan, Z., 2018. Hydrothermal pretreatment on the anaerobic digestion of washed vinegar residue. Bioresour. Technol. 248, 265–271.
Sierra-Alvarez, R., Lettinga, G., 1991. The methanogenic toxicity of wastewater lignins and lignin related compounds. J. Chem. Technol. Biotechnol. 50, 443–455. https://doi.org/10.1002/jctb.280500403.
Summers, S.R., Sprenger, K.G., Pfaendtner, J., Marchant, J., Summers, M.F., Kaar, J.L., 2017. Mechanism of Competitive Inhibition and Destabilization of Acidothermus cellulolyticus Endoglucanase 1 by Ionic Liquids. J. Phys. Chem. B 121, 10793–10803.
Tian, H., Karachalios, P., Angelidaki, I., Fotidis, I.A., 2018. A proposed mechanism for the ammonia-LCFA synergetic co-inhibition effect on anaerobic digestion process. Chem. Eng. J. 349, 574–580.
Venturin, B., Frumi Camargo, A., Scapini, T., Mulinari, J., Bonatto, C., Bazoti, S., Pereira Siqueira, D., Maria Colla, L., Alves, S.L., Paulo Bender, J., Luís Radis Steinmetz, R., Kunz, A., Fongaro, G., Treichel, H., 2018. Effect of pretreatments on corn stalk chemical properties for biogas production purposes. Bioresour. Technol. 266, 116–124.
Verein Deutscher Ingenieure, 2014. VDI 4630 – Gärsubstrate.
Wang, B.Y., Gabbard, H.D., Pai, P., 1992. Inhibition of acetate methanogenesis by phenols. J. Environ. Eng. 117, 487–500.
Wintsche, B., Jehmlich, N., Popp, D., Harms, H., Kleinsteuber, S., 2018. Metabolic adaptation of methanogens in anaerobic digesters upon trace element limitation. Front. Microbiol. 9, 1–10.
Xin, L., Guo, Z., Xiao, X., Xu, W., Geng, R., Wang, W., 2018. Feasibility of anaerobic digestion for contaminated rice straw inoculated with waste activated sludge. Bioresour. Technol. 266, 45–50.
Yeh, A.I., Huang, Y.C., Chen, S.H., 2010. Effect of particle size on the rate of enzymatic hydrolysis of cellulose. Carbohydr. Polym. 79, 192–199.
Yin, C.R., Seo, D.Il, Kim, M.K., Lee, S.T., 2000. Inhibitory effect of hardwood lignin on acetate-utilizing methanogens in anaerobic digester sludge. Biotechnol. Lett. 22, 1531–1535.
Yu, L., Chen, Z.X., Tong, X., Li, K., Li, W.W., 2012. Anaerobic degradation of microcrystalline cellulose: Kinetics and micro-scale structure evolution. Chemosphere 86, 348–353.
Zhang, W., Xing, W., Li, R., 2018. Real-time recovery strategies for volatile fatty acid-inhibited anaerobic digestion of food waste for methane production. Bioresour. Technol. 265, 82–92.
Zhu, J., Wan, C., Li, Y., 2010. Enhanced solid-state anaerobic digestion of corn stover by alkaline pretreatment. Bioresour. Technol. 101, 7523–7528.

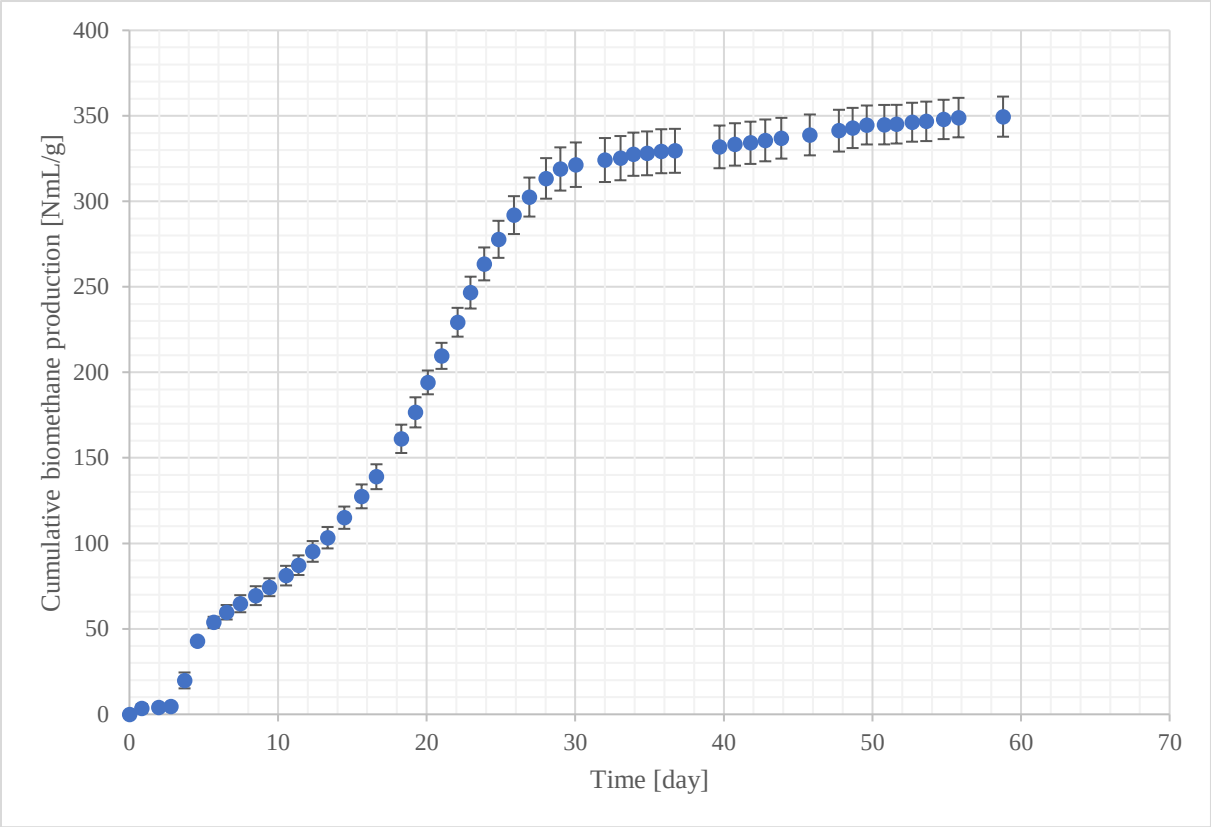

Figure S1. The biomethane production curve of the reference sample (10 g of cellulose only) in the first batch test.

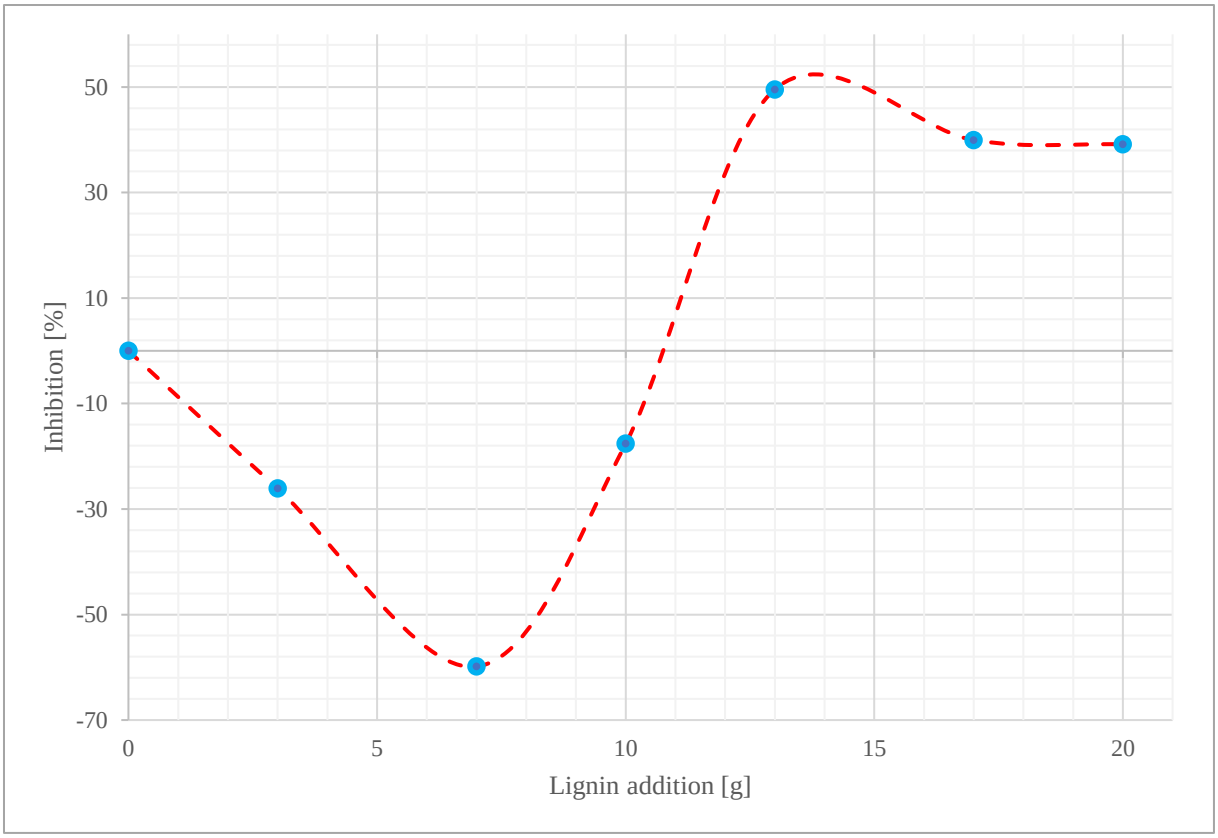

Figure S2. The effects of addition of lignin on inhibition during interval 2–3.

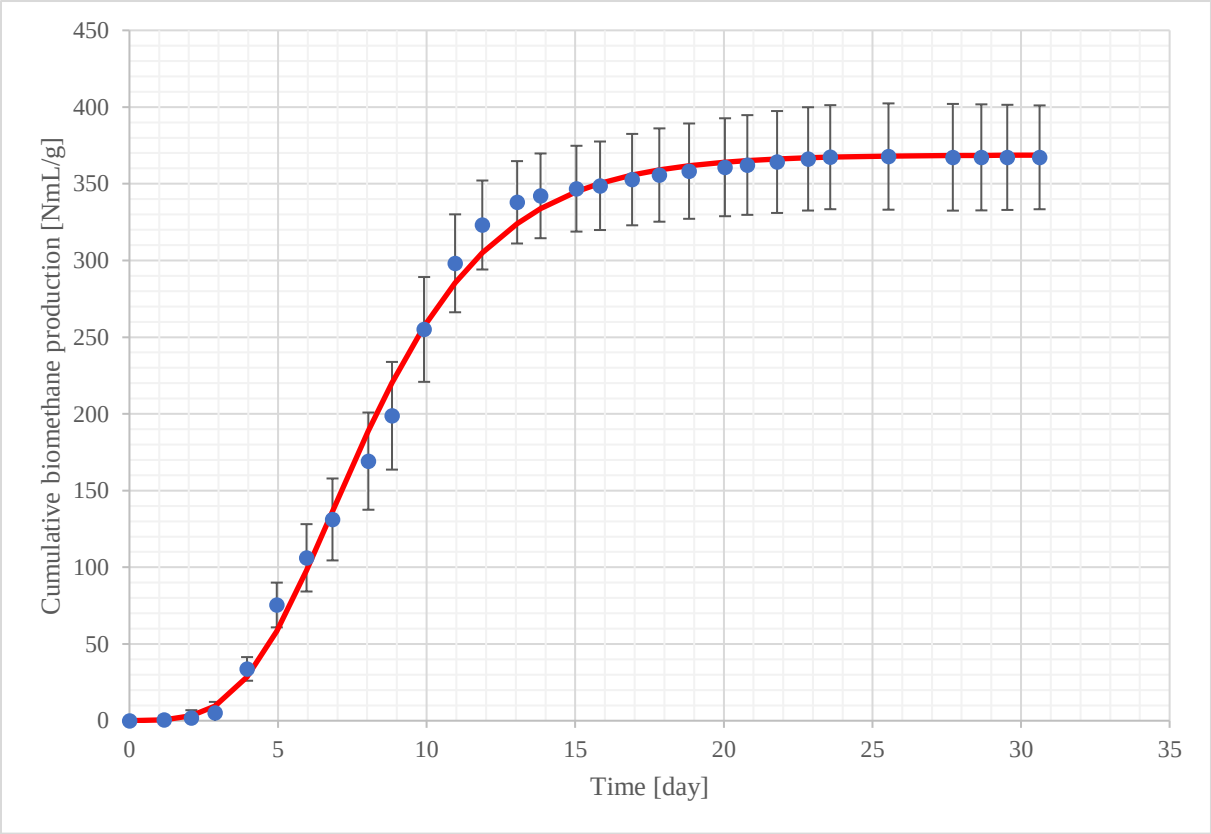

Figure S3. The biomethane production curve of the reference sample (10 g of cellulose only) in the second batch test. The solid, red line is the Modified Gompertz Model approximation.